RCA REVIEW

a technical journal

RADIO AND ELECTRONICS
RESEARCH • ENGINEERING

VOLUME XIV MARCH 1953 NO. 1

PRINTED IN U.S.A.

RCA REVIEW, published quarterly in March, June, September and December by RCA Laboratories Division, Radio Corporation of America, Princeton, New Jersey. Entered as second class matter July 3, 1950 at the Post Office at Princeton, New Jersey, under the act of March 3, 1879. Subscription price in the United States, Canada and Postal Union; one year $2.00, two years $3.50, three years $4.50: in other countries; one year $2.40, two years $4.30, three years $5.70. Single copies in the United States, $.75; in other countries, $.85.

RCA REVIEW

a technical journal

RADIO AND ELECTRONICS
RESEARCH • ENGINEERING

Published quarterly by
RCA Laboratories Division
Radio Corporation of America
in cooperation with

RCA Victor Division
Radiomarine Corporation of America
RCA International Division
RCA Communications, Inc.
National Broadcasting Company, Inc.
RCA Institutes, Inc.

Volume XIV | March, 1953 | Number 1

CONTENTS

RCA REVIEW is regularly abstracted and indexed by *Industrial Arts Index, Science Abstracts* (I.E.E.-Brit.), *Electronic Engineering Master Index, Chemical Abstracts, Proc. I.R.E., and Wireless Engineer.*

RCA REVIEW

BOARD OF EDITORS

SOME APPLICATIONS OF PERMANENTLY MAGNETIZED FERRITE MAGNETOSTRICTIVE RESONATORS*

By

W. Van B. Roberts†

Formerly with Research Department, RCA Laboratories Division, Princeton, N. J.

Summary—There are many cases in which the reaction of a sharply resonant mechanical body upon an electrical circuit can be advantageously employed. Probably the most familiar of these involve quartz crystals as frequency control of oscillators, elements of lattice filters, and the like. The use of magnetostrictively coupled resonators is less well established, probably because in the past such resonators have seriously reduced the Q of their actuating coils and have usually required a magnet for "bias." The advent of the so-called ferrite material has eliminated these drawbacks and makes the magnetostrictive resonator a practical device of negligible cost compared to a crystal, at least for frequencies of the order of a megacycle or less. The discussion in this paper is limited largely to ferrite resonators of toroidal form permanently magnetized with closed lines of biasing flux.

General Discussion

A FAMILIAR magnetostrictive resonator is shown in Figure 1. A nickel rod *R* is maintained in a partly magnetized condition by a horseshoe magnet, and alternating current in the winding alternately increases and decreases the magnetization of the rod. This

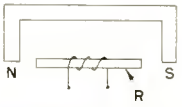

Fig. 1—Magnetostriction rod resonator.

results in a corresponding decrease and increase in the length of the rod because a nickel rod shrinks in proportion to its magnetization. If the frequency of the alternating current is made the same as the natural frequency of longitudinal vibration of the rod, the amount of motion produced by a given amplitude of current is greatly increased. The "mechanical Q" of the rod may be defined as the ratio of the natural frequency of the rod to the difference between the two frequencies (one a little above and the other a little below the rod

* Decimal Classification: 538.11.

† President, Applied Science Corporation of Princeton, Princeton, N. J.

frequency) at which the rod motion is equal to its maximum value divided by the square root of two.

The resonator described has the merit that if the rod is thin compared to its length, it retains enough magnetization to continue to operate even after the magnet is removed. However, it has the drawback that eddy currents in the nickel, even if the rod is laminated, cause losses which make the apparent Q of the coil low. Furthermore, the mechanical Q of a nickel rod is not very high, being only of the order of two or three hundred.

Ferrites as Magnetostrictive Resonators

If, in Figure 1, a rod of a suitable ferrite is substituted for the nickel, the Q of the coil is not only not lowered but may be greatly increased, because the resistivity of the ferrite is so great as to preclude eddy currents. Furthermore, the mechanical Q of the ferrite is quite high, of the order of several thousand, the exact value depending on the composition used and to some extent on the amplitude of vibration, the intensity of magnetization and various other factors. Unfortunately, however, the coercive force of the ferrites best suited for resonator use is so small that even in the case of very thin rods, the free poles developed at the rod ends by magnetization are sufficient to demagnetize the rod if the magnet is removed.

Permanent Magnetization of Ferrites

If, instead of a rod, a torus of ferrite is magnetized (by direct current flowing in a toroidal winding), no free poles are created and a considerable residual magnetization remains in the torus after the magnetizing current ceases. In some ferrites the intensity of this residual magnetization is very near optimum for magnetostriction purposes. The number of ampere turns required to produce this magnetization is small, so that the torus can be magnetized by passing a single wire through it and connecting the wire momentarily to an ordinary storage battery. The circuit can be completed by the very short duration contact of a hammer against a block of metal.

It is also possible to produce the same kind of magnetization of the torus, although of lesser intensity, by means of a magnet, as shown in Figure 2. Here, pole pieces P of iron are placed on the poles of the magnet to provide a narrow gap in the magnetic circuit. The ferrite torus R is placed against this gap as shown, and then pulled straight away. Due to the easy saturation of ferrite, more magnetic energy is stored in the form of clockwise lines of flux going around the larger

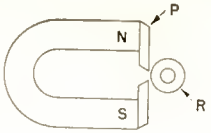

Fig. 2—Magnet arrangement for circularly magnetizing a ferrite rod.

portion of the torus which is remote from the pole pieces, than in the short portion adjacent to the pole pieces in which the flux lines run counterclockwise. When the torus is pulled away, there remains a circular magnetization of intensity determined by the difference in path lengths through the ferrite between pole pieces. If the gap is small compared to the torus diameter, the residual magnetization is of the order of one half that produced by the direct-current method of magnetizing. This method is, therefore, of value only when it is necessary to magnetize a solid cylinder or disc or other body which has no hole in it through which to pass a wire.

Bias and Driving Fluxes Not in the Same Direction

The basic method for producing mechanical forces in a magnetostrictive material is to superpose a "driving" magnetic field upon a constant or "bias" flux in the material. If the driving field is colinear with the bias flux, the result is a simple contraction or extension of the material along the common direction of the bias and driving fields, as in Figure 1. If, however, the driving field is at right angles to the bias flux, a shearing force is produced. Figure 3 shows a small square sample of magnetostrictive material in which magnet poles N and S produce a bias flux indicated by the vertical vector, while current in a driving coil L wrapped around the sample produces a driving flux indicated by the horizontal vector. Each of these vectors can be thought of as composed of two components at right angles, as shown in Figure 4. It will be seen that along one diagonal of the sample the driving flux component adds to the bias component, while along the other diagonal they oppose. The result is to shorten the one diagonal and elongate the other, so that the sample becomes slightly diamond

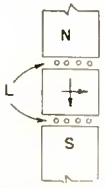

Fig. 3—Magnet and driving fields for producing shear.

shaped. But such a deformation of a square constitutes a shearing strain of the material, and the axis of the shear may be defined as being perpendicular to the plane of the sample. If the driving field had not been taken as at right angles to the bias, only its component at right angles would create shearing stress, so that finally the shearing stress may be defined as proportional to the vector product of the bias and driving fluxes. That is, its magnitude is proportional to the scalar product of the two fluxes multiplied by the sine of the angle between them, and its direction is perpendicular to the plane containing the bias and driving fluxes.

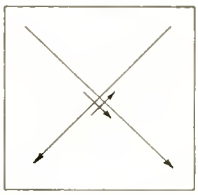

Fig. 4—Diagram of flux components producing shear.

Some Combinations of Bias and Driving Fluxes in Toroids

In a toroid (or disc or cylinder) the three coordinates may be called radial, circumferential, and axial. The nine combinations of bias and driving fluxes along these three coordinates are shown in Table I.

In Table I, the first column shows a pair of bar magnets with like poles together to produce radial bias flux, the third column shows the torus between unlike poles to have axial bias flux, while the middle column shows no magnet because the torus can be permanently magnetized in the circumferential direction. The same types of vibration are found in squares symmetrically located with respect to the main diagonal of the table, as interchanging the bias and driving fluxes makes no difference except to the practicability of the arrangement. The various types of vibration are:

"Radial Vibration with Node," where the inner part of the ring moves radially while the outer part moves in the opposite direction, although also radially.

"Radial Vibration," where all parts of the torus move radially and in the same sense. It is the "fundamental" of which the preceding mode is the first overtone.

"Longitudinal Vibration" implies simple longitudinal motion as in Figure 1, although, due to Poisson's ratio, there is some concomitant radial motion just as in the radial vibrations there will be some axial motion.

"Concentric Shear," where the outer part of the torus moves circumferentially in one sense while the inner part rotates in the opposite sense.

"Torsion" is a simple twisting of the torus on its axis, the ends turning in opposite senses.

"Coaxial Shear" is axial motion of concentric shells, the outer ones moving in opposite sense to the inner ones.

Of the various arrangements of Table I, the middle column is of special interest as no magnets are required. The arrangements in the other columns, however, are not necessarily less desirable for some

Table I—Various Combinations of Driving Coil Arrangements and Bias Fluxes for Toroidal-Ferrite Resonators.

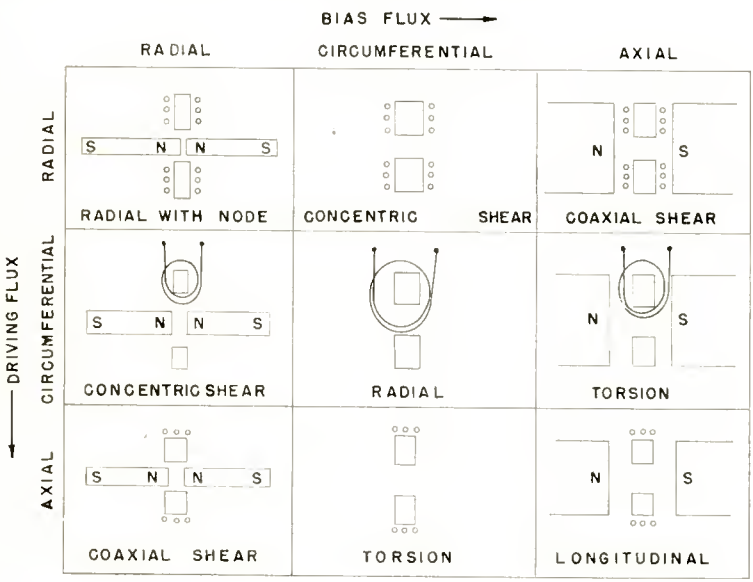

applications. For example, a stronger coupling can be obtained by using the torsion drive shown in column 3 than that in column 2. The frequencies of vibration in these three modes are given in the Appendix. It may be noted, however, that the torsion frequency depends only on axial length, the concentric shear only on radial dimensions, while radial frequency depends on all the dimensions, although very little on axial lengths. The radial and torsional modes are generally the most useful, as the "winding" for the radial mode may consist of a single conductor passing through the torus, while the torsional mode may be used for driving a torsion mechanical filter.

Coefficient of Coupling

In any magnetostrictive resonator, the efficiency of operation depends upon the magnetostrictive activity of the resonator material. From the point of view of circuit analysis and design, however, the most useful measure of efficiency is what may be termed the coefficient of coupling between a given coil and the resonator with which it is associated. If the coil is tuned by a condenser to the same frequency as the resonator, the system will be found to have two natural frequencies, one above and one below the resonator frequency. The difference between these two, divided by the resonator frequency, is the coefficient of coupling. (The same definition gives the coefficient of coupling between the coils of any pair of like-tuned electrical circuits.) This coefficient can be readily measured with a Q-meter. The coil, with resonator in place, is connected to the Q meter and the condenser thereof is adjusted until the coil is tuned to the same frequency as the resonator as evidenced by equality of the two

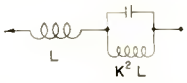

Fig. 5—Equivalent circuit for magnetostriction resonator.

responses observed when the frequency alone is varied. The difference between the frequencies at which the response peaks occur, divided by the mean frequency, is very closely equal to the coefficient of coupling. The coefficient depends on how closely the winding can be associated with the resonator. With a toroidal winding and the radial mode of vibration, coefficients up to about 10 per cent are obtainable. The combination of coil and resonator can be replaced, for purposes of circuit analysis, by the equivalent circuit of Figure 5, where L is the inductance of the coil with resonator in place, and K is the coefficient of coupling (expressed as a fraction of unity, not as a percentage). The antiresonant frequency of the divided circuit is the same as the natural frequency of the resonator, and its Q the same as the mechanical Q of the resonator.

Applications

(1) Perhaps the simplest application of a permanently magnetized ferrite torus is in frequency control of an oscillator. Figure 6 shows a simple circuit for the purpose which requires only one winding on the resonator, and this may consist of only a single wire passing through the torus. In the absence of mechanical vibrations of the

ring, the circuit between junctions *a* and *b* is inductive, so that oscillation cannot occur. But this circuit can become nearly purely capacitive at a frequency slightly above the natural frequency of the resonator if the Q of the resonator is high and the coefficient of coupling sufficiently large. Then oscillations will occur when the circuit *L-C* is tuned to approximately the resonator frequency if the transductance of the tube exceeds a value determined by the circuit impedances. A 6J6 tube with 90 volts or more on the plate has been found sufficient with a reasonably high Q coil at *L*. The non-oscillating plate current is limited to 4 milliamperes by the cathode bias resistor. By varying the tuning of *L-C*, higher frequency oscillations at resonator modes other than the simple radial mode can often be produced. To give an idea of resonator size it may be noted that a torus of 0.82 centimeter outer diameter and a hole of about 0.15 centimeter diameter gives radial frequency oscillations at 380 kilocycles.

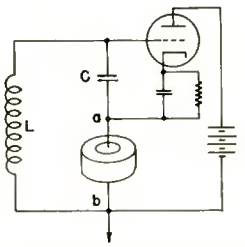

Fig. 6—Oscillator circuit employing magnetostriction resonator.

Oscillations are more easily obtained if a toroidal winding of several turns is put on the ring. Or, equivalently, if the primary of a transformer with very small leakage inductance is connected between points *a* and *b*, the secondary of the transformer being a single turn linked with the torus.

The oscillator circuit is, of course, not limited to radial vibrations of the torus, but may be operated in any mode where sufficient coefficient of coupling is obtainable; in particular, the torus may be arranged for torsional operation as shown in the lower middle square of Table I. In this case the coupling is improved, if the torus is short, by putting inert magnetic core material on each side of the torus. The oscillator described is intermediate in frequency stability between a tuned-circuit oscillator and a quartz-crystal oscillator, but the cost of the ferrite element is negligible.

(2) A simple three-circuit filter may be made by employing a long torus (a pipe or cylinder) as an intermediate "circuit" between a pair of tuned circuits. See Figure 7. In this case the resonator *R* operates

in torsion and is preferably three or more half-waves long. It passes through a metal pipe P and shielding S which prevents direct coupling between coils L_1 and L_2. Current in L_1 drives the resonator in torsion, and, by the inverse process, torsional vibrations in the output half wave length induce voltage in L_2. The band width obtainable in this filter is limited by the coefficient of coupling, and this in turn varies inversely with the square root of the number of half waves in the resonator. Figure 8 shows the transmission characteristic of a filter of this sort, operating at the third harmonic of the rod and adjusted to give a Tchebyscheff characteristic with 1.3 decibels peak-to-valley ratio.

(3) Another way to eliminate direct coupling between input and output coils is to provide auxiliary mutual inductance to buck out the undesired coupling. Figure 9 shows such an arrangement using a toroidal resonator in the radial mode. To avoid winding many turns on the torus, a step-down transformer arrangement is used. The bucking mutual is adjusted by a movable magnetic core M. Figure

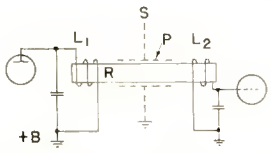

Fig. 7—A three-circuit filter with a ferrite rod as middle circuit.

10 shows the performance of such a filter. The dotted curve shows the effect of incomplete bucking. The output falls to 0.06 millivolt at 298 kilocycles, then rises again to a maximum of 0.067 at 303 kilocycles.

(4) If, for the bucking transformer in the above circuit, another resonator torus is used, and the two have suitably different frequencies, a differential type of filter results. Figure 11 shows a curve of such a filter.

Lattice filters with more than two ferrite rings can be readily designed and easily constructed by putting the rings on thin wall tubes through which only two wires need to be run. Figure 12 shows, for example, how eight rings, each of a different frequency, are arranged to form a lattice equivalent to a cascade of eight tuned circuits. The chief difficulty encountered in this type of filter is in obtaining a selection of rings each having the required coefficient of coupling as well as the proper frequency.

(5) A somewhat different way to add a ferrite resonator to an ordinary pair of tuned circuits is shown in Figure 13, and its perform-

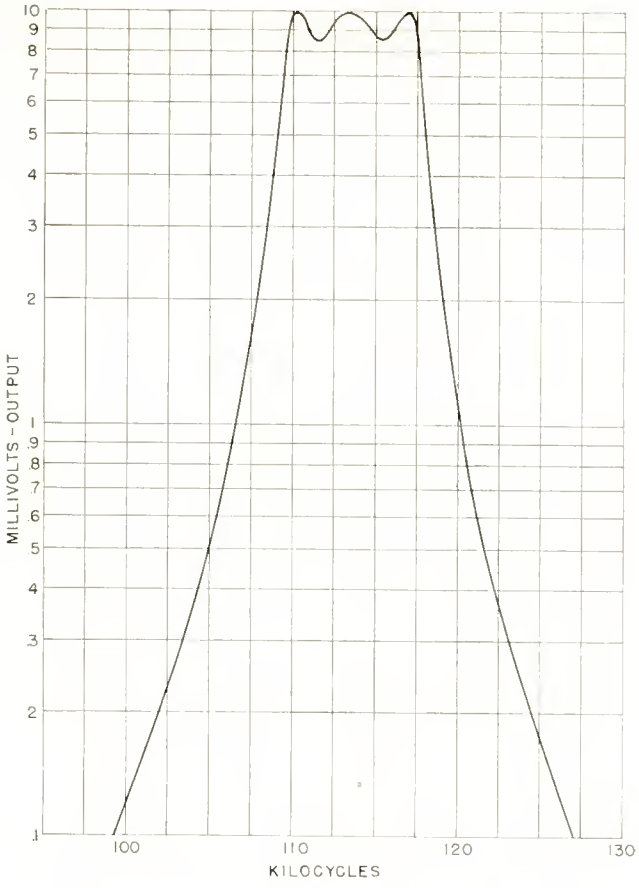

Fig. 8—Performance curve of the filter of Figure 7.

ance curve in Figure 14. Here all coils are tuned by their correspondingly numbered condensers to the (torsion) frequency of the ferrite ring in L_3, which is flanked by cylinders of unmagnetized ferrite to increase the coefficient of coupling. This is particularly necessary if the rejection points are to be pushed far apart, since the separation of these points divided by the mid-band frequency is equal to the coefficient of coupling between L_3 and the ring. From the equivalent

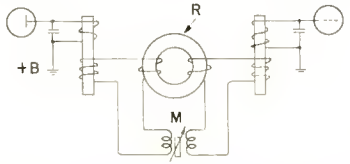

Fig. 9—Another three-circuit filter.

circuit (Figure 5) it will be seen that this is a "mid-series-terminated m-derived constant K" filter section. The broken curves of Figure 14 show the performance of the same end circuits (L_1C_1 and L_2C_2) coupled by simple mutual inductance, as in an ordinary intermediate-frequency transformer. The narrow curve is for loose coupling, and

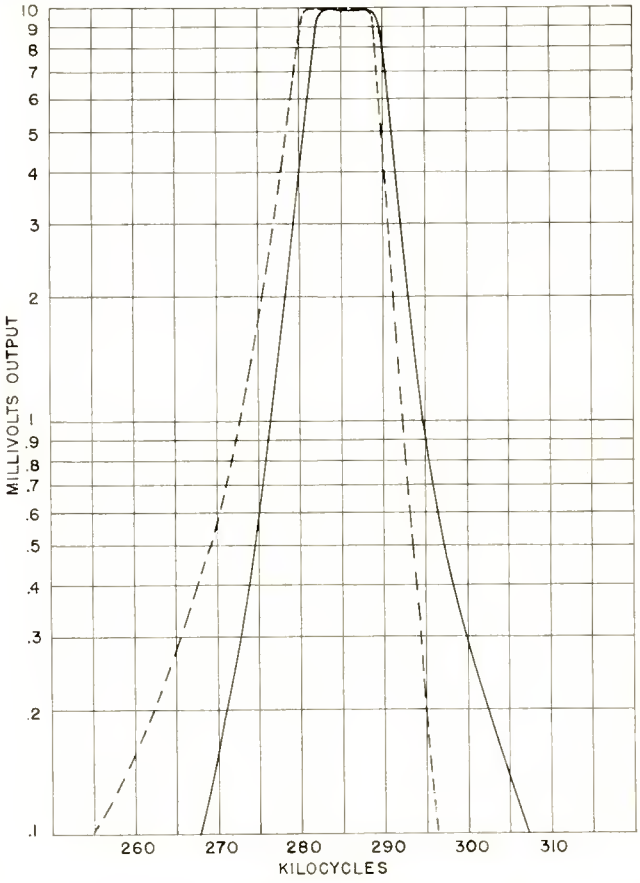

Fig. 10—Performance curves of the filter of Figure 9 with different adjustments.

the wide curve is for critical coupling. It is seen that considerable improvement is obtained by the addition of the ferrite and its circuit.

The inherent frequency constancy of the ferrite resonator makes it possible to tune this filter in a radio receiver without requiring a signal generator to provide the proper intermediate frequency. The input and output circuits are first detuned, and any strong signal is tuned in. This will peak up sharply at the ferrite frequency, so that

the desired intermediate frequency is known to be impressed on the filter. Next, the junction of C_1 and C_2 may be shorted to ground so that input and output circuits are only very loosely coupled by the inductance of the shorting lead. They may therefore be peaked independently. On removing the short, the filter is in tune except for C_3, which must be adjusted so that the rejection points fall outside the

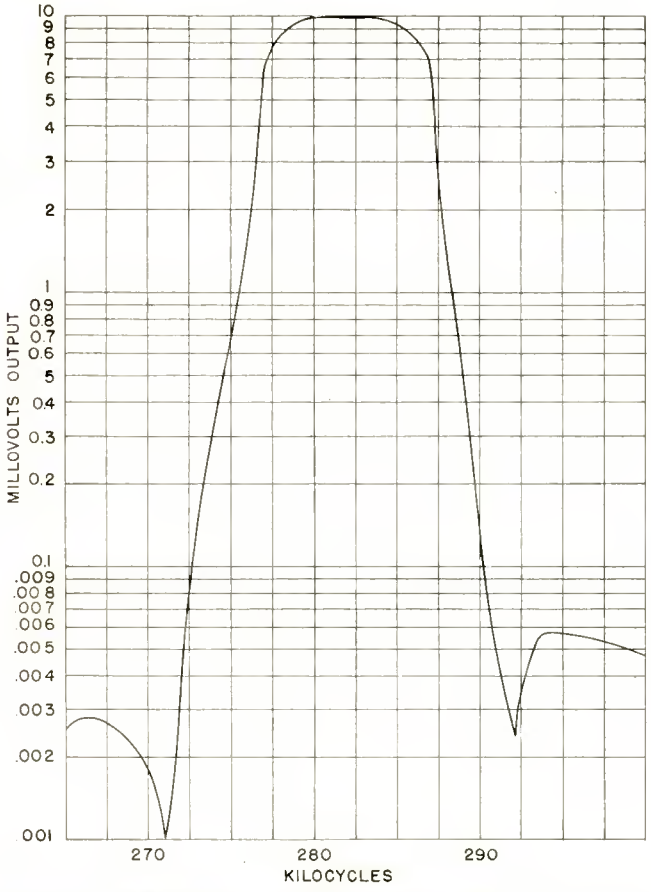

Fig. 11—Performance curves of a lattice filter employing two ferrite resonators.

transmission band, preferably at approximately equal distances on each side. The spacing between rejection points is not adjustable except in the original construction at which time the coefficient of coupling is fixed.

(6) Multisection torsion filters of high efficiency (low insertion loss) and great selectivity can be made if the end mechanical resonators

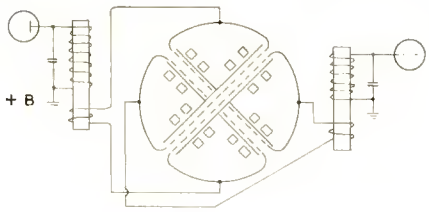

Fig. 12—A lattice filter employing eight ferrite ring-shaped resonators.

are ferrite tori. Provided the band width is not too great (not over approximately 5 per cent), the tuned circuits associated with the ferrite can act as the end circuits of the filter, the required terminating resistances being in the form of the electrical resistances in the tuned circuits. Inherent resistance in the electrical circuits sets the lower limit of the band width. The ferrite can be cemented to the metal part of the filter very satisfactorily with polyvinyl acetate.

Appendix

Velocities in Ferrites

In a homogeneous infinite medium, compression waves travel with a velocity which will be called V_2, and shear (or torsion) waves with a velocity V_1, which is roughly half of V_2. In a thin rod, the compression (or longitudinal) waves travel with a velocity V_r, which is a little less than V_2, while in a thin infinite sheet, the compression wave velocity V_s is between V_r and V_2. Wave lengths corresponding to these velocities will be indicated by λ with corresponding subscripts. In every case $V = \lambda f$, where f is the frequency.

The velocities in ferrite depend considerably upon its composition and heat treatment, and to some extent upon intensity of magnetization and temperature. As to temperature, the frequency of a longitudinally vibrating rod falls about 30 parts in a million for each degree centigrade rise in temperature. The frequency increases somewhere in the order of 1 per cent in going from weak to strong bias magnetization.

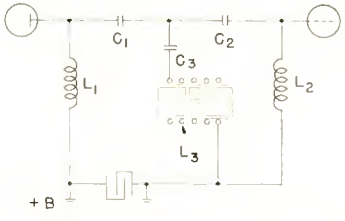

Fig. 13—An "m-derived" filter employing a ferrite torsion resonator.

Typical values for the velocities in a strongly magnetostrictive ferrite are:

$$V_1 = 3.33 \times 10^5 \text{ centimeters per second,}$$

$$V_2 = 5.7 \times 10^5 \text{ centimeters per second,}$$

$$V_r = 5.25 \times 10^5 \text{ centimeters per second,}$$

$$V_s = 5.4 \times 10^5 \text{ centimeters per second.}$$

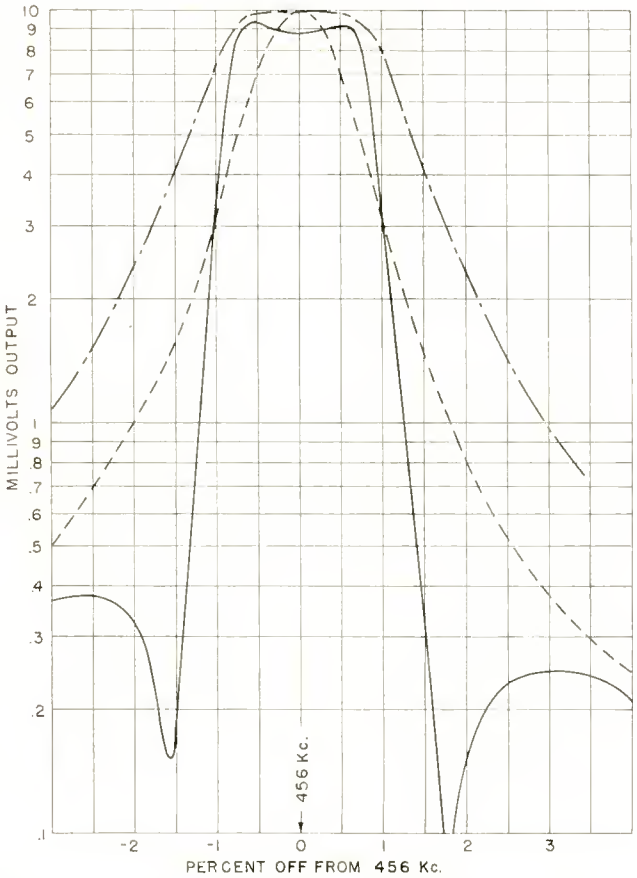

Fig. 14—Performance curve of the filter of Figure 13; dashed curves are for ordinary coupled circuits for comparison.

Frequency Formulas for Toroids

The fundamental frequency of a longitudinally vibrating thin rod is $V_r/2L$ where L is its length in centimeters.

A torsion rod (or pipe or torus) has frequency $V_1/2L$.

A thin disc with no hole has lowest radial frequency $\frac{2.166}{2\pi a} V_s$, where a is the radius, if Poisson's ratio for the material is 1/3, which is approximately the case for aluminum.

The formula for the radial frequency of a long solid cylinder is the same except that V_2 is used in place of V_s.

The presence of a hole in a disc lowers the radial frequency by an amount not readily given by any simple formula. However, if the hole in a thin disc is so large that a thin ring results, the perimeter of the ring is one wave length at V_r, so that $f = V_r/2\pi a$.

A long thin-walled pipe has the slightly higher radial frequency $V_s/2\pi a$.

A solid disc of any thickness vibrates in concentric shear according to the relation $\frac{\lambda_1}{a} = \frac{2\pi}{5.135}$ at its lowest frequency, i.e., $f = \frac{5.135}{2\pi} \frac{V_1}{a}$.

If there is a large hole, the frequency approaches $V_1/2W$ where W is the radial thickness of the wall.

Ferrites for Magnetostriction

Almost any ferrite exhibits some magnetostriction, but best results have been obtained with a simple nickel ferrite (74.69 grams of NiO plus 159.68 grams of Fe_2O_3) heated to 1300°-1400°C for approximately an hour and a half, and cooled slowly.

FACTORS IN THE DESIGN OF POINT-CONTACT TRANSISTORS*

By

B. N. Slade

Tube Department, RCA Victor Division,
Harrison, N. J.

Summary—*Electrical characteristics of point-contact transistors depend essentially on four main factors: (1) the materials used for the point contacts, (2) the spacing of the point contacts, (3) the resistivity of the germanium, and (4) the electrical forming process. Control of these four factors during transistor fabrication makes possible the control of equivalent circuit resistances, current amplification factor, static characteristic curves, and frequeny response and, therefore, permits the design of different transistors each suitable for use in a specific type of circuit application. This paper discusses the design of point-contact transistors for use in radio-frequency amplifiers, oscillators, and switching or counter circuits, and the effects of electrical forming on the electrical characteristics.*

Transistors for Radio-Frequency Amplifiers

TRANSISTORS designed for use as amplifiers at radio frequencies must be electrically stable when no appreciable external impedances are present in the emitter or collector circuits. This requirement, known as "short-circuit" stability, is particularly important in radio-frequency stages having parallel-tuned circuits in both the input and output of the transistor, because the impedance of the tuned circuits approaches zero in the off-resonance condition. For transistor stability under these short-circuit conditions, the following condition must exist:

$$\frac{r_e}{r_b} + \frac{r_e}{r_c} + 1 > \frac{r_m}{r_c}, \qquad (1)$$

where r_e is the emitter resistance, r_b is the base resistance, r_c is the collector resistance, r_m is the transfer resistance, and r_m/r_c is approximately equal to α_{cc}, the collector to emitter current amplification factor.[1,2]

---

* Decimal Classification: R282.12.

[1] B. N. Slade, "Control of Frequency Response and Stability of Point Contact Transistors," *Proc. I.R.E.*, Vol. 40, p. 1382, November, 1952.

[2] R. M. Ryder and R. J. Kircher, "Some Circuit Aspects of the Transistor," *Bell Sys. Tech. Jour.*, Vol. 28, pp. 317-401, July, 1949.

The effect of various equivalent-circuit resistances on transistor stability may be analyzed by the substitution of typical values in this expression. For example, typical equivalent circuit resistances for a transistor having germanium resistivity of 5 ohm-centimeters and a point spacing of 0.002 inch might be

$$r_e = 180 \text{ ohms},$$

$$r_b = 200 \text{ ohms},$$

$$r_c = 20000 \text{ ohms},$$

$$\alpha_{cc} = 2.0.$$

If these values are substituted in Expression (1), it is seen that the specified condition is not met, and, therefore, the transistor would not be stable under "short-circuit" conditions. Although either the germanium resistivity or the point spacing may be varied to achieve the resistance values required for stability, variation of the point spacing has a decided effect upon the frequency response of the transistor. From available design data for point-contact transistors,[1] it is possible to select a combination of germanium resistivity and point spacing which provides stability at a desired frequency of operation.

Before the resistivity and point-spacing values are selected, the value of equivalent base resistance required for stability must be determined from the expression given above. The term r_e/r_c can be neglected in these approximations because it is very small compared to the other terms of the expression. Since forming techniques allow control of α_{cc}, as will be shown later, a typical value of 2.0 may be assumed for this term. A value of r_b greater than that of r_e, therefore, causes instability, and a value less than that of r_e results in stability.

The value of r_b used in these expressions refers to only one direct-current operating point. Figures 1a and 1b show the feed-back characteristics of two developmental point-contact transistors. The slope of this curve at any point indicates the value of the equivalent base resistance. Since the slope increases as the collector current increases, the transistor may be stable at one value of collector current, but unstable at another. If the value of r_b in the above example should be less than that of r_e at 2.0 milliamperes, for instance, but greater than that of r_e at 2.5 milliamperes, it would be necessary to limit the operation of the transistor to 2.0 milliamperes or less to avoid unstable operation. Because of the nonlinearity of the feed-back characteristic, it is desirable to provide a value of r_b low enough to assure stability regardless of the direct-current operating conditions of the point-

contact transistor. With few exceptions, a value less than 120 ohms for r_b assures short-circuit stability in a common-base amplifier circuit.

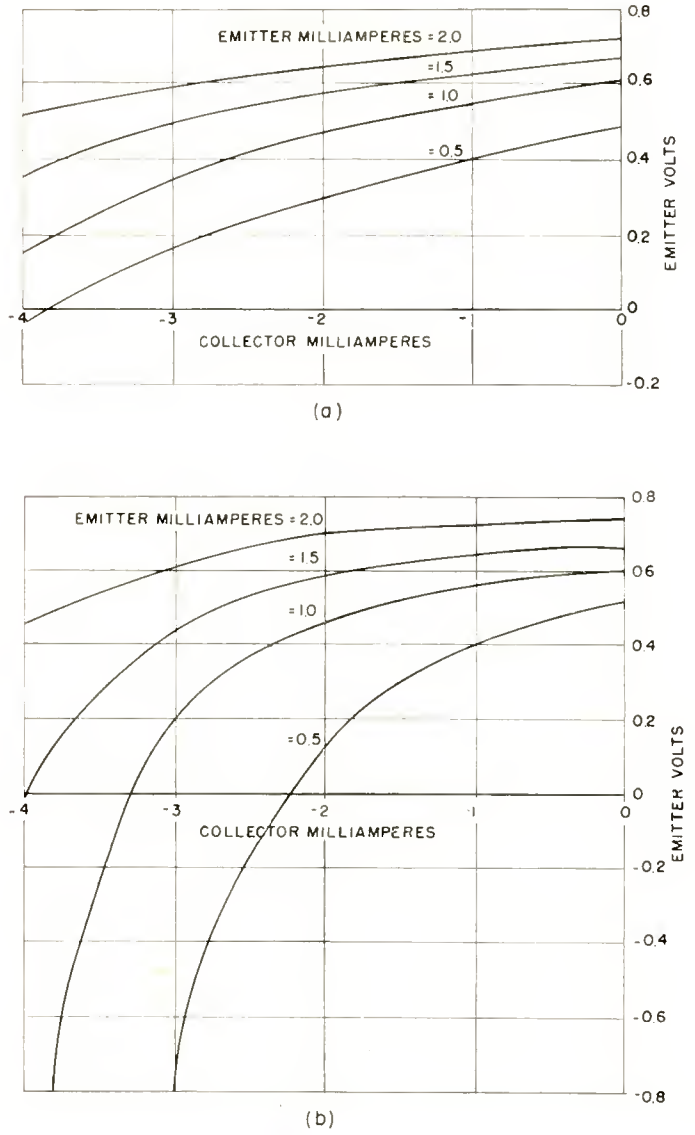

Fig. 1—Feedback characteristics of two developmental point-contact transistors.

If stability is extremely important, an additional safety factor of approximately 20 ohms is desirable. Within the range of resistivities

discussed here, the value of r_e is usually sufficiently large to assure stability if the value of α_{cc} is approximately 2.0. As the value of α_{cc} increases, however, the transistor tends to become unstable, and the value of r_b must be decreased even further.

When transistors are designed for operation at specific frequencies, the curves given in Figure 2 may be used to determine values of point-spacing and resistivity which will provide the equivalent base resistance necessary for stability at the desired frequency. These curves represent a composite of design curves given in a previous paper.[1] The dashed line shows the variation of cutoff frequency (3 decibels down in current amplification factor) with point spacing for transistors

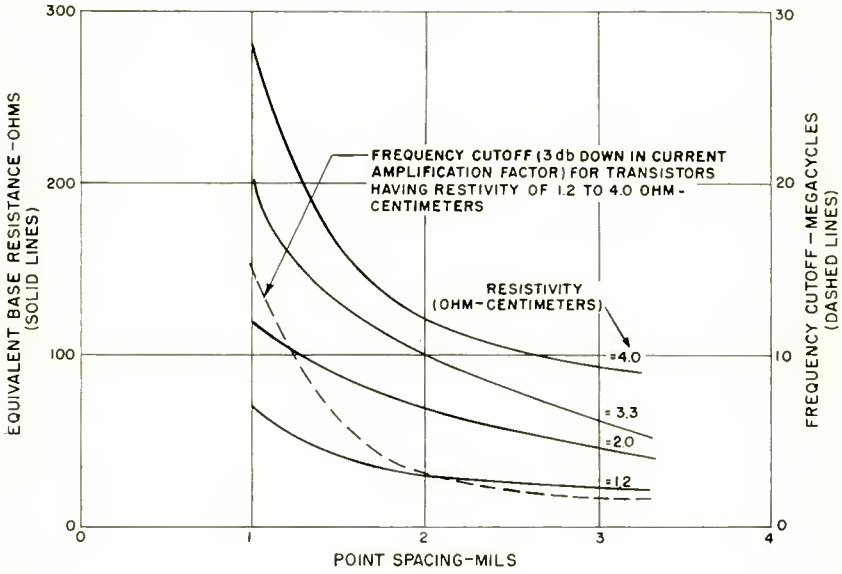

Fig. 2—Effect of variation of point spacing and germanium resistivity on frequency cutoff and equivalent base resistance.

having a resistivity ranging from 1.2 to 4.0 ohm-centimeters. In a transistor having a resistivity of 1.2 ohm-centimeters, a spacing of 1.0 mil, and an equivalent base resistance of 70 ohms, for example, a frequency cutoff of 15 megacycles can be obtained. If, for reasons to be discussed later, it is desirable to utilize a higher value of germanium resistivity, such as 3.3 ohm-centimeters, stability can be achieved at a spacing of 2.0 mils with a 100-ohm value of r_b, but the frequency cutoff would be only about 3.0 megacycles.

Although the curves included in this paper cannot be used as exact design data, their general shape serves as a guide to transistor design.

The curves were obtained by careful measurement of the resistivity of individual germanium specimens, and by variation of the spacing on each specimen to attain the separate resistivity curves. It is quite difficult, however, to maintain accurate point spacings, and measurement of the germanium resistivity is subject to some error. Because the transistors had to be formed electrically for each point on the curves, some error also arises due to the difficulty in reproducing the same forming conditions for each point.

For most amplifier applications, it is necessary to consider power gain and current amplification as well as frequency response and stability. A point-contact transistor usually should have a low-frequency power gain of at least 17 decibels and a current amplification factor of at least 2.0. It is possible to achieve a 17-decibel power gain using practically any value of resistivity within the range from one to 15 ohm-centimeters provided appropriate point spacings are used. If germanium having a resistivity of 10 ohm-centimeters is used, power gains greater than 17 decibels can be obtained at spacings greater than 10 mils.[3] When smaller resistivities are used, smaller spacings must be used to provide power-gain values of approximately 17 decibels or greater. When resistivities ranging from 1 to 5 ohm-centimeters and spacings of less than 3 mils are used, power-gain values greater than 17 decibels can usually be obtained for any combination of point spacing and resistivity. The small-signal power gain for radio-frequency applications, therefore, is not a serious consideration in the selection of a value of point spacing and resistivity.

Transistors for Switching Circuits

In the design of point-contact transistors for switching or counter circuits, the selection of point spacing and resistivity involves additional considerations. Figure 3 shows the output characteristics of several typical developmental point-contact transistors. Collector current is plotted as a function of collector to base voltage for varying values of emitter current. The current amplification factor may be computed from the curves of Figure 3 by dividing an increment of collector current along a line of constant collector voltage by the corresponding increment of emitter current. For most switching applications, I_{CO}, the collector current when there is no emitter current, should be as low as possible. In addition, the transistor should be capable of drawing a large amount of collector current at a low value of collector voltage when the emitter current is high. α_{ce} should be as constant

[3] B. N. Slade, "A High-Performance Transistor with Wide Spacing Between Contacts," *RCA Review*, Vol. XI, No. 4, p. 517, December, 1950.

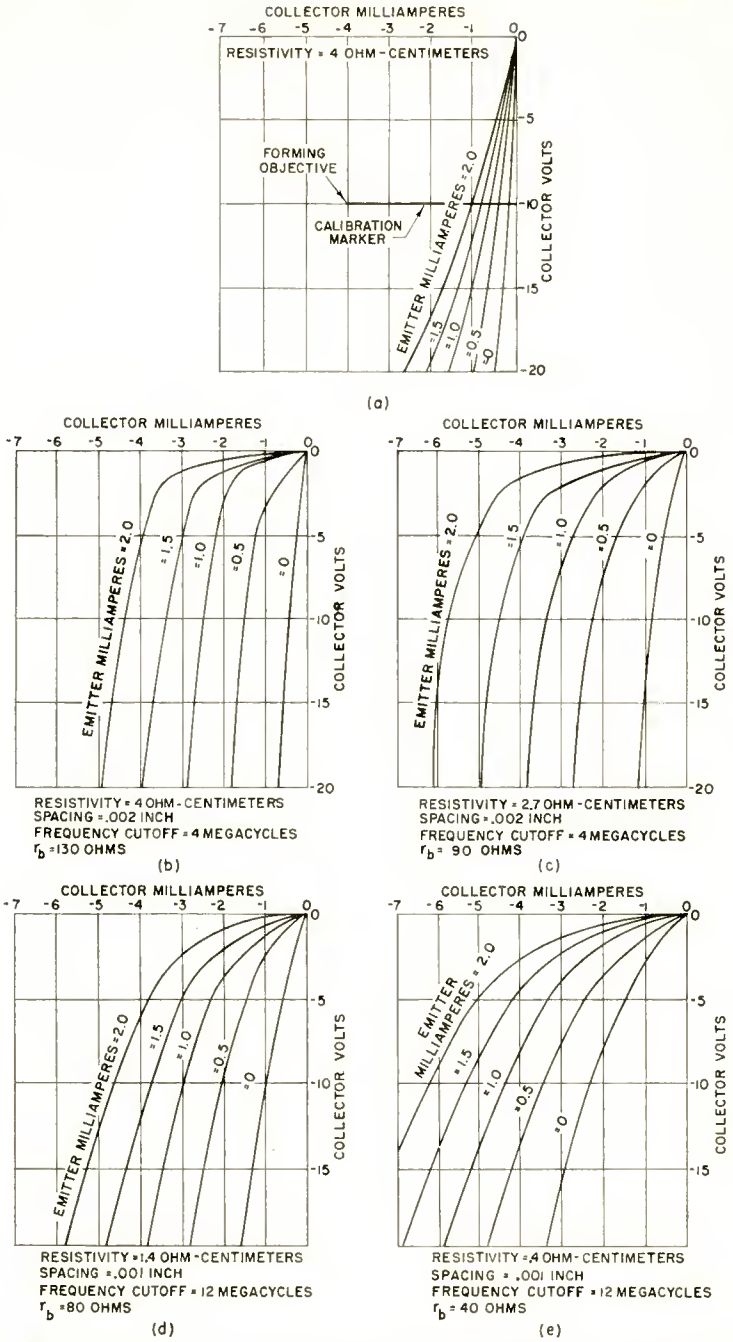

Fig. 3—Output characteristics of several developmental point-contact transistors: (a) before forming; (b), (c), (d), (e) after forming.

as possible over the entire range of collector voltages, and should generally be on the order of 2.0 or more. If the germanium resistivity is too low (on the order of 1 to 2 ohm-centimeters), it is difficult to obtain a high current amplification factor and still maintain a low value of collector current when there is no emitter current. This difficulty is due in part to the electrical forming treatment, which will be discussed later. Values of germanium resistivity greater than 3 ohm-centimeters permit higher current amplification factors with fairly low values of I_{CO}.

For switching circuits, it is not essential that the transistor be short-circuit stable. Relatively small point spacings, therefore, may be used with germanium having higher resistivities. Even in switching circuits, however, the value of the equivalent base resistance is subject to some limitations. If extremely narrow spacings are used with very high resistivities, the value of r_b may increase rapidly with increasing collector current because of the nonlinearity of the feed-back characteristic. In some cases, r_b of a transistor may vary from a few hundred ohms to a few thousand ohms over a collector-current range of three milliamperes, as evidenced by the shape of the curves in Figure 1b. The nonlinearity of the feed-back characteristic is much less pronounced when wider spacings or lower resistivities are used. If the speed of the switching circuits is not too high, therefore, wider point spacings and germanium having a higher resistivity may be used to achieve a low value of equivalent base resistance together with a high current amplification factor, and a low value of I_{CO}. As shown in Figure 3, a transistor using germanium having a resistivity of 4.0 ohm-centimeters and a point spacing of 2 mils would have an equivalent base resistance of approximately 120 ohms and a frequency cutoff of 3 megacycles. A higher value of resistivity could also be used at the same spacing without the equivalent base resistance becoming excessive for this type of application.

Transistor Oscillators

Transistors normally will oscillate at frequencies much higher than the so-called "cutoff" frequency. For instance, a transistor having a frequency cutoff of 4 megacycles may oscillate at frequencies as high as 10 megacycles or more because the current amplification and the power gain at these higher frequencies is still sufficient to enable oscillations to occur. By utilizing point spacings of less than 0.001 inch, it is possible to achieve cutoff frequencies of 30 megacycles or more, and thus make possible oscillations at even higher frequencies. With spacings of approximately 0.0005 inch, transistors can be made

which will oscillate at frequencies well above 100 megacycles.[4] Germanium resistivities less than 2 ohm-centimeters can be used at these narrow spacings if low equivalent base resistance is desired.

Electrical Forming[5]

The material used for the point contacts greatly affects the transistor characteristics. The use of phosphor bronze for the collector contact is desirable because this material responds well to the electrical forming process. In the transistors discussed in this paper, phosphor bronze was also used for the emitter contacts. Because the emitter is not electrically formed, however, other point materials such as tungsten, steel, or berryllium copper can be used for the emitter without appreciably affecting major transistor characteristics.

The electrical forming treatment is very important in the fabrication of point-contact transistors. In a typical circuit used in the forming of transistors, as shown in Figure 4, a capacitor is charged to a

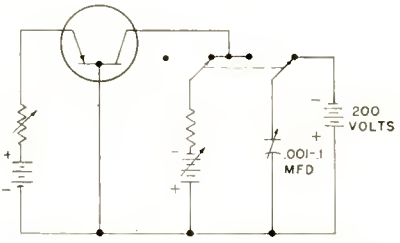

Fig. 4—Forming circuit for point-contact transistors.

voltage of approximately 200 volts and then discharged between the collector and base. The resulting surge of current causes a reduction in the collector resistance and an increase in the current amplification factor. Output characteristic curves for an unformed transistor are shown in Figure 3a and the output characteristic for the same transistor after it has been formed, is given in Figure 3b. The value of I_{CO} increases slightly after forming, and the current amplification factor increases considerably. The shape of the curves also changes, and α_{ce} becomes fairly uniform over the entire range from low voltages to the higher voltages. When the emitter current is zero, the collector draws only a few tenths of a milliampere; when the emitter current

[4] G. M. Rose and B. N. Slade, "Transistors Oscillate at 300 Mc," *Electronics*, Vol. 25, p. 116, November, 1952.

[5] J. Bardeen and W. G. Pfann, "Effects of Electrical Forming on the Rectifying Barriers of n- and p-Germanium Transistors," *Phys. Rev.*, Vol. 77, pp. 401-402, February, 1950.

is 2 milliamperes, however, the collector draws approximately 5 milliamperes at a voltage of only 10 volts.

This type of characteristic may be achieved by the repeated pulsing of the transistor by the capacitor-discharge method until the desired transistor characteristics are obtained, as observed on the oscilloscope of a curve tracer. The curve tracer may be switched in and out of the transistor circuit between discharges of the capacitor. The transistor can be pulsed to a desired operating point on the output characteristic. A calibration mark on the oscilloscope of a curve tracer can be set to this operating point. If, for example, a transistor is to be formed to the following operating point: emitter current = 2 milliamperes, collector voltage = —10 volts, collector current = —4.0 milliamperes, the calibration marker on the oscilloscope is set to this operating point, as shown in Figure 3a. The output characteristic is then plotted as the collector is swept with an alternating-current voltage while the emitter current is varied in steps from zero to 2 milliamperes. As the capacitor in Figure 4 is charged and discharged, the zero-emitter-current curve rises slightly while the constant-emitter-current curves begin to spread out. The value of the capacitor or charging voltage may be increased as additional pulses are applied until the 2-milliampere emitter-current curve passes through the —10-volt and —4.0-milliampere point marked by the calibrating marker.

The shape of the output characteristic obtained during the pulsing operation depends to some extent upon the germanium resistivity. If resistivities of about 2 ohm-centimeters or more are used, the shape of the characteristic curve approaches that of the plate characteristic curve of a pentode-type vacuum tube. When larger values of resistivities are used, I_{CO} may be decreased. When resistivities much smaller than 2 ohm-centimeters are used, it is often difficult to achieve values of α_{cc} much greater than 2 and maintain low values of I_{CO}. A "short-circuit-stable" transistor having a cutoff frequency of approximately 15 megacycles would have the output characteristic shown in Figure 3d, because germanium having fairly low resistivity would be used. Figures 3b through 3e indicate types of output characteristics that can be obtained with different germanium resistivities. Typical values of frequency cutoff and equivalent base resistance are given for each curve family.

Effect of Ambient Temperature

An important consideration in the design of point-contact transistors is the dependence of transistor characteristics upon variations in ambient temperatures. As ambient temperatures are increased, the

equivalent circuit resistances decrease, in some cases to an intolerable degree. The amount of change that may be tolerated depends upon the application. As the ambient temperature increases from room temperature (25°C) to 60°C, r_e, r_b, and r_c tend to decrease while α_{ce} tends to increase. r_c changes most rapidly, and becomes very low at temperatures greater than 60°C. At elevated temperatures, however, the increase in α_{ce} tends to compensate for the decrease in r_c, and the power gain is kept fairly constant. For small-signal applications, therefore, changes in ambient temperatures may not be too serious up to temperatures of 50 or 60°C. For large-signal applications, however, large changes in I_{CO} are very serious, particularly in switching circuits.

The temperature problem in small-signal circuits is alleviated some-

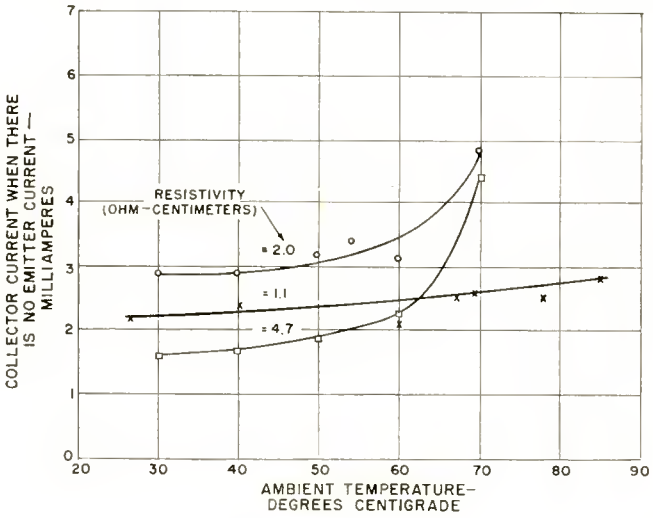

Fig. 5—Effect of variation of ambient temperature on collector current when there is no emitter current.

what because the temperature dependence of point-contact transistors decreases as the germanium resistivity decreases. Figure 5 shows a curve of I_{CO} versus ambient temperature for three different values of resistivities. When germanium having low resistivity is used, I_{CO} is less dependent upon temperature changes and the temperature at which the transistor may satisfactorily operate is extended beyond 60°C. The curves of Figure 6 show the variation of gain, r_e, and r_b with ambient temperature for developmental transistors having varying values of germanium resistivity. The dependence of the low-resistivity transistors on temperature is considerably less than that

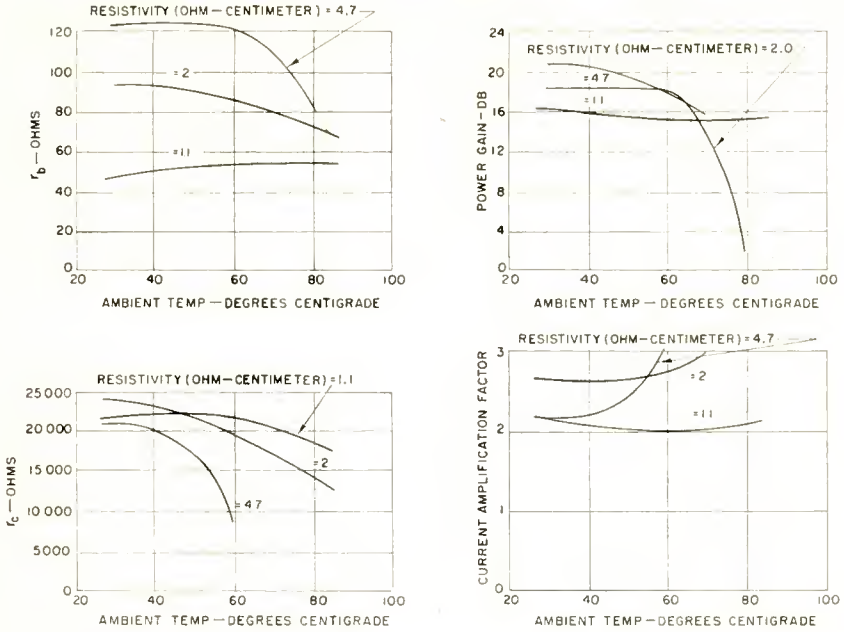

Fig. 6—Effect of variation of ambient temperature on current amplification factor, power gain, r_b, and r_c of developmental point-contact transistors.

of high-resistivity units. Thus, the temperature characteristics of the device may also be controlled to some extent by the proper choice of germanium resistivity.

TERMINOLOGY AND EQUATIONS FOR LINEAR ACTIVE FOUR-TERMINAL NETWORKS INCLUDING TRANSISTORS*

By

L. J. Giacoletto

Research Department, RCA Laboratories Division,
Princeton, N. J.

Summary—With the advent of transistors, considerably greater usage has been made of linear active four-terminal network theory. Some of this usage has been complicated because of differences in terminology. In this paper a unified system of nomenclature is developed for a linear active four-terminal network, and this system is then applied to transistors. It is hoped that this paper will serve as a step towards a standard system of nomenclature.

Section I deals with the general properties of a linear active four-terminal network. Section II is devoted to a tabulation of circuits associated with transistors. Several quantitative examples of the application of material in Sections I and II to transistor circuits are given in Section III.

Section I—Linear Active Four-Terminal Networks and Equations

In general, any linear active four-terminal network (Figure 1) is characterized by two equations which interrelate the currents and voltages at its input and output terminals. These equations may be written in either nodal or loop equation form.

A. Circuit with Associated Generator and Load, and Equations

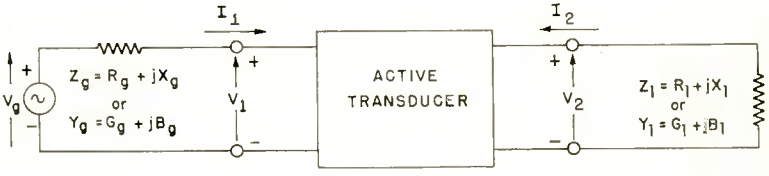

Fig. 1—General active transducer circuit.

Nodal Equations	**Loop Equations**
$I_1 = y_{11}V_1 + y_{12}V_2$	$V_1 = z_{11}I_1 + z_{12}I_2$
$I_2 = y_{21}V_1 + y_{22}V_2$	$V_2 = z_{21}I_1 + z_{22}I_2$

* Decimal Classification: R282.12.

B. Definition of Transducer Parameters

The above circuit equations, which completely describe the small-signal operation of the transducer, also serve as a guide to defining the parameters. Thus, for example, if $V_2 = 0$, i.e., the output is shorted, then $y_{11} = I_1/V_1$ defines y_{11} as the input admittance when the output is shorted. Continuing in this manner all of the parameters may be similarly defined.

Nodal	Loop
$y_{11} = g_{11} + jb_{11}$ = input admittance with output shorted	$z_{11} = r_{11} + jx_{11}$ = input impedance with output open
$y_{12} = g_{12} + jb_{12}$ = reverse transfer (feedback) admittance with input shorted	$z_{12} = r_{12} + jx_{12}$ = reverse transfer (feedback) impedance with input open
$y_{21} = g_{21} + jb_{21}$ = forward transfer admittance with output shorted	$z_{21} = r_{21} + jx_{21}$ = forward transfer impedance with output open
$y_{22} = g_{22} + jb_{22}$ = output admittance with input shorted	$z_{22} = r_{22} + jx_{22}$ = output impedance with input open

C. Transformation Equations

In general, the parameters within each pair of equations are independent of each other. The two sets of parameters, however, are related by the following transformation equations:

Nodal	Loop
$y_{11} = z_{22}/\Delta_z$	$z_{11} = y_{22}/\Delta_y$
$y_{12} = -z_{12}/\Delta_z$	$z_{12} = -y_{12}/\Delta_y$
$y_{21} = -z_{21}/\Delta_z$	$z_{21} = -y_{21}/\Delta_y$
$y_{22} = z_{11}/\Delta_z$	$z_{22} = y_{11}/\Delta_y$
$\Delta_z = \begin{vmatrix} z_{21} & z_{22} \\ z_{11} & z_{12} \end{vmatrix} = z_{11}z_{22} - z_{12}z_{21}$	$\Delta_y = \begin{vmatrix} y_{11} & y_{12} \\ y_{21} & y_{22} \end{vmatrix} = y_{11}y_{22} - y_{12}y_{21}$

D. Definition of Amplification Factors

In addition to the parameters already discussed, it is convenient to define various amplification factors which serve as indexes of performance. Since the network may, in general, be bilateral, each factor must be defined in the reverse as well as in the forward direction.

Current Amplification Factors—The current amplification factor is defined as the ratio of the negative current at one pair of shorted terminals to the current introduced at the other pair of terminals.

α_{21} = *forward* current amplification factor

= ratio of the *negative* current at the shorted *output* terminals to the current introduced at the *input* terminals.

α_{12} = *reverse* current amplification factor

= ratio of the *negative* current at the shorted *input* terminals to the current introduced at the *output* terminals.

Voltage Amplification Factors—The voltage amplification factor is defined as the ratio of the voltage at one pair of open terminals to the voltage applied to the other pair of terminals.

μ_{21} = *forward* voltage amplification factor

= ratio of the voltage at the open *output* terminals to the voltage introduced at the *input* terminals.

μ_{12} = *reverse* voltage amplification factor

= ratio of the voltage at the open *input* terminals to the voltage introduced at the *output* terminals.

Power Amplification Factors—The power amplification factor is defined as the maximum power amplification in a given direction when the transfer impedance or the transfer admittance in the opposite direction is zero. These factors are introduced here for the first time. It is believed that the forward power amplification factor in particular may be more useful than either the forward current or the forward voltage amplification factor as a single index of performance.

ϕ_{21} = *forward* power amplification factor

= maximum power amplification from the *input to the output* terminals when the *reverse* transfer (feedback) impedance or the *reverse* transfer (feedback) admittance is zero.

ϕ_{12} = *reverse* power amplification factor

= maximum power amplification from the *output to the input* terminals when the *forward* transfer impedance or the *forward* transfer admittance is zero.

E. Equation for Amplification Factors

The amplification factors can be readily determined in terms of the impedance or admittance parameters already defined.

Nodal	Loop
$\alpha_{21} = -y_{21}/y_{11}$	$\mu_{21} = z_{21}/z_{11}$
$\alpha_{12} = -y_{12}/y_{22}$	$\mu_{12} = z_{12}/z_{22}$
$\mu_{21} = -y_{21}/y_{22}$	$\alpha_{21} = z_{21}/z_{22}$
$\mu_{12} = -y_{12}/y_{11}$	$\alpha_{12} = z_{12}/z_{11}$
$\phi_{21} = \dfrac{\lvert y_{21}\rvert^2}{4g_{11}g_{22}}$	$\phi_{21} = \dfrac{\lvert z_{21}\rvert^2}{4r_{11}r_{22}}$
$\phi_{12} = \dfrac{\lvert y_{12}\rvert^2}{4g_{11}g_{22}}$	$\phi_{12} = \dfrac{\lvert z_{12}\rvert^2}{4r_{11}r_{22}}$

F. Input and Output Impedances

The input and output impedances of the transducer under circuit conditions are, of course, dependent on the actual load and source impedances respectively. These impedances are readily determined by conventional analysis and are given by

Nodal	Loop
$y_i = g_i + jb_i =$ input admittance	$z_i = r_i + jx_i =$ input impedance
$= y_{11} - \dfrac{y_{12}y_{21}}{y_{22} + Y_l}$	$= z_{11} - \dfrac{z_{12}z_{21}}{z_{22} + Z_l}$
$y_o = g_o + jb_o =$ output admittance	$z_o = r_o + jx_o =$ output impedance
$= y_{22} - \dfrac{y_{12}y_{21}}{y_{11} + Y_g}$	$= z_{22} - \dfrac{z_{12}z_{21}}{z_{11} + Z_g}$

G. Amplification under Arbitrary Conditions

The values of amplification for arbitrary values of generator and load impedances are given by the following equations. Note that voltage amplification as defined in Reference (7) is only the magnitude of voltage amplification defined below.

Nodal	Loop
Forward Current Amplification	Forward Voltage Amplification
$= \dfrac{y_{21}Y_l}{y_{11}(y_{22} + Y_l) - y_{12}y_{21}}$	$= \dfrac{z_{21}Z_l}{z_{11}(z_{22} + Z_l) - z_{12}z_{21}}$

Reverse Current Amplification

$$= \frac{y_{12}Y_g}{y_{22}(y_{11} + Y_g) - y_{12}y_{21}}$$

Reverse Voltage Amplification

$$= \frac{z_{12}Z_g}{z_{22}(z_{11} + Z_g) - z_{12}z_{21}}$$

Forward Voltage Amplification

$$= -\frac{y_{21}}{y_{22} + Y_l}$$

Forward Current Amplification

$$= -\frac{z_{21}}{z_{22} + Z_l}$$

Reverse Voltage Amplification

$$= -\frac{y_{12}}{y_{11} + Y_g}$$

Reverse Current Amplification

$$= -\frac{z_{12}}{z_{11} + Z_g}$$

Forward Power Amplification

$$= \left|\frac{y_{21}}{y_{22} + Y_l}\right|^2 \frac{G_l}{g_i}$$

Forward Power Amplification

$$= \left|\frac{z_{21}}{z_{22} + Z_l}\right|^2 \frac{R_l}{r_i}$$

Reverse Power Amplification

$$= \left|\frac{y_{12}}{y_{11} + Y_g}\right|^2 \frac{G_g}{g_o}$$

Reverse Power Amplification

$$= \left|\frac{z_{12}}{z_{11} + Z_g}\right|^2 \frac{R_g}{r_o}$$

H. Equation for Conjugate Impedance Match

The maximum power amplification is obtained when the generator and the load impedances are the conjugate of the input and output impedances respectively.

Nodal

Let

$$G_N = \frac{g_{12}g_{21} - b_{12}b_{21}}{g_{11}g_{22}}$$

$$B_N = \frac{b_{12}g_{21} - b_{21}g_{12}}{2g_{11}g_{22}}$$

Then

Input Admittance

$$= g_{11}\sqrt{1 - G_N - B_N^2} + j(b_{11} - g_{11}B_N)$$

Loop

Let

$$R_N = \frac{r_{12}r_{21} - x_{12}x_{21}}{r_{11}r_{22}}$$

$$X_N = \frac{x_{12}r_{21} - x_{21}r_{12}}{2r_{11}r_{22}}$$

Then

Input Impedance

$$= r_{11}\sqrt{1 - R_N - X_N^2} + j(x_{11} - r_{11}X_N)$$

Output Admittance	Output Impedance
$= g_{22}\sqrt{1-G_N-B_N^2} + j(b_{22}-g_{22}B_N)$	$= r_{22}\sqrt{1-R_N-X_N^2} + j(x_{22}-r_{22}X_N)$
Forward Power Amplification	Forward Power Amplification
$= \dfrac{\lvert y_{21}\rvert^2}{g_{11}g_{22}[2+2\sqrt{1-G_N-B_N^2}-G_N]}$	$= \dfrac{\lvert z_{21}\rvert^2}{r_{11}r_{22}[2+2\sqrt{1-R_N-X_N^2}-R_N]}$
Reverse Power Amplification	Reverse Power Amplification
$= \dfrac{\lvert y_{12}\rvert^2}{g_{11}g_{22}[2+2\sqrt{1-G_N-B_N^2}-G_N]}$	$= \dfrac{\lvert z_{12}\rvert^2}{r_{11}r_{22}[2+2\sqrt{1-R_N-X_N^2}-R_N]}$

I. Equations for Image Impedance Match

The transducer is image impedance matched when the generator and load impedances are equal to the input and output impedances respectively.

Nodal	**Loop**
Input Admittance $= y_{11}\sqrt{1-\alpha_{12}\alpha_{21}}$	Input Impedance $= z_{11}\sqrt{1-\alpha_{12}\alpha_{21}}$
Output Admittance $= y_{22}\sqrt{1-\alpha_{12}\alpha_{21}}$	Output Impedance $= z_{22}\sqrt{1-\alpha_{12}\alpha_{21}}$

$$\text{Forward current amplification} = -\frac{\alpha_{21}}{1+\sqrt{1-\alpha_{12}\alpha_{21}}}$$

$$\text{Reverse current amplification} = -\frac{\alpha_{12}}{1+\sqrt{1-\alpha_{12}\alpha_{21}}}$$

$$\text{Forward voltage amplification} = \frac{\mu_{21}}{1+\sqrt{1-\alpha_{12}\alpha_{21}}}$$

$$\text{Reverse voltage amplification} = \frac{\mu_{12}}{1+\sqrt{1-\alpha_{12}\alpha_{21}}}$$

If all transducer parameters are real,

$$\text{Forward power amplification} = \frac{\alpha_{21}\mu_{21}}{(1+\sqrt{1-\alpha_{12}\alpha_{21}})^2}$$

$$\text{Reverse power amplification} = \frac{\alpha_{12}\mu_{12}}{(1+\sqrt{1-\alpha_{12}\alpha_{21}})^2}$$

J. Equations for Iterative Impedance Match

The transducer is iterative impedance matched if it is an element of an infinite number (or the equivalent thereof) of cascaded identical transducers.

Nodal

Let

$$y_m = \frac{y_{11}+y_{22}}{2}$$

Then

Input Admittance

$$= -y_{22} + y_m\left[1 \pm \sqrt{1-\frac{y_{12}y_{21}}{y_m}}\right]$$

Output Admittance

$$= -y_{11} + y_m\left[1 \pm \sqrt{1-\frac{y_{12}y_{21}}{y_m}}\right]$$

Loop

Let

$$z_m = \frac{z_{11}+z_{22}}{2}$$

Then

Input Impedance

$$= -z_{22} + z_m\left[1 \pm \sqrt{1-\frac{z_{12}z_{21}}{z_m}}\right]$$

Output Impedance

$$= -z_{11} + z_m\left[1 \pm \sqrt{1-\frac{z_{12}z_{21}}{z_m}}\right]$$

The equations in Section I-*G* may be used to obtain the various circuit amplifications.

K. Equivalent Circuits

While formal manipulation of the admittance and impedance parameters of a network will result in the correct algebraic expression for whatever quantity is desired, it is, nevertheless, convenient to be able to express the basic relationships of Section I-*A* in terms of an equivalent circuit.

Two-Generator Equivalent Circuits—When two generators are used, as shown in Figure 2, the circuit follows directly from the equations of Section I-*A*.

Single-Generator Equivalent Circuits—It is often desirable to express the network in terms of a single-generator equivalent circuit.

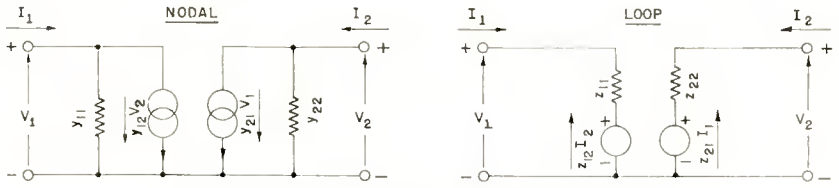

Fig. 2—Two-generator equivalent circuits.

This may be done in several ways. For example, z_{21} may be separated into two parts:

$$z_{21} = z_{12} + (z_{21} - z_{12}).$$

The basic equations then become

$$\begin{aligned} V_1 &= z_{11} I_1 + z_{12} I_2 \\ V_2 &= z_{12} I_1 + z_{22} I_2 \end{aligned} \quad \Big| \quad + (z_{21} - z_{12}) I_1 .$$

The expressions to the left of the vertical line represent a passive network with a common mutual impedance. This network is representable by a T network. The remainder of the expression represents a voltage source. Hence the corresponding loop network (Figure 3) can readily be drawn. For an indication of the numerous other equivalent circuits that can be derived, see Reference (3).

Measurement of the actual parameters of a given network may be made by the methods outlined in References (4), (6), (8), and (9).

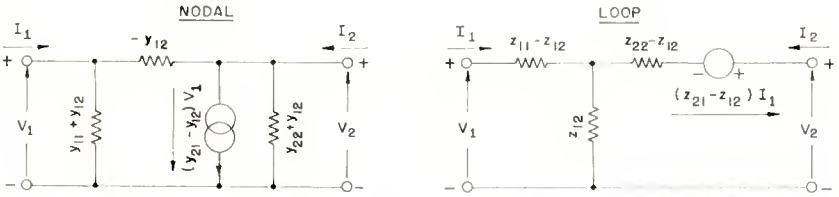

Fig. 3—Single-generator equivalent circuits.

Section II — Equivalent Circuits of Transistors

A compilation of the more useful transistor equivalent circuits is given in the four charts on pages 36-39. Included with the circuits are the amplification factors and the transformation equations which enable one to go readily from a nodal- (or loop-) derived equivalent circuit to any other nodal- (or loop-) derived equivalent circuit. However, in order to go from a nodal to the corresponding loop-derived

NODAL-DERIVED EQUIVALENT CIRCUITS

	COMMON EMITTER	COMMON BASE	COMMON COLLECTOR
EQUATIONS	$I_b = y_{bbe} V_{be} + y_{bce} V_{ce}$ $I_c = y_{cbe} V_{be} + y_{cce} V_{ce}$	$I_e = y_{eeb} V_{eb} + y_{ecb} V_{cb}$ $I_c = y_{ceb} V_{eb} + y_{ccb} V_{cb}$	$I_b = y_{bbc} V_{bc} + y_{bec} V_{ec}$ $I_e = y_{ebc} V_{bc} + y_{eec} V_{ec}$
TWO – GEN.	(1N) 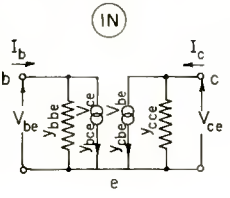	(2N) 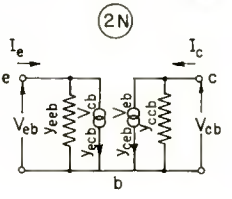	(3N) 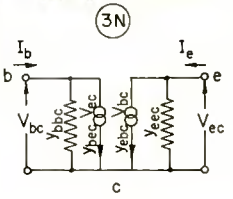
AMP. FACTORS	FORWARD / REVERSE	FORWARD / REVERSE	FORWARD / REVERSE
	$\alpha_{cb} = -\frac{y_{cbe}}{y_{bbe}}$ $\mu_{cb} = -\frac{y_{cbe}}{y_{cce}}$ $\phi_{cb} = \frac{\lvert y_{cbe}\rvert^2}{4 g_{bbe} g_{cce}}$	$\alpha_{bc} = -\frac{y_{bce}}{y_{cce}}$ $\mu_{bc} = -\frac{y_{bce}}{y_{bbe}}$ $\phi_{bc} = \frac{\lvert y_{bce}\rvert^2}{4 g_{bbe} g_{cce}}$	$\alpha_{ce} = -\frac{y_{ceb}}{y_{eeb}}$ $\mu_{ce} = -\frac{y_{ceb}}{y_{ccb}}$ $\phi_{ce} = \frac{\lvert y_{ceb}\rvert^2}{4 g_{eeb} g_{ccb}}$	$\alpha_{ec} = -\frac{y_{ecb}}{y_{ccb}}$ $\mu_{ec} = -\frac{y_{ecb}}{y_{eeb}}$ $\phi_{ec} = \frac{\lvert y_{ecb}\rvert^2}{4 g_{eeb} g_{ccb}}$	$\alpha_{eb} = -\frac{y_{ebc}}{y_{bbc}}$ $\mu_{eb} = -\frac{y_{ebc}}{y_{eec}}$ $\phi_{eb} = \frac{\lvert y_{ebc}\rvert^2}{4 g_{bbc} g_{eec}}$	$\alpha_{be} = -\frac{y_{bec}}{y_{eec}}$ $\mu_{be} = -\frac{y_{bec}}{y_{bbc}}$ $\phi_{be} = \frac{\lvert y_{bec}\rvert^2}{4 g_{bbc} g_{eec}}$
TRANSFORMATION EQUATIONS	(4N) → (1N) $y_{bbe} = {}_e y_{be} + {}_e y_{bc}$ $y_{bce} = -{}_e y_{bc}$ $y_{cbe} = {}_e y_m - {}_e y_{bc}$ $y_{cce} = {}_e y_{ce} + {}_e y_{bc}$	(5N) → (2N) $y_{eeb} = {}_b y_{eb} + {}_b y_{ec}$ $y_{ecb} = -{}_b y_{ec}$ $y_{ceb} = {}_b y_m - {}_b y_{ec}$ $y_{ccb} = {}_b y_{cb} + {}_b y_{ec}$	(6N) → (3N) $y_{bbc} = {}_c y_{bc} + {}_c y_{be}$ $y_{bec} = -{}_c y_{be}$ $y_{ebc} = {}_c y_m - {}_c y_{be}$ $y_{eec} = {}_c y_{ec} + {}_c y_{be}$	
	(2N) → (1N) $V_{be} = -V_{eb}$; $V_{ce} = V_{cb} - V_{eb}$ $y_{bbe} = y_{eeb} + y_{ecb} + y_{ceb} + y_{ccb}$ $y_{bce} = -(y_{ccb} + y_{ecb})$ $y_{cbe} = -(y_{ccb} + y_{ceb})$ $y_{cce} = y_{ccb}$	(3N) → (2N) $V_{eb} = V_{ec} - V_{bc}$; $V_{cb} = -V_{bc}$ $y_{eeb} = y_{eec}$ $y_{ecb} = -(y_{eec} + y_{ebc})$ $y_{ceb} = -(y_{eec} + y_{bec})$ $y_{ccb} = y_{bbc} + y_{bec} + y_{ebc} + y_{eec}$	(1N) → (3N) $V_{bc} = V_{be} - V_{ce}$; $V_{ec} = -V_{ce}$ $y_{bbc} = y_{bbe}$ $y_{bec} = -(y_{bbe} + y_{bce})$ $y_{ebc} = -(y_{bbe} + y_{cbe})$ $y_{eec} = y_{bbe} + y_{cbe} + y_{bce} + y_{cce}$	
	(3N) → (1N) $V_{be} = V_{bc} - V_{ec}$; $V_{ce} = -V_{ec}$ $y_{bbe} = y_{bbc}$ $y_{bce} = -(y_{bbc} + y_{bec})$ $y_{cbe} = -(y_{bbc} + y_{ebc})$ $y_{cce} = y_{bbc} + y_{bec} + y_{ebc} + y_{eec}$	(1N) → (2N) $V_{eb} = -V_{be}$; $V_{cb} = V_{ce} - V_{be}$ $y_{eeb} = y_{bbe} + y_{cbe} + y_{bce} + y_{cce}$ $y_{ecb} = -(y_{cce} + y_{bce})$ $y_{ceb} = -(y_{cce} + y_{cbe})$ $y_{ccb} = y_{cce}$	(2N) → (3N) $V_{bc} = -V_{cb}$; $V_{ec} = V_{eb} - V_{cb}$ $y_{bbc} = y_{eeb} + y_{ecb} + y_{ceb} + y_{ccb}$ $y_{bec} = -(y_{eeb} + y_{ceb})$ $y_{ebc} = -(y_{eeb} + y_{ecb})$ $y_{eec} = y_{eeb}$	

Chart 1—Transistor Circuits and Equations

NODAL-DERIVED EQUIVALENT CIRCUITS

	COMMON EMITTER	COMMON BASE	COMMON COLLECTOR
EQUATIONS	$I_b=(e y_{be}+e y_{bc})V_{be}-e y_{bc}\,V_{ce}$ $I_c=(e y_m-e y_{bc})V_{be}+(e y_{ce}+e y_{bc})V_{ce}$	$I_e=(b y_{eb}+b y_{ec})V_{eb}-b y_{ec}V_{cb}$ $I_c=(b y_m-b y_{ec})V_{eb}+(b y_{cb}+b y_{ec})V_{cb}$	$I_b=(c y_{bc}+c y_{be})V_{bc}-c y_{be}V_{ec}$ $I_e=(c y_m-c y_{be})V_{bc}+(c y_{ec}+c y_{be})V_{ec}$
ONE – GEN.	(4N) 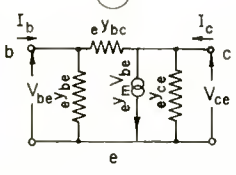 	(5N) 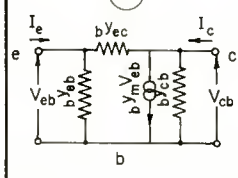 	(6N) 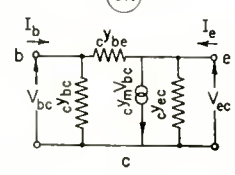
AMP. FACTORS	FORWARD / REVERSE	FORWARD / REVERSE	FORWARD / REVERSE
	$\alpha_{cb}=-\frac{e y_m-e y_{bc}}{e y_{be}+e y_{bc}}$ $\alpha_{bc}=+\frac{e y_{bc}}{e y_{be}+e y_{bc}}$ $\mu_{cb}=-\frac{e y_m-e y_{bc}}{e y_{ce}+e y_{bc}}$ $\mu_{bc}=+\frac{e y_{bc}}{e y_{be}+e y_{bc}}$ $\phi_{cb}=\frac{\lvert e y_m-e y_{bc}\rvert^2}{4(e g_{be}+e g_{bc})(e g_{ce}+e g_{bc})}$ $\phi_{bc}=\frac{\lvert e y_{bc}\rvert^2}{4(e g_{be}+e g_{bc})(e g_{ce}+e g_{bc})}$	$\alpha_{ce}=-\frac{b y_m-b y_{ec}}{b y_{eb}+b y_{ec}}$ $\alpha_{ec}=+\frac{b y_{ec}}{b y_{cb}+b y_{ec}}$ $\mu_{ce}=-\frac{b y_m-b y_{ec}}{b y_{cb}+b y_{ec}}$ $\mu_{ec}=+\frac{b y_{ec}}{b y_{eb}+b y_{ec}}$ $\phi_{ce}=\frac{\lvert b y_m-b y_{ec}\rvert^2}{4(b g_{eb}+b g_{ec})(b g_{cb}+b g_{ec})}$ $\phi_{ec}=\frac{\lvert b y_{ec}\rvert^2}{4(b g_{eb}+b g_{ac})(b g_{cb}+b g_{ec})}$	$\alpha_{eb}=-\frac{c y_m-c y_{be}}{c y_{bc}+c y_{be}}$ $\alpha_{be}=+\frac{c y_{be}}{c y_{ec}+c y_{be}}$ $\mu_{eb}=-\frac{c y_m-c y_{be}}{c y_{ec}+c y_{be}}$ $\mu_{be}=+\frac{c y_{be}}{c y_{ec}+c y_{be}}$ $\phi_{eb}=\frac{\lvert c y_m-c y_{be}\rvert^2}{4(c g_{bc}+c g_{be})(c g_{ec}+c g_{be})}$ $\phi_{be}=\frac{\lvert c y_{be}\rvert^2}{4(c g_{bc}+c g_{be})(c g_{ec}+c g_{be})}$
TRANSFORMATION EQUATIONS	(1N) → (4N) $e y_{be}=y_{bbe}+y_{bce}$ $e y_{bc}=-y_{bce}$ $e y_{ce}=y_{cce}+y_{bce}$ $e y_m=y_{cbe}-y_{bce}$	(2N) → (5N) $b y_{eb}=y_{eeb}+y_{ecb}$ $b y_{ec}=-y_{ecb}$ $b y_{cb}=y_{ccb}+y_{ecb}$ $b y_m=y_{ceb}-y_{ecb}$	(3N) → (6N) $c y_{bc}=y_{bbc}+y_{bec}$ $c y_{be}=-y_{bec}$ $c y_{ec}=y_{eec}+y_{bec}$ $c y_m=y_{ebc}-y_{bec}$
	(5N) → (4N) $V_{be}=-V_{eb}$; $V_{ce}=V_{cb}-V_{eb}$ $e y_{be}=b y_{eb}+b y_m$ $e y_{bc}=b y_{cb}$ $e y_{ce}=b y_{ec}$ $e y_m=-b y_m$	(6N) → (5N) $V_{eb}=V_{ec}-V_{bc}$; $V_{cb}=-V_{bc}$ $b y_{eb}=c y_{be}-c y_m$ $b y_{ec}=c y_{ec}+c y_m$ $b y_{cb}=c y_{bc}$ $b y_m=c y_m$	(4N) → (6N) $V_{bc}=V_{be}-V_{ce}$; $V_{ec}=-V_{ce}$ $c y_{bc}=e y_{bc}$ $c y_{be}=e y_{be}$ $c y_{ec}=e y_{ce}+e y_m$ $c y_m=-e y_m$
	(6N) → (4N) $V_{be}=V_{bc}-V_{ec}$; $V_{ce}=-V_{ec}$ $e y_{be}=c y_{be}$ $e y_{bc}=c y_{bc}$ $e y_{ce}=c y_{ec}+c y_m$ $e y_m=-c y_m$	(4N) → (5N) $V_{eb}=-V_{be}$; $V_{cb}=V_{ce}-V_{be}$ $b y_{eb}=e y_{be}+e y_m$ $b y_{ec}=e y_{ce}$ $b y_{cb}=e y_{bc}$ $b y_m=-e y_m$	(5N) → (6N) $V_{bc}=-V_{cb}$; $V_{ec}=V_{eb}-V_{cb}$ $c y_{bc}=b y_{cb}$ $c y_{be}=b y_{eb}+b y_m$ $c y_{ec}=b y_{ec}-b y_m$ $c y_m=b y_m$

Chart 2—Transistor Circuits and Equations

LOOP-DERIVED EQUIVALENT CIRCUITS

	COMMON EMITTER	COMMON BASE	COMMON COLLECTOR
EQUATIONS	$V_{be}=z_{bbe}\,I_b+z_{bce}\,I_c$ $V_{ce}=z_{cbe}\,I_b+z_{cce}\,I_c$	$V_{eb}=z_{eeb}\,I_e+z_{ecb}\,I_c$ $V_{cb}=z_{ceb}\,I_e+z_{ccb}\,I_c$	$V_{bc}=z_{bbc}\,I_b+z_{bec}\,I_e$ $V_{ec}=z_{ebc}\,I_b+z_{eec}\,I_e$
TWO-GEN.	(1L) 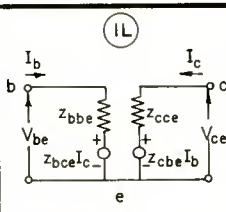	(2L) 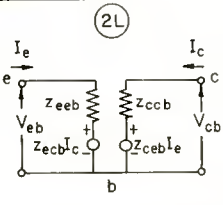	(3L) 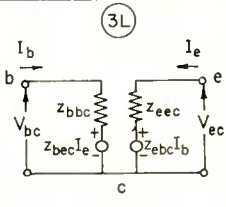
AMP. FACTORS	FORWARD / REVERSE	FORWARD / REVERSE	FORWARD / REVERSE
	$\alpha_{cb}=+\frac{z_{cbe}}{z_{cce}}$ $\mu_{cb}=+\frac{z_{cbe}}{z_{bbe}}$ $\phi_{cb}=\frac{\lvert z_{cbe}\rvert^2}{4r_{bbe}\,r_{cce}}$	$\alpha_{bc}=+\frac{z_{bce}}{z_{bbe}}$ $\mu_{bc}=+\frac{z_{bce}}{z_{cce}}$ $\phi_{bc}=\frac{\lvert z_{bce}\rvert^2}{4r_{bbe}\,r_{cce}}$	$\alpha_{ce}=+\frac{z_{ceb}}{z_{ccb}}$ $\mu_{ce}=+\frac{z_{ceb}}{z_{eeb}}$ $\phi_{ce}=\frac{\lvert z_{ceb}\rvert^2}{4r_{eeb}\,r_{ccb}}$	$\alpha_{ec}=+\frac{z_{ecb}}{z_{eeb}}$ $\mu_{ec}=+\frac{z_{ecb}}{z_{ccb}}$ $\phi_{ec}=\frac{\lvert z_{ecb}\rvert^2}{4r_{eeb}\,r_{ccb}}$	$\alpha_{eb}=+\frac{z_{ebc}}{z_{eec}}$ $\mu_{eb}=+\frac{z_{ebc}}{z_{bbc}}$ $\phi_{eb}=\frac{\lvert z_{ebc}\rvert^2}{4r_{bbc}\,r_{eec}}$	$\alpha_{be}=+\frac{z_{bec}}{z_{bbc}}$ $\mu_{be}=+\frac{z_{bec}}{z_{eec}}$ $\phi_{be}=\frac{\lvert z_{bec}\rvert^2}{4r_{bbc}\,r_{eec}}$
TRANSFORMATION EQUATIONS	(4L)→(1L) $z_{bbe}={}_e z_b+{}_e z_e$ $z_{bce}={}_e z_e$ $z_{cbe}={}_e z_m+{}_e z_e$ $z_{cce}={}_e z_c+{}_e z_e$	(5L)→(2L) $z_{eeb}={}_b z_e+{}_b z_b$ $z_{ecb}={}_b z_b$ $z_{ceb}={}_b z_m+{}_b z_b$ $z_{ccb}={}_b z_c+{}_b z_b$	(6L)→(3L) $z_{bbc}={}_c z_b+{}_c z_c$ $z_{bec}={}_c z_c$ $z_{ebc}={}_c z_m+{}_c z_c$ $z_{eec}={}_c z_e+{}_c z_c$
	(2L)→(1L) $V_{be}=-V_{eb}\;;\;V_{ce}=V_{cb}-V_{eb}$ $z_{bbe}=z_{eeb}$ $z_{bce}=z_{eeb}-z_{ecb}$ $z_{cbe}=z_{eeb}-z_{ceb}$ $z_{cce}=z_{eeb}-z_{ecb}-z_{ceb}+z_{ccb}$	(3L)→(2L) $V_{eb}=V_{ec}-V_{bc};\;V_{cb}=-V_{bc}$ $z_{eeb}=z_{bbc}-z_{bec}-z_{ebc}-z_{eec}$ $z_{ecb}=z_{bbc}-z_{ebc}$ $z_{ceb}=z_{bbc}-z_{bec}$ $z_{ccb}=z_{bbc}$	(1L)→(3L) $V_{bc}=V_{be}-V_{ce}\;;\;V_{ec}=-V_{ce}$ $z_{bbc}=z_{bbe}-z_{bce}-z_{cbe}+z_{cce}$ $z_{bec}=z_{cce}-z_{bce}$ $z_{ebc}=z_{cce}-z_{cbe}$ $z_{eec}=z_{cce}$
	(3L)→(1L) $V_{be}=V_{bc}-V_{ec}\;;\;V_{ce}=-V_{ec}$ $z_{bbe}=z_{bbc}-z_{ebc}-z_{bec}+z_{eec}$ $z_{bce}=z_{eec}-z_{bec}$ $z_{cbe}=z_{eec}-z_{ebc}$ $z_{cce}=z_{eec}$	(1L)→(2L) $V_{eb}=-V_{be}\;;\;V_{cb}=V_{ce}-V_{be}$ $z_{eeb}=z_{bbe}$ $z_{ecb}=z_{bbe}-z_{bce}$ $z_{ceb}=z_{bbe}-z_{cbe}$ $z_{ccb}=z_{bbe}-z_{bce}-z_{cbe}+z_{cce}$	(2L)→(3L) $V_{bc}=-V_{cb}\;;\;V_{ec}=V_{eb}-V_{cb}$ $z_{bbc}=z_{ccb}$ $z_{bec}=z_{ccb}-z_{ceb}$ $z_{ebc}=z_{ccb}-z_{ecb}$ $z_{eec}=z_{eeb}-z_{ecb}-z_{ceb}+z_{ccb}$

Chart 3—Transistor Circuits and Equations

LOOP-DERIVED EQUIVALENT CIRCUITS

EQUATIONS

COMMON EMITTER	COMMON BASE	COMMON COLLECTOR
$V_{be}=({}_eZ_b+{}_eZ_e)I_b+{}_eZ_e\,I_c$	$V_{eb}=({}_bZ_e+{}_bZ_b)I_e+{}_bZ_b\,I_c$	$V_{bc}=({}_cZ_b+{}_cZ_c)I_b+{}_cZ_c\,I_e$
$V_{ce}=({}_eZ_m+{}_eZ_e)I_b+({}_eZ_c+{}_eZ_e)I_c$	$V_{cb}=({}_bZ_m+{}_bZ_b)I_e+({}_bZ_c+{}_bZ_b)I_c$	$V_{ec}=({}_cZ_m+{}_cZ_c)I_b+({}_cZ_e+{}_cZ_c)I_e$

ONE - GEN.

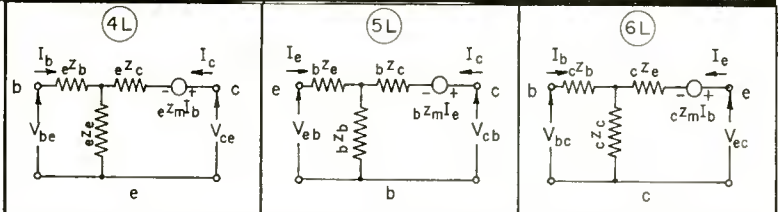

AMP. FACTORS

COMMON EMITTER		COMMON BASE		COMMON COLLECTOR	
FORWARD	REVERSE	FORWARD	REVERSE	FORWARD	REVERSE
$\alpha_{cb}=\frac{{}_eZ_m+{}_eZ_e}{{}_eZ_c+{}_eZ_e}$	$\alpha_{bc}=\frac{{}_eZ_e}{{}_eZ_b+{}_eZ_e}$	$\alpha_{cb}=\frac{{}_bZ_m+{}_bZ_b}{{}_bZ_c+{}_bZ_b}$	$\alpha_{eb}=\frac{{}_bZ_b}{{}_bZ_e+{}_bZ_b}$	$\alpha_{eb}=\frac{{}_cZ_m+{}_cZ_c}{{}_cZ_e+{}_cZ_c}$	$\alpha_{be}=\frac{{}_cZ_c}{{}_cZ_b+{}_cZ_c}$
$\mu_{cb}=\frac{{}_eZ_m+{}_eZ_e}{{}_eZ_b+{}_eZ_e}$	$\mu_{bc}=\frac{{}_eZ_e}{{}_eZ_c+{}_eZ_e}$	$\mu_{cb}=\frac{{}_bZ_m+{}_bZ_b}{{}_bZ_e+{}_bZ_b}$	$\mu_{eb}=\frac{{}_bZ_b}{{}_bZ_c+{}_bZ_b}$	$\mu_{eb}=\frac{{}_cZ_m+{}_cZ_c}{{}_cZ_b+{}_cZ_c}$	$\mu_{be}=\frac{{}_cZ_c}{{}_cZ_e+{}_cZ_c}$
$\phi_{cb}=\frac{\lvert{}_eZ_m+{}_eZ_e\rvert^2}{4({}_eR_b+{}_eR_e)({}_cR_c+{}_eR_e)}$		$\phi_{ce}=\frac{\lvert{}_bZ_m+{}_bZ_b\rvert^2}{4({}_bR_e+{}_bR_b)({}_bR_c+{}_bR_b)}$		$\phi_{eb}=\frac{\lvert{}_cZ_m+{}_cZ_c\rvert^2}{4({}_cR_b+{}_cR_c)({}_cR_e+{}_cR_c)}$	
$\phi_{bc}=\frac{\lvert{}_eZ_e\rvert^2}{4({}_eR_b+{}_eR_e)({}_cR_c+{}_eR_e)}$		$\phi_{eb}=\frac{\lvert{}_bZ_b\rvert^2}{4({}_bR_e+{}_bR_b)({}_bR_c+{}_bR_b)}$		$\phi_{be}=\frac{\lvert{}_cZ_c\rvert^2}{4({}_cR_b+{}_cR_c)({}_cR_e+{}_cR_c)}$	

TRANSFORMATION EQUATIONS

COMMON EMITTER	COMMON BASE	COMMON COLLECTOR
(1L) → (4L)	(2L) → (5L)	(3L) → (6L)
${}_eZ_b={}_bZ_{be}-{}_bZ_{ce}$	${}_bZ_e={}_eZ_{eb}-{}_eZ_{cb}$	${}_cZ_b={}_bZ_{bc}-{}_bZ_{ec}$
${}_eZ_e={}_bZ_{ce}$	${}_bZ_b={}_eZ_{cb}$	${}_cZ_c={}_bZ_{ec}$
${}_eZ_c={}_cZ_{ce}-{}_bZ_{ce}$	${}_bZ_c={}_cZ_{cb}-{}_eZ_{cb}$	${}_cZ_e={}_eZ_{ec}-{}_bZ_{ec}$
${}_eZ_m={}_cZ_{be}-{}_bZ_{ce}$	${}_bZ_m={}_cZ_{eb}-{}_eZ_{cb}$	${}_cZ_m={}_eZ_{bc}-{}_bZ_{ec}$
(5L) → (4L)	(6L) → (5L)	(4L) → (6L)
$V_{be}=-V_{eb}\;;\;V_{ce}=V_{cb}-V_{eb}$	$V_{eb}=V_{ec}-V_{bc}\;;\;V_{cb}=-V_{bc}$	$V_{bc}=V_{be}-V_{ce}\;;\;V_{ec}=-V_{ce}$
${}_eZ_b={}_bZ_b$	${}_bZ_e={}_cZ_e$	${}_cZ_b={}_eZ_b-{}_eZ_m$
${}_eZ_e={}_bZ_e$	${}_bZ_b={}_cZ_b-{}_cZ_m$	${}_cZ_c={}_eZ_c$
${}_eZ_c={}_bZ_c-{}_bZ_m$	${}_bZ_c={}_cZ_c+{}_cZ_m$	${}_cZ_e={}_eZ_e$
${}_eZ_m=-{}_bZ_m$	${}_bZ_m={}_cZ_m$	${}_cZ_m=-{}_eZ_m$
(6L) → (4L)	(4L) → (5L)	(5L) → (6L)
$V_{be}=V_{bc}-V_{ec}\;;\;V_{ce}=-V_{ec}$	$V_{eb}=-V_{be}\;;\;V_{cb}=V_{ce}-V_{be}$	$V_{bc}=-V_{cb}\;;\;V_{ec}=V_{eb}-V_{cb}$
${}_eZ_b={}_cZ_b-{}_cZ_m$	${}_bZ_e={}_eZ_e$	${}_cZ_b={}_bZ_b+{}_bZ_m$
${}_eZ_e={}_cZ_e$	${}_bZ_b={}_eZ_b$	${}_cZ_c={}_bZ_c-{}_bZ_m$
${}_eZ_c={}_cZ_c$	${}_bZ_c={}_eZ_c-{}_eZ_m$	${}_cZ_e={}_bZ_e$
${}_eZ_m=-{}_cZ_m$	${}_bZ_m=-{}_eZ_m$	${}_cZ_m={}_bZ_m$

Chart 4—Transistor Circuits and Equations

equivalent circuit, or vice versa, the transformation equations of Section I-*C* are required.

The notation used in this tabulation was chosen in order to avoid ambiguity among the various circuit parameters. When applied to the two-generator equivalent circuits, this notation basically consists of the conventional two-letter subscript. To this conventional notation a third subscript has been added which designates the common terminal between the input and output circuit. Thus z_{bbc} is the base self impedance of the transistor in a common-emitter circuit, and y_{ceb} is the transfer admittance to the collector from the emitter in a common-base circuit. If only one circuit connection is being considered, or if no ambiguity arises, the last subscript designating the common electrode may be omitted.

When applied to the single-generator equivalent circuit, a presubscript designates the common electrode between the input and output circuits. For the π-equivalent or nodal-derived network, admittances are used with the two postsubscripts designating the terminals between which the admittance is located. Thus ${}_{c}y_{be}$ is the admittance between the base and the emitter in a common-collector circuit. For the T-equivalent or loop-derived network there is one node in common with all the elements of the T. Thus only one postsubscript is necessary to designate the terminal to which the impedance is connected. Accordingly ${}_{b}z_{c}$ is the impedance in a common-base circuit between the collector and the center of the T. In both the π and T networks, the generator parameter is designated by the subscript m. If only one circuit connection is being considered, or if no ambiguity arises, the presubscript designating the common electrode may be omitted.

When it is desirable to use admittances in place of impedances, or vice versa, ambiguity may be avoided by using reciprocal notation. Thus, $1/y_{eeb}$ is the emitter self impedance in the two-generator, common-base, nodal-derived, equivalent circuit, and $1/{}_{e}z_{m}$ is the generator admittance in the single-generator, common-emitter, loop-derived, equivalent circuit.

Section III — Illustrative Calculations

Consider a junction transistor in a common-base circuit for which the following low-frequency, open-circuited, impedance measurements have been made:

$$z_{11} = z_{eeb} = 199 \text{ ohms},$$

$$z_{12} = z_{ecb} = 182 \text{ ohms},$$

$$z_{21} = z_{ccb} = 0.503 \text{ megohm},$$

$$z_{22} = z_{ccb} = 0.5145 \text{ megohm}.$$

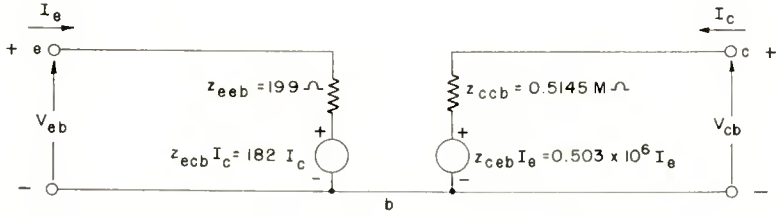

Fig. 4—Two-generator, loop-derived, common-base equivalent circuit.

The two-generator equivalent circuit (2L) of Section II is shown in Figure 4. Using the values shown in Figure 4, the amplification factors can be computed from Section I-*E*.

$$\mu_{21} = \mu_{ce} = z_{ceb}/z_{ccb} = 2{,}530,$$

$$\mu_{12} = \mu_{ec} = z_{ecb}/z_{ccb} = 354 \times 10^{-6},$$

$$\alpha_{21} = \alpha_{ce} = z_{ceb}/z_{ccb} = 0.977,$$

$$\alpha_{12} = \alpha_{ec} = z_{ecb}/z_{eeb} = 0.915,$$

$$\varphi_{21} = \varphi_{ce} = \frac{|z_{ceb}|^2}{4\, r_{eeb}\, r_{ccb}} = 620,$$

$$\varphi_{12} = \varphi_{ec} = \frac{|z_{ecb}|^2}{4\, r_{eeb}\, r_{ccb}} = 81 \times 10^{-6}.$$

Since all elements are real, the image match equations of Section I-*I* can be used. Thus the input and output match impedances are

$$\text{Input Impedance} = z_{eeb}\sqrt{1 - \alpha_{ec}\,\alpha_{ce}} = 64.8 \text{ ohms},$$

$$\text{Output Impedance} = z_{ccb}\sqrt{1 - \alpha_{ec}\,\alpha_{ce}} = 167{,}000 \text{ ohms},$$

and the amplification values for the image-matched condition are

$$\text{Forward current amplification} = -\frac{\alpha_{ce}}{1+\sqrt{1-\alpha_{ec}\,\alpha_{ce}}} = -0.737,$$

$$\text{Reverse current amplification} = -\frac{\alpha_{ec}}{1+\sqrt{1-\alpha_{ec}\,\alpha_{ce}}} = -0.690,$$

$$\text{Forward voltage amplification} = \frac{\mu_{ce}}{1+\sqrt{1-\alpha_{ec}\,\alpha_{ce}}} = 1{,}910,$$

$$\text{Reverse voltage amplification} = \frac{\mu_{ec}}{1+\sqrt{1-\alpha_{ec}\,\alpha_{ce}}} = 267\times 10^{-6},$$

$$\text{Forward power amplification} = \frac{\alpha_{ce}\,\mu_{ce}}{(1+\sqrt{1-\alpha_{ec}\,\alpha_{ce}})^2} = 1{,}408$$

$$= 31.5 \text{ decibels},$$

$$\text{Reverse power amplification} = \frac{\alpha_{ec}\,\mu_{ec}}{(1+\sqrt{1-\alpha_{ec}\,\alpha_{ce}})^2} = 184\times 10^{-6}.$$

The one-generator equivalent circuit can be obtained by using the (2L) → (5L) transformation equations of Section II. Thus,

$${}_bz_e = z_{ceb} - z_{ecb} = 17 \text{ ohms},$$

$${}_bz_b = z_{ecb} = 182 \text{ ohms},$$

$${}_bz_c = z_{ccb} - z_{ecb} = 0.5145 \text{ megohm},$$

$${}_bz_m = z_{ceb} - z_{ecb} = 0.503 \text{ megohm}.$$

so that the equivalent circuit (5L) of Section II is that shown in Figure 5.

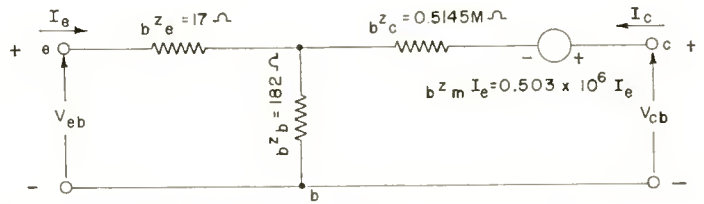

Fig. 5—Single-generator, loop-derived, common-emitter equivalent circuits.

If the common-emitter, one-generator, equivalent circuit is desired, the (5L) → (4L) transformation equations of Section II are used. Thus,

$$V_{be} = -V_{eb},$$

$$V_{ce} = V_{cb} - V_{eb},$$

$${}_cz_b = {}_hz_b = 182 \text{ ohms},$$

$${}_cz_e = {}_bz_c = 17 \text{ ohms},$$

$${}_cz_c = {}_bz_c - {}_bz_m = 11.5 \text{ K ohms},$$

$${}_ez_m = -{}_bz_m = -0.503 \text{ megohm},$$

so that the equivalent circuit (4L) of Section II is that shown in Figure 6.

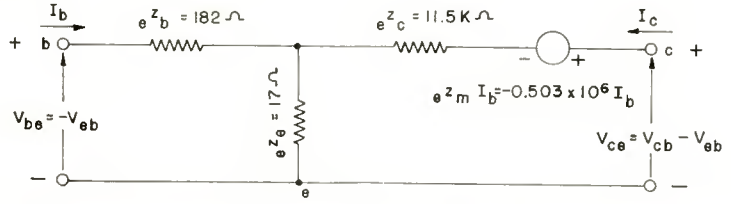

Fig. 6—Two-generator, loop-derived, common-emitter equivalent circuit.

If the common-collector, one-generator equivalent circuit is desired, the (5L) → (6L) transformation equations of Section II are used. Thus,

$$V_{bc} = -V_{cb},$$

$$V_{cc} = V_{cb} - V_{cb},$$

$${}_cz_b = {}_bz_b + {}_bz_m = 0.503 \text{ megohm},$$

$${}_cz_c = {}_bz_c - {}_bz_m = 11.5 \text{ K ohms},$$

$${}_cz_e = {}_bz_e = 17 \text{ ohms},$$

$${}_cz_m = {}_bz_m = 0.503 \text{ megohm},$$

so that the equivalent circuit (6L) of Section II is that shown in Figure 7.

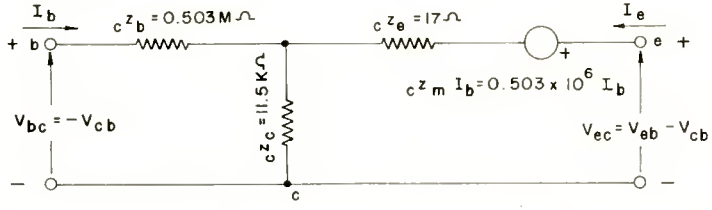

Fig. 7—Single-generator, loop-derived, common-collector equivalent circuit.

The amplification factors and the circuit amplifications for the common-emitter and the common-collector circuits will of course be different from those values computed above for the common-base circuit. The appropriate equations can be used to compute the new values.

If a nodal-derived equivalent circuit is desired, the transformation equations of Section I-*C* must be used. Thus, suppose that the common-emitter, one-generator, equivalent circuit (4N) of Section II is desired. There are several different successive transformations that can be employed to arrive at circuit (4N). The following successive transformation will be employed: (2L) → (1L) → (1N) → (4N). Thus, (2L) → (1L)

$$V_{be} = -V_{cb},$$

$$V_{ce} = V_{cb} - V_{cb},$$

$$z_{bbe} = z_{ceb} = 199 \text{ ohms},$$

$$z_{bce} = z_{ceb} - z_{ccb} = 17 \text{ ohms},$$

$$z_{cbe} = z_{ceb} - z_{ccb} = -0.503 \times 10^6 \text{ ohms},$$

$$z_{cce} = z_{ceb} - z_{ecb} - z_{ceb} + z_{ccb} = 11.5 \times 10^3 \text{ ohms},$$

and (1L) → (1N)

$$\Delta_z = z_{bbe}z_{cce} - z_{bce}z_{cbe} = 10.84 \times 10^6 \text{ ohm}^2,$$

$$y_{bbe} = z_{cce}/\Delta_z = 1.06 \times 10^{-3} \text{ mho},$$

$$y_{bce} = -z_{bce}/\Delta_z = -1.568 \times 10^{-6} \text{ mho},$$

$$y_{cbe} = -z_{cbe}/\Delta_z = 0.0464 \text{ mho},$$

$$y_{cce} = z_{bbe}/\Delta_z = 18.37 \times 10^{-6} \text{ mho.}$$

Finally, (1N) → (4N)

$$_e y_{be} = y_{bbe} + y_{bce} = 1.059 \times 10^{-3} \text{ mho,}$$

$$_e y_{bc} = -y_{bce} = 1.568 \times 10^{-6} \text{ mho,}$$

$$_e y_{ce} = y_{cce} + y_{bce} = 16.8 \times 10^{-6} \text{ mho,}$$

$$_e y_m = y_{cbe} - y_{bce} = 0.0464 \text{ mho,}$$

so that the equivalent circuit (4N) is that shown in Figure 8.

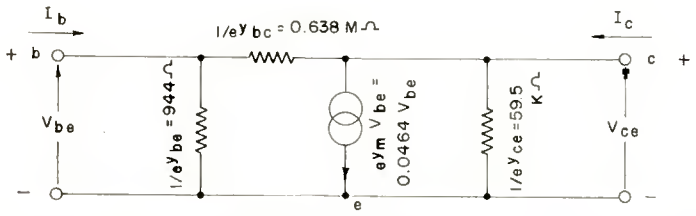

Fig. 8—Single-generator, nodal-derived, common-emitter equivalent circuit.

References

1. ASA C42-1941, "American Standard Definitions of Electrical Terms," *American Institute of Electrical Engineers*, New York, N. Y., 1941.

2. "Standards on Abbreviations, Graphical Symbols, Letter Symbols, and Mathematical Signs," *The Institute of Radio Engineers*, New York, N. Y., 1948.

3. L. C. Peterson, "Equivalent Circuits of Linear Active Four-Terminal Networks," *Bell Sys. Tech. Jour.*, Vol. 27, pp. 593-622, October, 1948.

4. K. Lehovec, "Testing Transistors," *Electronics*, Vol. 22, pp. 88-89, June, 1949.

5. "Standards on Electron Tubes; Definition of Terms, 1950," *Proc. I.R.E.*, Vol. 38, pp. 426-438, April, 1950.

6. "Standards on Electron Tubes: Methods of Testing, 1950," *Proc. I.R.E.*, Vol. 38, pp. 917-948, August, 1950.

7. "Standards on Transducers: Definitions of Terms, 1951," *Proc. I.R.E.*, Vol. 39, pp. 897-899, August, 1951.

8. F. E. Terman and J. M. Pettit, *Electronic Measurements*, McGraw-Hill Book Co., Inc., New York, N. Y., 1952, pp. 289-310.

9. L. J. Giacoletto, "Junction Transistor Characteristics at Low and Medium Frequencies," National Electronics Conference, Sept. 30, 1952; published in the *Proceedings* of the conference.

THE UNIAXIAL MICROPHONE *

By

Harry F. Olson, John Preston, and John C. Bleazey

Research Department, RCA Laboratories Division,
Princeton, N. J.

Summary—*A small unidirectional microphone has been developed with the following features: maximum sensitivity along the axis of the microphone; a high ratio of electrical output to size; a sharper directivity pattern than a cardioid; a directivity pattern that is independent of the frequency; a blastproof vibrating system. The high discrimination which this microphone exhibits to sounds which originate from the sides and rear makes it particularly suitable for long distance sound pickup in radio, television, sound motion pictures, and sound reinforcing systems.*

Introduction

THE general trend in microphones for use in television is in the direction of smaller and more unobtrusive units. One of the first high-quality units of this type was the small "Bantam" velocity microphone.[1] Another example is the "Starmaker," a nondirectional pressure ribbon microphone.[2] However, for boom use and other long distance pickup applications a directional microphone is required. The "77D" unidirectional microphone is almost universally used for these applications. This microphone was developed almost ten years ago. Over this period, research and development work has been carried on with the objective of improving the acoustic and magnetic systems of microphones. An example, incorporating some of these developments, is the "Starmaker" microphone referred to above. A review of the unidirectional microphone indicated that it would be possible to reduce the size and improve the directivity. Furthermore, a new requirement was a blastproof vibrating system capable of withstanding blast from guns, pistols and small explosions. This review also indicated that a blastproof feature could be incorporated. The vibrating system which appeared to be the most suitable for obtaining the above enumerated features was one similar to that used in the Starmaker. In the unidirectional form this system has been termed the uniaxial microphone

---

* Decimal Classification: R385.54.

[1] L. J. Anderson and L. M. Wigington, "The Bantom Velocity Microphone," *Audio Eng.*, Vol. 34, p. 13, January, 1950.

[2] H. F. Olson and J. Preston, "Unobtrusive Pressure Microphone," *Audio Eng.*, Vol. 34, p. 18, July, 1950.

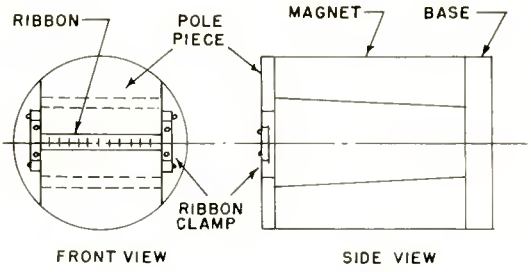

Fig. 1—Front and side views of the motor of the uniaxial microphone.

because the maximum sensitivity corresponds to the axis of the system. It is the purpose of this paper to describe the uniaxial microphone.

Theory

The motor selected for this microphone is shown in Figure 1. Among the advantages of this motor is the simple and efficient magnetic structure. Simplicity is accomplished by the use of a small number of easily machined parts. High magnetic efficiency is obtained due to the small leakage inherent in magnetic designs of this type.

The next consideration is a blastproof system. A typical sound wave produced by the firing of a gun is shown in Figure 2. The total time depends upon the type of gun. It appears to range from 1/20 to 1/40 of a second from a .45- to a .22-caliber gun. The low-frequency components of this wave are not reproduced through the complex chain of elements which constitute the sound channel in recording or broadcasting. However, these low-frequency components in the blast pulse produce the large deflections in the ribbon and stress it beyond the elastic limit and thereby introduce a permanent deformation in the

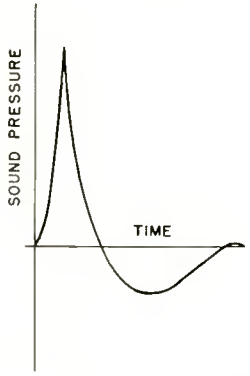

Fig. 2—A graph of the sound wave produced by the firing of a gun.

ribbon. What is required is a system which will reduce the low-frequency amplitude of the sound pressure delivered to the ribbon.

The sound pressure delivered to the ribbon in the low-frequency range can be reduced by the use of an acoustical resistance placed over each side of the ribbon as shown in Figure 3. The acoustical circuit is also shown in Figure 3. The components of the acoustical impedance of the elements of the system shown in Figure 3 are shown in Figure 4. These components are as follows:

The acoustical resistance is

$$r_A = r_{A1} + r_{A2}\,, \tag{1}$$

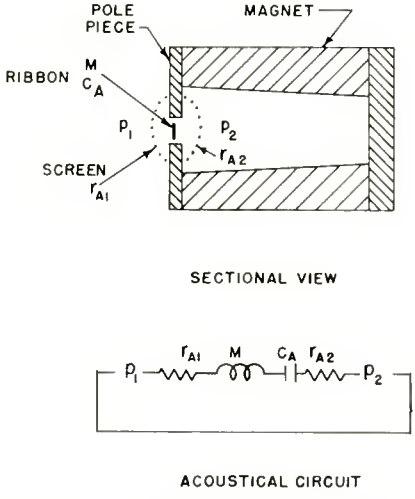

Fig. 3—Sectional view and acoustical circuit of a simplified vibrating system of a uniaxial microphone to show the effect of the blast baffles. In the acoustical circuit: p_1 is the sound pressure on the front of the microphone; r_{A1} and r_{A2} the acoustical resistances of the blast baffles; M and C_A the inertance and acoustical capacitance of the ribbon; and P_2 the sound pressure on the back of the microphone.

where r_{A1} = acoustical resistance of the screen on the front of the ribbon,

r_{A2} = acoustical resistance of the screen on the back of the ribbon.

The positive acoustical reactance of the ribbon is given by

$$X_{AM} = 2\pi f M, \tag{2}$$

where M = inertance of the ribbon.

The negative acoustical reactance of the ribbon is given by

$$X_{AC} = \frac{1}{2\pi f C_A}, \tag{3}$$

where C_A = acoustical capacitance of the ribbon.

The volume current in the system of Figure 3 is given by

$$\dot{X} = \frac{p_1 - p_2}{r_A + jX_{AM} + jX_{AC}}, \tag{4}$$

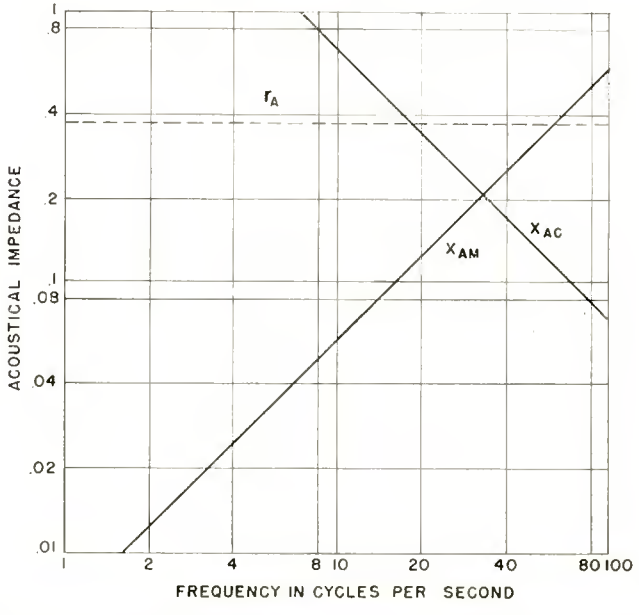

Fig. 4—The components of the acoustical impedance of the system of Figure 3. r_A is the total acoustical resistance, x_{AM} the positive acoustical reactance, and x_{AC} the negative acoustical reactance.

where p_1 = pressure on the front of the ribbon, and

p_2 = pressure on the back of the ribbon.

The driving pressure, $p_1 - p_2$, is proportional to the frequency. The reason is as follows: The magnitudes of p_1 and p_2 are the same. However, the phase difference between p_1 and p_2 is proportional to the frequency. Therefore, in the frequency range in which the distance between the front and back is small compared to the wave length, the

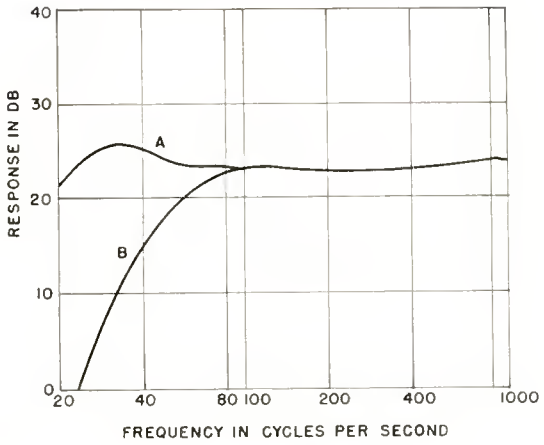

Fig. 5—Response frequency characteristic of the system of Figure 3: A. Without acoustical resistance; B. With acoustical resistance.

difference in pressure between the front and back will be proportional to the frequency.

Referring to Figures 3 and 4 it will be seen that the low-frequency response will be attenuated by the addition of the acoustical resistances. The response–frequency characteristics with and without the acoustical resistances are shown in Figure 5. These characteristics show the high attenuation in the low-frequency region due to the addition of the acoustical resistance.

A sectional view of the complete vibrating system is shown in Figure 6. The magnetic system is similar to the one shown in Figure 1. The ribbon is connected to the damped folded pipe or labyrinth by means of a connector which couples the rectangular cross-sectional area at the ribbon to the circular cross-sectional area at the labyrinth. The connector is provided with two holes, one on each small side near

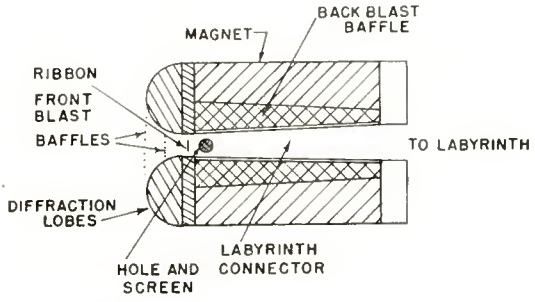

Fig. 6—A sectional view showing the elements of the motor of the uniaxial microphone.

the connection to the ribbon. These two holes provide the essential portion of the phase-shifting acoustical network so that the directional pattern will be of the unidirectional type. The front face of the microphone is equipped with two lobes. The lobes perform three functions: the reduction of the deleterious effects of diffraction, the accentuation of the high-frequency response, and the support of the blast baffles. The front of the microphone is equipped with two blast baffles held in place by the lobes. The side of the microphone is equipped with a single blast baffle. The action of the different elements and the

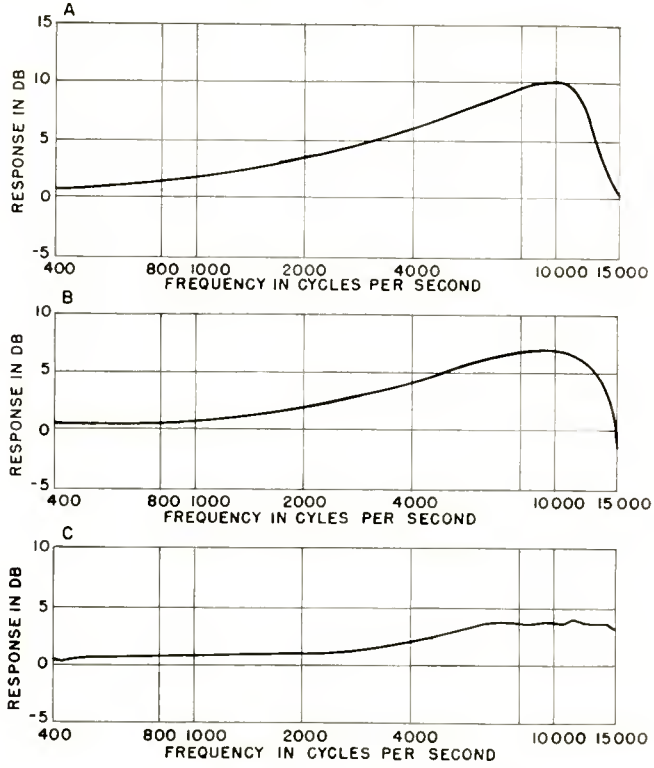

Fig. 7—A. The response at the center of a cylinder; B. The response of the uniaxial microphone without the diffraction lobes; C. The response of the uniaxial microphone with the diffraction lobes.

complete microphone will be described in the discussion which follows.

The front face of the microphone is circular. Therefore, the response will be nonuniform in the high-frequency range due to the diffraction effects produced at the face of the cylinder. The sound-pressure response-frequency characteristic at the center of the cylinder for normal incidence of the impinging sound wave of uniform sound

pressure in free space is shown in Figure 7A. The response–frequency characteristic of the system shown in Figure 6 operating as a pressure microphone and without the lobes is shown in Figure 7B. The deviation of this response–frequency characteristic from that of Figure 7A is due to the fact that the ribbon covers a length of about one inch on the surface rather than a single point at the center. The response–frequency characteristic of the system of Figure 6 operating with the lobes is shown in Figure 7C. The addition of the lobes reduces the effects of diffraction. The net result is a smoother response–frequency characteristic. The lobes also act as a small horn which accentuates the response in the extreme high-frequency range.

A sectional view and acoustical network of the complete microphone are shown in Figure 8. It is of the single-ribbon type in which the back of the ribbon is coupled to a damped pipe and an inertance in the form of an aperture in the pipe.

The action of the microphone can be obtained from a consideration of the acoustical network. The sound pressure on the open side of the ribbon may be written

$$p_1 = p_0 \epsilon^{j\omega t}, \tag{5}$$

where p_0 = amplitude of the pressure, in dynes per square centimeter,

$\omega = 2\pi f$,

f = frequency, in cycles per second,

t = time.

The sound pressure acting upon the air load of the aperture and the aperture may be written

$$p_2 = p_0 \epsilon^{j(\omega t + \phi_1)}, \tag{6}$$

where ϕ_1 = phase angle between the pressure p_1 and the pressure p_2.

Referring to Figures 6 and 8 it will be seen that there is a cavity between the magnets filled with damping material. This cavity is coupled to the aperture as shown in the acoustical network. This cavity is also acted upon by a sound pressure which may be written

$$p_3 = p_0 \epsilon^{j(\omega t + \phi_2)}. \tag{7}$$

The phase angles ϕ_1 and ϕ_2 are a function of the angle of the incident sound as follows:

$$\phi_1 = \Phi_1 \cos \theta, \tag{8}$$

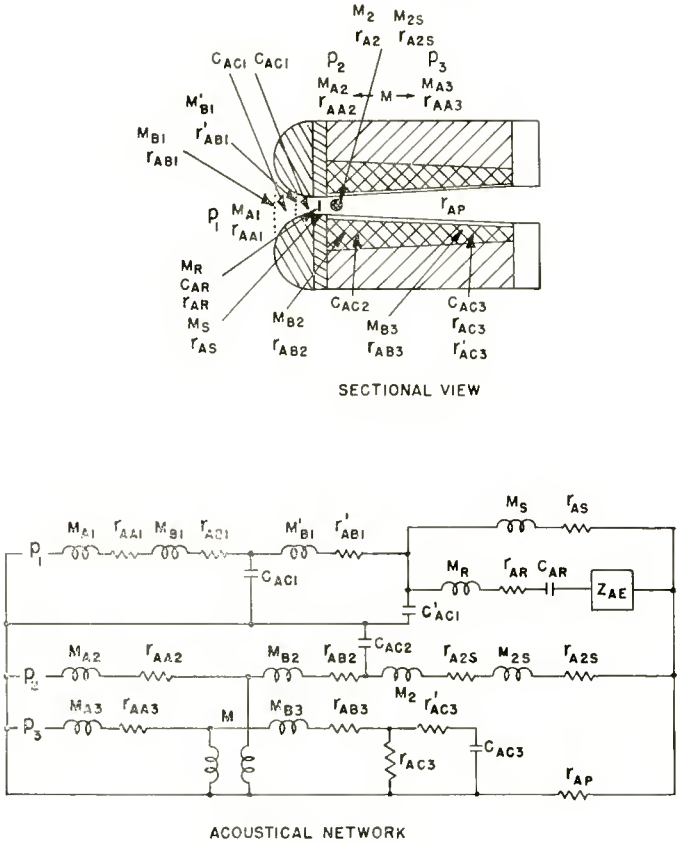

Fig. 8—Sectional view and acoustical network of a uniaxial microphone. In the acoustical network: p_1 is the sound pressure on the front of the microphone; M_{A1} and r_{AA1} the inertance and acoustical resistance of the air load on the front of the microphone; M_{B1}, r_{AB1}, M'_{B1}, and r'_{AB1} the inertances and acoustical resistances of the blast baffles on the front of the microphone; C_{AC1} and C'_{AC1} the acoustical capacitances of the volumes between the blast baffles; M_S and r_{AS} the inertance and acoustical resistance of the slit between the ribbon and pole pieces; M_R, r_{AR}, and C_{AR}, the inertance, acoustical resistance and acoustical capacitance of the ribbon; Z_{AE} the acoustical impedance due to the electrial circuit; p_2 the sound pressure at the apertures in the labyrinth connector; M_{A2} and r_{AA2} the inertance and acoustical resistance of the air load at the apertures of the labyrinth connector; M_{B2} and r_{AB2} the inertance and acoustical resistance of the blast baffles on the side of the microphone; C_{AC2} the acoustical capacitance of the volume behind the blast baffle; M_{2S} and r_{A2S} the inertance and acoustical resistance of the screen covering the hole in the labyrinth connector; M_2 and r_{A2} the inertance of the hole in the labyrinth connector; r_{AP} the acoustical resistance of the labyrinth; p_3 the sound pressure at the damped cavity between the magnets; M_{A3} and r_{AA3} the inertance and acoustical resistance of the air load upon the damped cavity; M_{B3} and r_{AB3} the inertance and acoustical resistance of the blast baffle over the damped cavity; C_{AC3}, r_{AC3} and r'_{AC3} the acoustical capacitance and accustical resistances of the cavity between the magnets; M the coupling between the cavity and the apertures.

and $$\phi_2 = \Phi_2 \cos\theta, \tag{9}$$

where θ = angle between the normal to the surface of the ribbon and the direction of the incident sound wave,

Φ_1 = constant phase angle for the pressure p_2, and

ϕ_2 = constant phase angle for the pressure p_3.

The coupling M between the aperture and the damped cavity is complex function of the dimensions and configuration of the cavity and the relation of the cavity to the aperture. In addition, the coupling is a function of the direction of the incident sound. Under these conditions the acoustical network of Figure 8 is extremely complex. If the blast baffles are removed, the acoustical network is reduced to the one shown in Figure 9A. A further simplification can be obtained by lumping the elements into the impedances as shown in Figure 9B. The acoustical network of Figure 9B can be reduced to the acoustical network of Figure 9C in which the pressure

$$p'_2 = f_1\,(p_2)\; f_2\,(p_3)\; f_3\,(\theta), \tag{10}$$

and the acoustical impedance

$$z'_{A2} = f_4\,(z_{A2})\; f_5\,(z_{A3}). \tag{11}$$

In the acoustical network of Figure 9C, the volume current in the acoustical impedance z_{A1} due to pressure p_1 is

$$\dot{X}_1 = \frac{p_1\,(z'_{A2} + r_{AP})}{z_{A1}z'_{A2} + z_{A1}r_{AP} + z'_{A2}r_{AP}}. \tag{12}$$

The volume current in the acoustical impedance z_{A1} due to the pressure p'_2 is

$$\dot{X}_2 = \frac{p'_2\, r_{AP}}{z_{A1}z'_{A2} + z_{A1}r_{AP} + z'_{A2}r_{AP}}. \tag{13}$$

The resultant volume current in the acoustical impedance z_{A1} is the difference between the volume currents

$$\dot{X}_R = \dot{X}_1 - \dot{X}_2. \tag{14}$$

If the volume current through the slit between ribbon and the pole

is negligible, the volume current $\dot{X}_R$ is the volume current of the ribbon.

The velocity of the ribbon is

$$\dot{x}_R = \frac{\dot{X}_R}{A_R}, \tag{15}$$

where A_R = area of the ribbon.

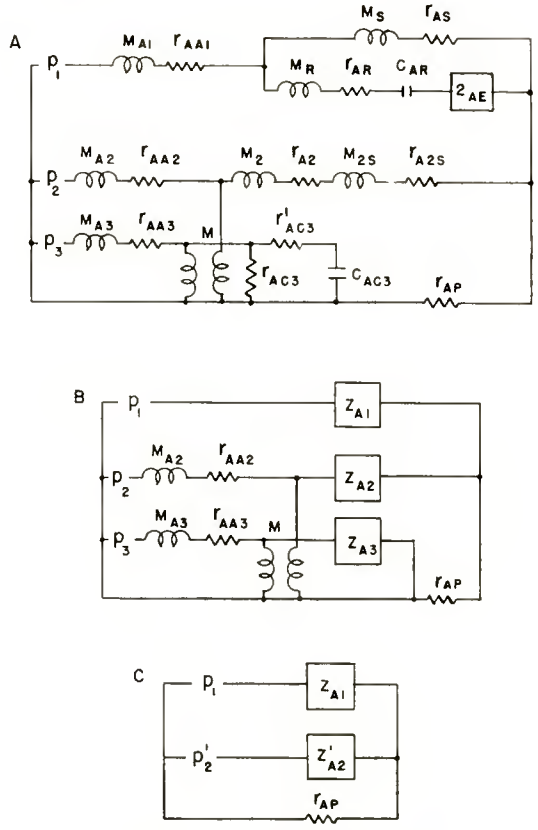

Fig. 9—A. Acoustical network of Figure 8 with the blast baffles removed; B. Acoustical network of A with the equivalent lumped acoustical impedances; C. The approximate equivalent acoustical network of B with the mutual coupling system and associated acoustical impedances replaced by a single pressure and acoustical impedance.

The voltage generated by the motion of the ribbon is given by

$$e = Bl\dot{x}_R, \tag{16}$$

where B = flux density in the air gap, and l = length of the ribbon.

The performance of the microphone can be predicted from Equations (5) to (16) inclusive. The directivity pattern of the uniaxial microphone shown in Figure 6, under a given set of constants, can be approximately expressed as

$$e = K\left(.3 + .7\cos\theta\cos\frac{\theta}{3}\right), \tag{17}$$

where K = sensitivity constant of the microphone.

The directivity pattern of the uniaxial microphone obtained from Equation (17) is shown in Figure 10.

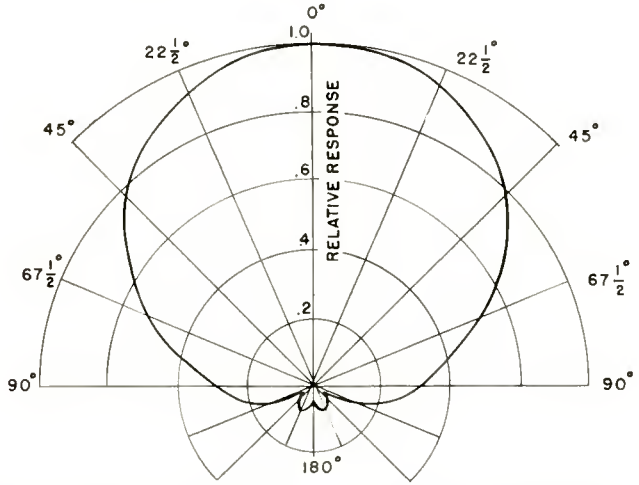

Fig. 10—Theoretical directional pattern of the uniaxial microphone.

It is interesting to compare the directional patterns of the uniaxial microphone with the conventional unidirectional microphone. If the damped cavity is omitted, then the microphone becomes the conventional unidirectional type with the acoustical network of Figure 11A. The acoustical network of Figure 11A can be reduced to the acoustical network of Figure 11B.

The resultant volume current through the acoustical impedance z_{A1} is given by

$$\dot{X}_R = \frac{p_1\,(z''_{A2} + r_{AP}) - p_2\,r_{AP}}{z_{A1}\,z''_{A2} + z_{A1}\,r_{AP} + z''_{A2}\,r_{AP}}. \tag{18}$$

The voltage generated by the ribbon can be obtained from Equations (15), (16), and (18). The directivity pattern of this microphone is given by

$$e = K\ (a + b \cos \theta),$$

where K = sensitivity constant of the microphone,

a and b = limaçon constants, $a + b = 1$.

A few of the directivity patterns which can be obtained from this microphone are shown in Figure 12.

Comparing Figures 10 and 12 it will be seen that it is not possible to obtain, in the conventional microphone, the same directivity in the

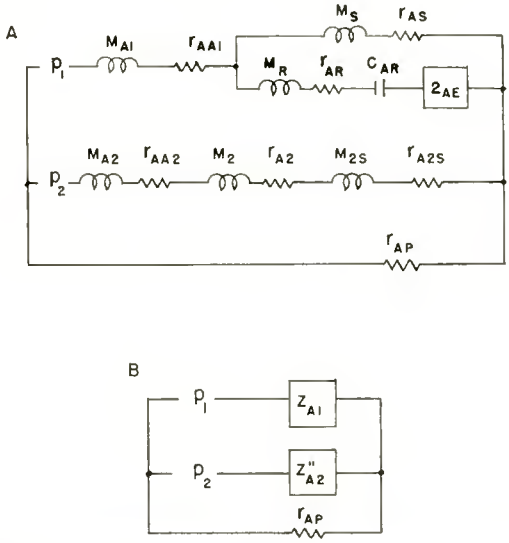

Fig. 11—A. The acoustical network of the acoustical system of Figure 9 with the damped cavity omitted; B. The equivalent acoustical network of A with the equivalent lumped acoustical impedances.

front hemisphere as that in the uniaxial microphone without sacrificing high discrimination in the rear hemisphere. For example, referring to Figure 12, the directivity pattern of the unidirectional microphone in the front hemisphere for $3a = b$ is approximately the same as the uniaxial microphone in the front hemisphere. However, the discrimination in the rear hemisphere for the unidirectional microphone for the same constants is only 6 decibels for 180 degrees as compared to 26 decibels for the uniaxial microphone.

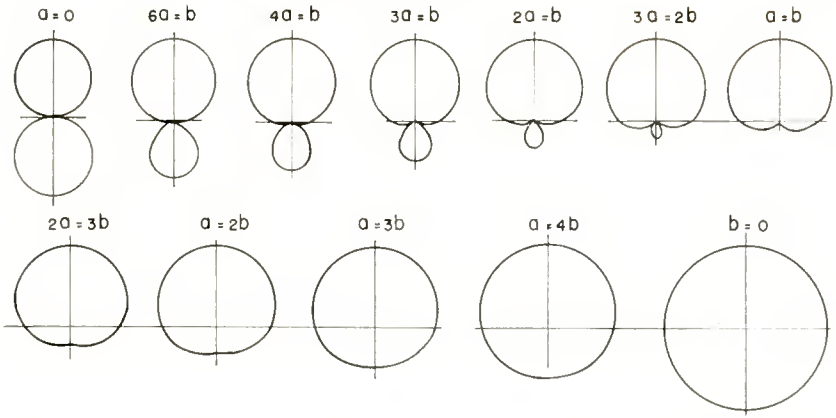

Fig. 12—A few of the single infinity of directional characteristics obtainable with the polydirectional microphone.

Performance Characteristics

The response frequency characteristics of the uniaxial microphone for the angles 0°, 45°, 90°, 135° and 180°, where 0° corresponds to the axis of the microphone are shown in Figure 13. The average polar directivity pattern of the uniaxial microphone is shown in Figure 14.

In order to show the effect of the damped cavity upon the directivity pattern, the cavity was covered with thick sheets of copper. The directivity pattern obtained under these conditions is shown in Figure 15. The directivity pattern under these conditions is slightly broader

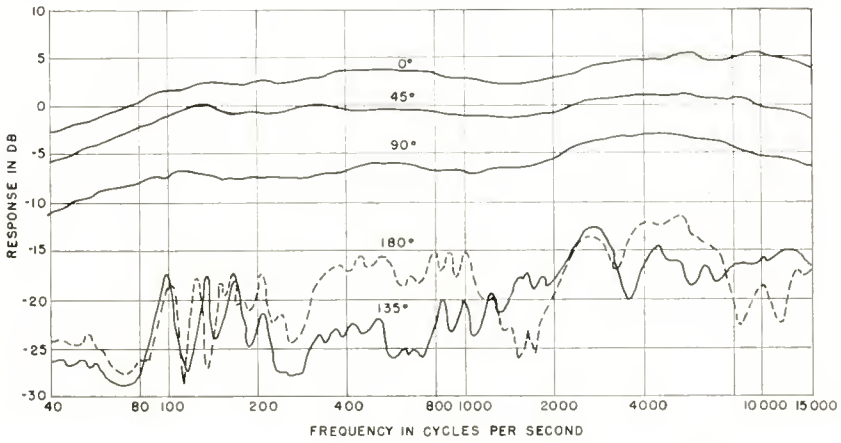

Fig. 13—The measured response frequency characteristics of the uniaxial microphone sound incident at 0°, 45°, 90°, 135° and 180°. 0° corresponds to the axis of the microphone.

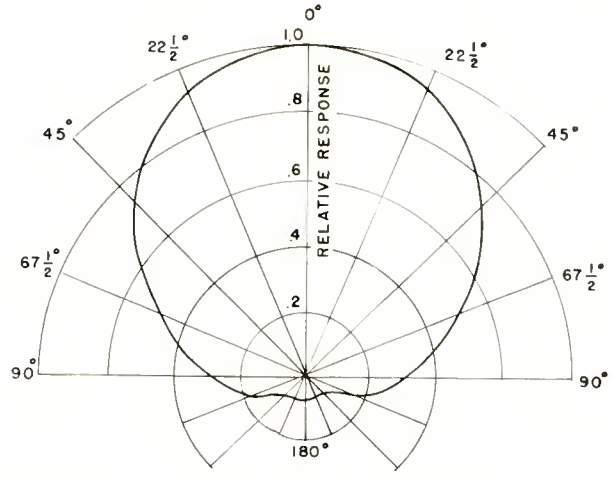

Fig. 14—The average of the measured directional patterns of the uniaxial microphone.

in the front hemisphere. Also, a large lobe has now appeared in the rear hemisphere. The directivity pattern shown in Figure 15 is not satisfactory as a unidirectional microphone because of the inadequate discrimination in the rear hemisphere. With the cavity covered, the holes in the connector were reduced in size until the cardioid pattern shown in Figure 16 was obtained. This is the typical pattern for a

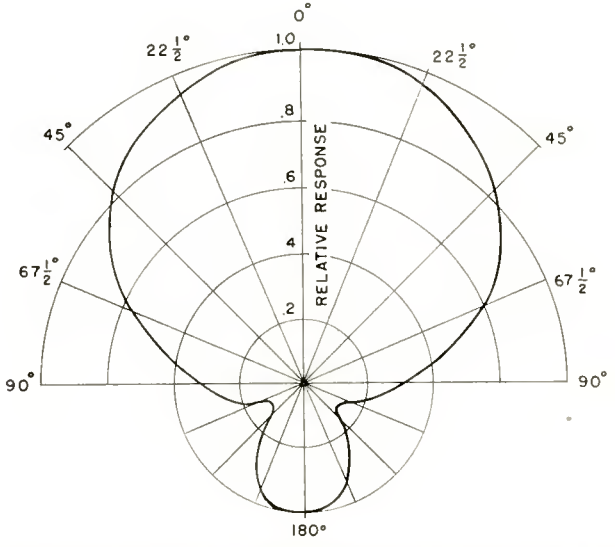

Fig. 15—The average of the measured directional patterns of a conventional unidirectional microphone set for the pattern $e = .3 + .7 \cos \theta$.

unidirectional microphone with high discrimination against sound coming from the rear. Now the directivity pattern is much broader in the front hemisphere. The response of a unidirectional microphone with a cardioid directivity pattern to random sounds, with all directions equally probable and of equal strength, is ⅓ that of a nondirectional microphone. The response of the uniaxial to random sounds is ⅕ that of a nondirectional microphone. This means that the response of the uniaxial microphone to random sounds is 60 per cent that of a microphone with a cardioid pattern. From the standpoint of sound pickup distance, the uniaxial microphone will operate at 30 per cent greater distance for the same reverberation or undesirable sounds or noise.

Tests have been made of the effectiveness of the blastproofiing. The

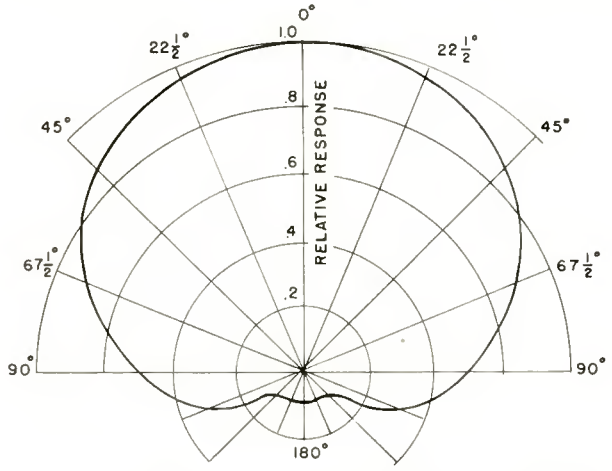

Fig. 16—The average of the measured directional patterns of a conventional unidirectional microphone set for a cardioid pattern.

uniaxial microphone will stand the blast of a .45 pistol firing blanks at a distance of 5 feet indoors, with the direction of firing at right angles to the microphone. It will withstand the same blasts at a smaller distance outdoors. However, a distance of 5 feet should be ample for practically all conditions of use because the effective operating pickup distance of the uniaxial microphone is greater than the conventional unidirectional microphone.

Applications

One of the applications for this microphone is the pickup of sound in television where the microphone is mounted on a boom and kept out

of the picture. The directional properties of the microphone are particularly suitable for this application because the discrimination against unwanted sounds which originate at the sides and the rear is very high. A photograph of the cradle which has been developed for this microphone for use on a boom is shown in Figure 17. The cradle design provides an underslung mounting of the microphone so that the microphone is the lowest part of the system. This condition allows for minimum distance between the source of sound and the microphone.

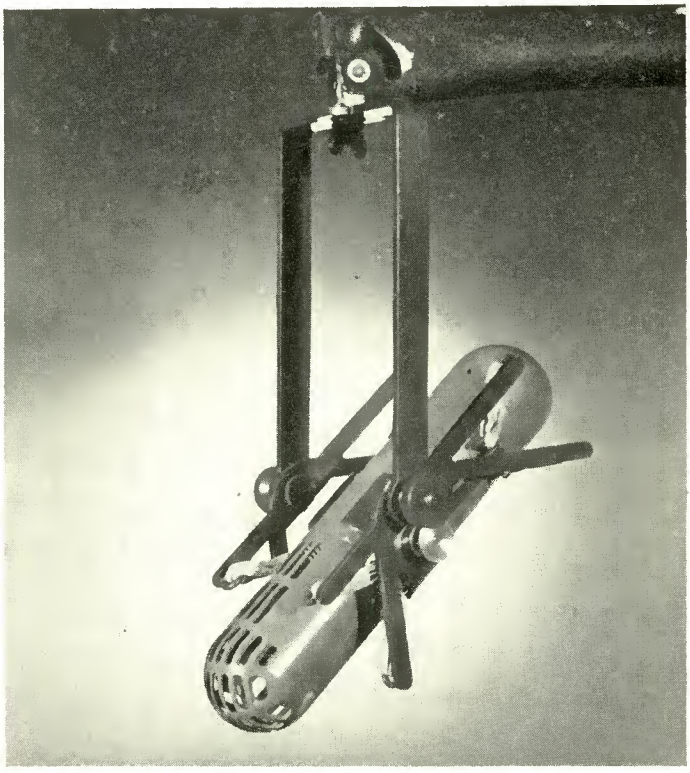

Fig. 17—The uniaxial microphone mounted in a cradle for boom operation.

Other applications for this microphone are the pickup of sound in television where the microphone is seen in the picture. Either floor or desk stands are used for these applications. A desk stand is shown in Figure 18. The uniaxial microphone is particularly suited for these applications because the maximum response occurs on the axis. Under these conditions the projected area of the microphone is a minimum as viewed by the camera.

Fig. 18—The uniaxial microphone mounted on a desk stand.

The uniaxial microphone is also useful for standard broadcast and sound reinforcing applications where the unidirectional microphone has already been established as the solution for sound pickup problems. It has been extensively field tested, including use at the 1952 political conventions.

IMPEDANCE MATCHING WITH TRANSFORMER SECTIONS*

By

R. W. Klopfenstein†

Iowa State College, Ames, Iowa

Summary—*A new viewpoint toward impedance matching by transmission line sections leading to greater flexibility in transformer design is presented. Step capacities which are significant at ultra-high frequencies are easily acounted for in design.*

Introduction

IT IS often convenient or necessary for impedance matching purposes to introduce a shunt susceptance or series reactance at a point in a transmission line. This is quite commonly accomplished by the use of an open-circuit terminated or short-circuit terminated transmission line stub section placed in series with or in shunt with the main transmission line. Unfortunately, these stub sections have quite large peak currents and voltages occurring in them in many applications. In addition to the problems that these high voltages and currents create by their nature, an additional problem is introduced by the concurrent power losses.

Due to the problems occurring with the use of open-circuit terminated and short-circuit terminated transmission line stub sections for impedance matching, it is usually desirable to use transformer sections for this purpose where possible. Quarter-wave transformer sections for matching one resistance to another and transformer sections an integral number of half wave lengths long are in common usage. However, it is also possible to simulate any given shunt susceptance or series reactance by the use of a transformer section. It is the object of this note to devise an equivalent circuit for any transmission line section which will display this equivalence and to discuss the application of the equivalence to several impedance matching problems.

Notation

All impedance and admittance values will be considered to be normalized to the characteristic impedance or admittance of the main transmission line. The symbolization to be used is as follows:

---

* Decimal Classification: R117.12.

† On leave of absence from the Engineering Products Department, RCA Victor Division, Camden, N. J.

Y_1, Z_1 = characteristic admittance and impedance, respectively, of the main transmission line,

Y_2, Z_2 = normalized characteristic admittance and impedance, respectively, of the transformer section,

B, X = normalized equivalent shunt susceptance and series reactance, respectively,

B_D = normalized susceptance introduced due to discontinuity effects at the beginning and end of the transformer section,

Y_L = normalized load admittance,

Y_L^* = complex conjugate of normalized load admittance,

l = physical length of transformer section,

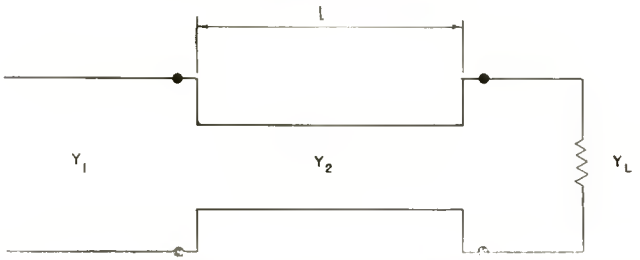

Fig. 1—Circuit diagram representing transformer section of length l and normalized characteristic admittance Y_2 with negligible end effects.

d = physical spacing in units of length between load and transformer,

β = phase constant of transmission line,

σ = voltage-standing-wave ratio.

Relations of Equivalent Circuits

As is well known, it is possible to match an arbitrary load admittance with a simple shunt susceptance or series reactance. This is accomplished by inserting a sufficient length of transmission line that the input conductance or resistance has the desired value. The susceptance or reactance part of the input admittance or impedance is then removed by a suitable shunt or series element (see Equation (5)). The same result can be obtained by using a transformer section designed in accordance with the equivalent circuit developed here.

As shown in Figures 1 and 2a, a short transformer section of

length l and normalized characteristic admittance Y_2 is equivalent to a length of transmission line of characteristic admittance Y_1 and length $l + \Delta l$ with a lumped shunt susceptance B at the center of the section. Alternatively, the short transformer section may be considered equivalent to a length of transmission line, $l + \Delta l + \lambda/2$, of characteristic impedance Z_1 with a lumped series reactance X at the center of the section as shown in Figure 2b.

The equivalent shunt susceptance and series reactance are given by the relation

$$B = X = \left(Y_2 - \frac{1}{Y_2} \right) \sin (\beta l). \tag{1}$$

Proof of this and the other relations in this section is deferred to the Appendix. Inspection of Equation (1) shows that Y_2 and l may be selected in many different ways to obtain a given equivalent sus-

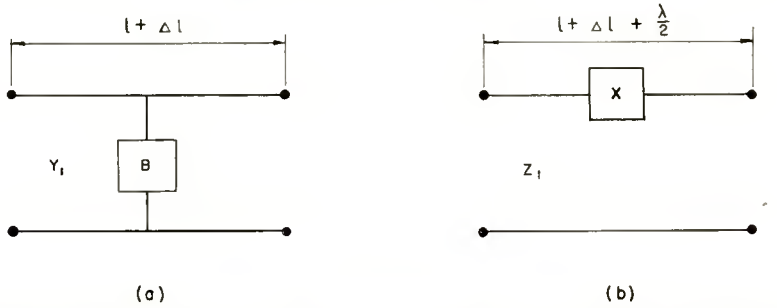

Fig. 2—Equivalent circuits for the transformer sections shown in Figures 1 and 3.

ceptance, B. This leads to the practical advantage that transformers may be limited to several standard sizes and different values of B can be obtained by cutting them to the proper length. In case the electrical length of the transformer is set equal to ninety degrees, it can be verified easily that Equation (1) reduces to the usual quarter-wave transformer relation.

An interesting feature of this approach to transformer design is that it can be extended readily to include the end effects occurring at the transition between the main line and the transformer section.[1] Figure 3 shows a transformer section with the parallel susceptances due to these end effects.

---

[1] J. R. Whinnery, H. W. Jamieson, and T. E. Robbins, "Coaxial Line Discontinuities," *Proc. I.R.E.*, Vol. 32, pp. 695-709, November, 1944.

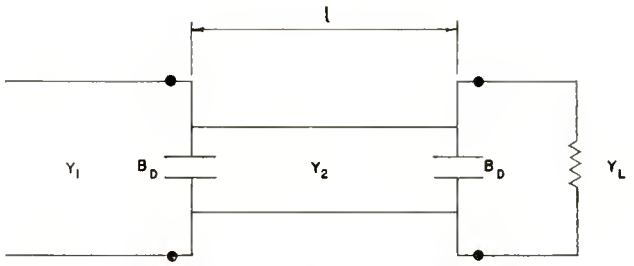

Fig. 3—Circuit diagram representing transformer section of length l and normalized characteristic admittance Y_2 with end effects represented by B_D.

In this case, the equivalent shunt susceptance and series reactance are given by the relation

$$B = X = \left(Y_2 - \frac{1 + B_D^2}{Y_2} \right) \sin(\beta l) + 2B_D \cos(\beta l). \qquad (2)$$

Several interesting conclusions can be drawn from Equation (2). The end effect susceptances are usually quite small ($B_D << 1$), and, in the case of a quarter-wave-length transformer, it is seen that they nearly compensate for each other. The length of a transformer of characteristic admittance Y_2 and end effect susceptances B_D which has the same equivalent susceptance as a quarter-wave-length transformer of characteristic admittance Y_2 without end effects is given by

$$\cos(\beta l) \simeq \frac{B_D}{2Y_2}, \qquad (3)$$

for small values of B_D. The correction in length of a transformer which is to be electrically an integral number of half wave-lengths long can also be obtained conveniently from Equation (2) by setting

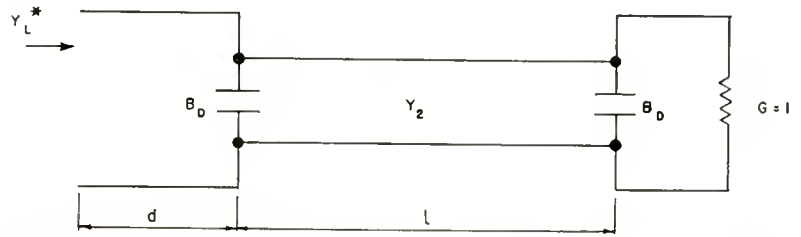

Fig. 4—Circuit diagram indicating the manner in which an impedance matching transformer with end effects can be designed without calculating the length correction, Δl.

the equivalent susceptance equal to zero. Thus, the length of such a transformer is given by

$$\tan(\beta l) = \frac{-2B_p Y_0}{Y_0^2 - B_p^2 - 1}. \tag{4}$$

Figures 5 and 6 illustrate the manner in which transformer lengths are altered by end effect susceptances in other cases.

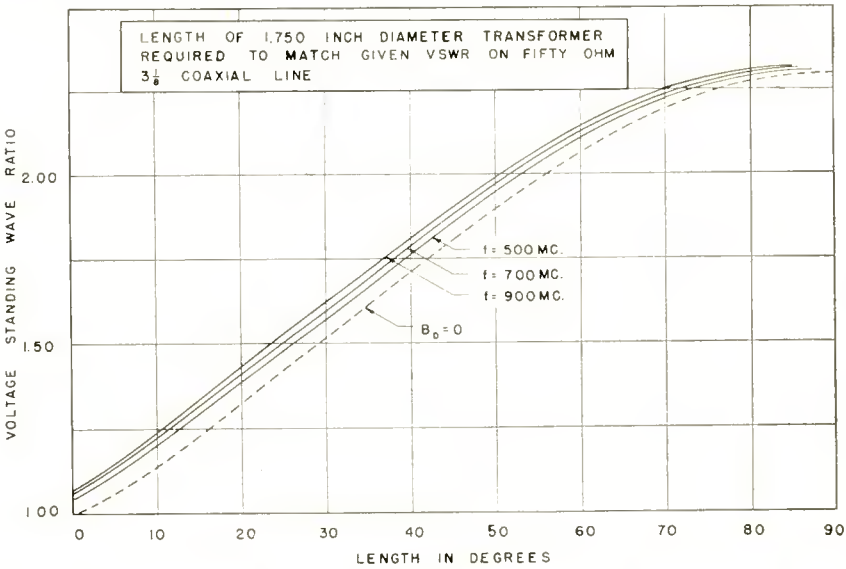

Fig. 5—Typical design curves for impedance matching transformers with end effects.

In general, the length of the equivalent circuits of Figures 2a and 2b is not the same as the physical length of the transformer section. A knowledge of this equivalent length is not necessary in many cases, however. The positioning of the transformer can be determined conveniently by a graphical procedure utilizing the Smith chart. The transformer dimensions can be determined from a knowledge of the voltage standing wave ratio, σ, on the line due to Y_L. The equivalent B of the transformer section to be used is given by[2]

$$B = \frac{\sigma - 1}{\sqrt{\sigma}}. \tag{5}$$

[2] T. Moreno, *Microwave Transmission Design Data*, McGraw-Hill Book Company, Inc., New York, N. Y., 1948, p. 56.

The transformer dimensions can then be determined from Equation (1) or Equation (2), and the load to transformer spacing, d, can be determined by examining the admittance seen from the load looking toward the generator as illustrated in Figure 4.

A match will have been achieved when the distance d is such that this admittance is equal to the complex conjugate of the load admittance.

The analytical expression for the equivalent lengths of transformer sections is quite involved. The equivalent length may be either longer or shorter than the physical length of the transformer section. For

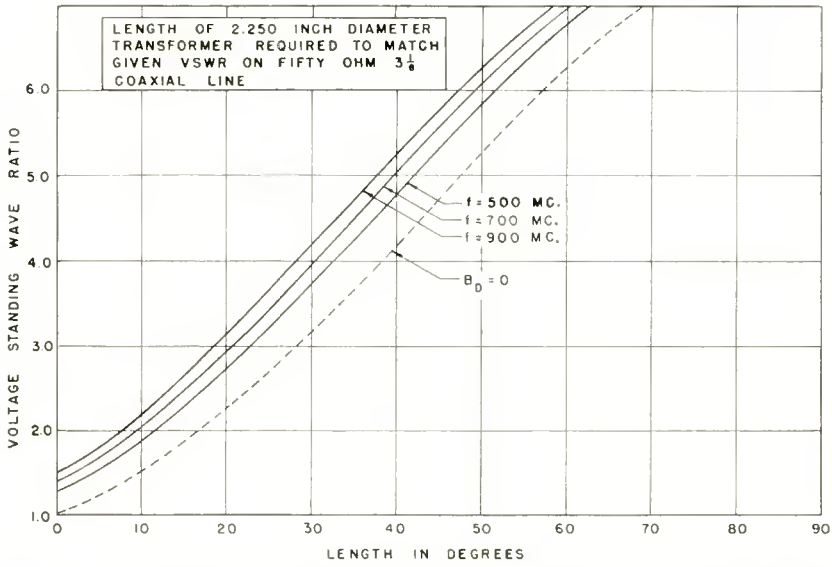

Fig. 6—Typical design curves for impedance matching transformers with end effects.

the configuration of Figure 1, the length correction is given by $\tan(\Delta\beta l) =$

$$\frac{2(2-Y_2-Z_2)\sin 2\beta l + (Y_2-Z_2)\sin\beta l\,[2+Z_2+Y_2+(2-Y_2-Z_2)\cos 2\beta l]}{(2-Y_2-Z_2)(Y_2-Z_2)\sin\beta l\sin 2\beta l - 2\,[2+Z_2+Y_2+(2-Y_2-Z_2)\cos 2\beta l]} \quad (6)$$

An approximation of the relation of Equation (6) valid when the length of the transformer section in wave lengths is small is

$$\tan(\Delta\beta l) \simeq \beta l\left(\frac{1}{Y_2}-1\right). \quad (7)$$

Equation (7) is the first term of a Maclaurin series expansion of $\tan(\Delta\beta l)$ as given by Equation (6) in powers of βl.

The corresponding expression for the configuration of Figure 3 is not given.

Conclusion

An equivalent circuit for a transformer section has been presented which allows considerable flexibility in transformer design. Through this equivalent circuit, end effects are easily taken into account.

Acknowledgment

The author would like to express his appreciation to T. U. Foley for his encouragement and his criticism of this paper.

Appendix

Only the equivalent susceptance for the configuration of Figure 3 will be derived here since the configuration of Figure 1 is a special case of this in which B_D is equal to zero. The equivalent susceptance is to be found by determining the susceptance, B, which will introduce the same voltage-standing-wave ratio on a matched transmission line as the given configuration. The fact that the same value of equivalent susceptance will hold for other values of terminating admittances is assured by network theory.[3]

The input admittance of the configuration of Figure 2a at the point of connection of the susceptance B is

$$Y = 1 + jB, \tag{8}$$

and, hence, the square of the magnitude of the voltage reflection coefficient is given by

$$|r|^2 = \frac{B^2}{4 + B^2}. \tag{9}$$

The input admittance of the configuration of Figure 3 is

$$Y = \frac{Y_2 - B_D \tan(\beta l) + j\,[2Y_2 B_D + (Y_2^2 - B_D^2)\tan(\beta l)\,]}{Y_2 - B_D \tan(\beta l) + j\tan(\beta l)}, \tag{10}$$

[3] T. E. Shea, *Transmission Networks and Wave Filters*, D. Van Nostrand and Co., New York, N. Y., 1929, pp. 67-71.

and, hence, the square of the magnitude of the voltage reflection coefficient is given by

$$|\gamma|^2 = \frac{4Y_2^2B_D^2 + 4Y_2B_D(Y_2^2 - B_D^2 - 1)\tan(\beta l)}{4Y_2^2(B_D^2 + 1) + 4Y_2B_D(Y_2^2 - B_D^2 - 1)\tan(\beta l)}$$

$$\frac{+ (Y_2^2 - B_D^2 - 1)^2\tan^2(\beta l)}{+ [(Y_2^2 - B_D^2 + 1)^2 + 4B_D^2]\tan^2(\beta l)}. \qquad (11)$$

When the expressions of Equations (9) and (11) are equated and solved for B, it is found that

$$B = \left(Y_2 - \frac{1 + B_D^2}{Y_2} \right) \sin(\beta l) + 2B_D\cos(\beta l), \qquad (12)$$

in which the positive square root has been chosen. This is the result given by Equation (2). It may be readily verified in a similar fashion that the equivalent series reactance is given by the same expression. The choice of the positive square root is consistent with the use of the principal inverse tangent function in finding the length correction from Equation (6) while a choice of the negative square root would not be consistent with this usage.

THE ELECTRON COUPLER — A DEVELOPMENTAL TUBE FOR AMPLITUDE MODULATION AND POWER CONTROL AT ULTRA-HIGH FREQUENCIES*

PART II. ENGINEERING ASPECTS

By

C. L. Cuccia

Research Department, RCA Laboratories Division,
Princeton, N. J.

Summary—*Part I*[1] *dealt with the theoretical and analytical aspects of a single-beam two-cavity Electron Coupler. This part will reconcile this theory with the engineering aspects which are associated with the various methods for modulating the power output of the Electron Coupler; actual developmental tubes utilizing these aspects are described in other papers.*

In the single-beam or basic Electron Coupler, modulation of the output power is possible only by use of beam-current control or output-cavity transit-time control. Only the latter method is of engineering value if the Electron Coupler is to operate as a unilateral impedance; it does, however, require an exceedingly high modulation voltage which may be reduced in magnitude by utilizing a specially biased collector.

For applications of the Electron Coupler when used as a modulator, criteria of linearity and depth of modulation (85 per cent) make it expedient to employ a more elaborate method of modulation — auxiliary beam modulation. In a tube employing this method, auxiliary spiral beams are installed in the output cavity; these beams both shunt the output load and produce a mismatch. For depths of voltage modulation up to 85 per cent, it may be necessary in such a tube to employ auxiliary beam currents of considerable magnitude. The design and operation of a 1-kilowatt, 800-megacycle, multi-beam Electron Coupler which employs coaxial cavities and which is capable of 85 per cent depth of modulation, a band width in excess of 5 megacycles, and excellent linearity characteristics is described.

Introduction

At ultra-high frequencies, power is obtained in a different manner than at the low and radio frequencies. High-efficiency generators, such as magnetrons, have been developed which are compact and capable of working at very high power levels; such generators may be frequency stabilized during continuous wave or pulse transmission by using signal injection, spiral electron beams, or external cavities. Although high power can be generated at ultra-high frequencies, its control presents difficult problems. It is for the

* Decimal Classification: R385.4.

[1] C. L. Cuccia, "The Electron Coupler — A Developmental Tube for Amplitude Modulation and Control at Ultra-High Frequencies," Part I, *RCA Review*, Vol. X, pp. 270-303, June, 1949.

purpose of providing a means of electronically controlling ultra-high-frequency power that the Electron Coupler was developed. The tube has the characteristics of a nonamplifying control impedance which can be made to have unilateral qualities.

The Electron Coupler is an absorption device in addition to being a variable-power-transfer tube. In applications where frequency stabilization is important, the driving generator will send a constant amount of power into the input of the tube—this power will either go to the output system or to a power sink such as a collector.

Because of this, the over-all operating efficiency during a modulation cycle will be relatively low thereby reducing the applicability of the Electron Coupler in continuous-wave systems designed to yield an output in excess of 5 kilowatts. It is, on the other hand, unique in its applicability as a buffer stage in ultra-high-frequency systems, as an isolation and control impedance, and as an electronic switch. In addition, the Electron Coupler is suitable for paralleling and multiple-output usage. The respective input cavities of several tubes in parallel can receive the ultra-high-frequency power from a single generator. The output cavities—each connected to a different load—can transfer this power to one or more of the output loads in a prescribed fashion.

The research to be described was intended to do more than simply deduce and demonstrate the fundamental principles of operation of an Electron Coupler; it was also intended to study methods of construction and assembly, particularly for high-power use. Because of this, the tubes to be described have moderately large dimensions. However, Electron Couplers of small geometry for low powers would, in many cases, be easier to design and construct, the precise design and shape being a function of the tube application.

In the study to follow, *only those aspects of tube construction and performance which follow from, or bear directly on, the physical theory presented in Part I will be described.* Extensive descriptions of the details of the two types of experimental Electron Couplers which were built and operated are presented elsewhere.[2, 3]

Basic Tube

The basic Electron Coupler, whose theory is discussed in Part I, is a spiral-electron-beam tube which consists essentially of two adjacent cavities which are electron coupled by a single electron beam. Unlike

[2] C. L. Cuccia and J. S. Donal, Jr., "The Electron Coupler — A Spiral Beam UHF Modulator," *Electronics*, Vol. 21, pp. 80-85, March, 1950.

[3] C. L. Cuccia, "The Multi-Beam Electron Coupler — An Improved UHF Modulator Tube," *Electronics*, to be published.

Klystron cavities, which present electric fields parallel to the electron flow, the cavities in the Electron Coupler present alternating-current electric fields transverse to the electron flow. The input cavity is connected to the generator and the output cavity is connected to the load. A configuration using suitable resonant cavities is pictured in Figure 1, where the arrangement is seen to include a collector and a magnetic field parallel to the axis of the cavities. It is assumed that there is no electromagnetic coupling between the input and output cavities. Power is absorbed by the electron beam in the form of spiral or rotational energy in the first cavity. The rotational energy is in addition to the energy due to a direct-current beam potential which transports the electrons through the tube and determines their transit time; this transport energy is not given up in second cavity but goes to the collector.

The resonant frequencies of the input and output cavities and

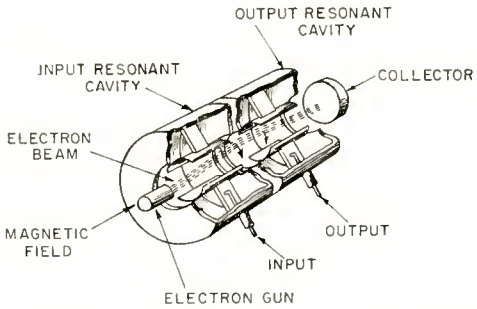

Fig. 1—Basic single-beam Electron Coupler structure showing the adjacent cavities, each of which produces a transverse electric field when excited, and the rotating electron coupling beam. The rotating beam configuration in the output cavity is illustrated for the case when all of the rotational energy is given up to the output load. In an operable Electron Coupler, the output cavity would be rotated 90 degrees with respect to the position shown here in order to prevent electromagnetic coupling between this cavity and the input cavity.

signal to the input cavity are adjusted to the cyclotron frequency; i.e., the frequency at which

$$f_c = \frac{1}{2\pi}\frac{e}{m} H \text{ (electrostatic units)}$$
$$= 2.794 \times H \text{ (practical units)}, \qquad (1)$$

where H is the magnetic field intensity in gausses, and f_c is the frequency in megacycles.

The Electron Coupler has enormous power-handling capabilities. The following discussion will illustrate this characteristic in terms of tube parameters employed in the various experimental Electron Couplers to be described.

The attainment of a certain spiral radius, x, by a cone-directrix beam in the input cavity as illustrated in Figure 1 corresponds to an absorption of power which is described by either of the equations

$$P = 1.122 \times 10^{-2} \times f_c^2 \times I_o \times x^2 \text{ watts}, \tag{2a}$$

$$P = \frac{1}{16} E_1^2 \frac{I_o}{V_{b_1}} l_1^2 \text{ watts}, \tag{2b}$$

where f_c is the frequency in megacycles, I_o is the beam current in amperes, x is the maximum cone-directrix beam radius in centimeters, E_1 is the peak value of the transverse electric field in volts per centimeter, l_1 is the distance which has been transversed by the electron beam in the input cavity in centimeters, and V_{b_1} is the direct-current beam voltage in volts. The spiral radius is related to the parameters of the first cavity by

$$x = 2.36 \frac{E_1 l_1}{V_{b_1}^{1/2} f_c}. \tag{3}$$

Consider an input cavity passing a coupling beam of $\frac{3}{8}$ inch diameter and 90 milliamperes at 800 megacycles; if $x = 1.25$, the value of power* which can be absorbed in the input cavity of the Electron Coupler is

$$P = 1.122 \times 10^{-2} \times 800^2 \times 0.090 \times 1.25^2 = 1{,}010 \text{ watts}. \tag{4}$$

This is not a maximum value but is one which is safely within the grazing limits. If the cavity pole faces are 6 centimeters long, the

* It is seen from Equation (2) that the power which can be absorbed by the electron beam in the first cavity is proportional to the beam current. It is evident, therefore, that space-charge limitations will have an important bearing on the power handling capabilities of the tube. For example, using formulation due to L. P. Smith and P. L. Hartman,[4] a cylindrical beam $\frac{3}{8}$ inch in diameter, concentric with respect to cylindrical boundaries of $1\frac{1}{2}$ inches diameter (which are closely approximated by the arcuate pole faces in the experimental tubes) will sustain a current of 150 milliamperes with a beam voltage of 750 volts.

[4] L. P. Smith and P. L. Hartman, "Formation and Maintenance of Electron and Ion Beams," *Jour. of Appl. Phys.*, Vol. II, pp. 220-229, March, 1940.

beam potential necessary to yield the deflection of 1.25 centimeters when, for example, $E_1 = 2{,}000$ volts per centimeter, is found from Equation (3) to be

$$V_{b_1} = \left[\frac{2.36 \times 2000 \times 6}{1.25 \times 800} \right]^2 = 804 \text{ volts.} \qquad (5)$$

Electron Beam Behavior in the Basic Electron Coupler

The general behavior of the electron beam during the operation of the Electron Coupler may be described as follows.

Consider first the interactions in the input cavity. In figures 2a and 2b it is seen that the electron trajectories in the input cavity are all the same, the major function of the cavity being the absorption by

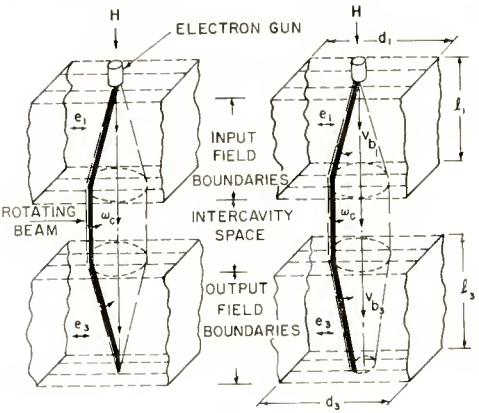

Fig. 2—Beam configuration in the Electron Coupler for two values of transit time or loading in the output cavity. (a) shows the case when the output cavity transit time and load are such that all of the rotational energy is extracted from the beam. (b) shows the beam configuration for increased loading or reduced transit time.

the electron beam of the ultra-high-frequency power. As the electrons pass through the input cavity, the frequency of the input power being equal to the cyclotron frequency, an absorption of energy by the beam takes place in increments of increasing magnitude as the electrons progress through the tube. Since this continued absorption can only take place if the electrons, regardless of where they may be in the cavity, see an accelerating electric field at all times, all electrons will lie on the line-directrix of a cone as shown. The beam spins with angular velocity $\omega = 2\pi f_c$.

As the rotating electron beam passes through the output cavity,

an induced current is produced in the load of the output system by virtue of the fact that these electrons represent oscillating space charge with periodicity, f_e, between the pole faces.

In general, the incremental current induced between a pair of parallel plane boundaries due to an oscillating charge, dq, between them is, for an incremental length of travel through these boundaries,

$$d\,I\,e^{j\omega_e t} = \frac{dq}{d} \times v_t\,, \tag{6}$$

where d is the spacing between the boundaries and v_t is the transversely directed velocity.

A discussion of the nature of the beam configuration in the output cavity as a function of transit time is particularly illuminating since it yields insight into the over-all operation of the Electron Coupler. Consider the case, illustrated in Figure 2a, when the voltage e_3 across the pole faces of the output cavity is equal in magnitude but 180 degrees out of phase with respect to e_1. If $l_1 = l_3$ and $d_1 = d_3$, the beam configuration in the output cavity will be an exact image of the beam configuration in the input cavity. This case represents a 100 per cent transfer of power to the output load with only the energy due to the beam voltage, V_{b_3}, remaining with the electrons as they reach the collector.

If the transit time τ_3 is decreased, the electrons will not remain in the output cavity long enough to give up all of their rotational energy and a truncated cone beam configuration, similar to that pictured in Figure 2b, will result. The rotational energy represented by the part of the cone which does occur between the pole faces, is, of course, lost to the output cavity and goes to the collector.

It is essential at this point to discuss the role of the output load in terms of what shall be termed "match" in the output cavity. The Electron Coupler is said to observe "match" in the output cavity when all the rotational power is transferred to the output load thereby producing the beam configuration pictured in Figure 2a. If the matched output load is R_{oo}, then as is shown in Part I, match is achieved with this load only when the following relationship is satisfied:

$$I_{oo} = 8\,\frac{V_{b_{3o}}}{R_{oo}}\left[\frac{d_3}{l_3}\right]^2. \tag{7}$$

where I_{oo} is the particular value of coupling beam current corresponding to the particular load R_{oo}, $V_{b_{3o}}$ is the beam voltage in the output

cavity, and l_3 and d_3 describe the length and width, respectively, of the pole faces in the output cavity.

The conditions represented by Equation (7) describe the special case when all of the power is transferred to the load. Since the primary function of the Electron Coupler is to control the power which reaches the load, it is evident that this control can be achieved by variation of any of three parameters: coupling beam current, output-cavity beam voltage, and the magnitude of the output load. Recognizing that I_{oo}, $V_{b_{3o}}$, and R_{oo} are optimum parameters defined by Equation (7), it is convenient to represent purely arbitrary values of beam current I_o, beam voltage V_{b_3} and output load R_o, as follows:

$$\alpha = \frac{I_o}{I_{oo}}, \tag{8}$$

$$\beta = \frac{V_{b_3}}{V_{b_{3o}}}, \tag{9}$$

$$\gamma = \frac{R_o}{R_{oo}}, \tag{10}$$

where α, β and γ represent the departures from optimum. Their physical significance and usefulness in a practical sense will be discussed in detail in the sections which follow.

Beam-Current Modulation

Of the three methods of modulating the Electron Coupler listed in the preceding section, it is evident that coupling-beam modulation affords the least promise. Except for specialized applications it is immediately obvious that as the coupling beam current is varied, the input impedance of the tube will vary thereby preventing the tube from operating as a unilateral impedance; the variation of the input impedance during modulation will result in the "pulling" of the frequency of the signal general resulting in attendant frequency distortion. If the driving signal frequency can be maintained constant however, or if frequency distortion is of negligible importance, this approach to modulation can be both simple and useful. Note that, it follows from Equation (A-8) of Part I of this paper, that if e_1 and e_2 represent the input and output voltages, respectively, of the Electron Coupler,

$$\frac{e_2}{e_1} = \frac{K\alpha}{1+\alpha}, \tag{11}$$

where K is a proportionality factor which is equal to 2 if the parameters of the input and output cavities are identical.

Transit-Time Modulation

Transit-time control of the output power of an Electron Coupler of the type pictured in Figure 1 is a useful and practical method of control since it permits the tube to function as a nonamplifying unilateral control impedance in which variations in output cavity beam voltage are not noticed by the input cavity which therefore maintains constant input impedance.

Consider now the theoretically predictable modulation performance of an Electron Coupler employing transit-time modulation. According to Equation A-18 of Part I, the power transfer efficiency of an Electron Coupler feeding into a matched load is expressible as follows:

$$\eta = \frac{\text{Power output}}{\text{Power input}} \times 100 = \frac{4}{\beta} \frac{1}{\left[1+\frac{1}{\beta}\right]^2} \times 100 \text{ per cent.} \tag{12}$$

β may be made to vary in either of two ranges: $0<\beta\leq 1$ and $1<\beta<\infty$. The range $0<\beta\leq 1$ is impractical in an experimental tube since it represents the case where the output cavity voltage is reduced toward zero. Since the Electron Coupler is a high-current device, and since it is appropriate to adjust the coupling beam current to some value close to the maximum value which the beam space can sustain for the adopted input cavity beam voltage, it is evident that reducing β to less than unity will mean reducing the secondary cavity voltage to a value which cannot sustain the coupling beam, whereupon a space change discontinuity will take place and the electron beam will turn back, thereby rendering the Electron Coupler inoperable in this region.

It is, therefore, obvious that if transit-time modulation is to be utilized, only the modulation-range $1<\beta<\infty$ can be adopted.

Consider now the dark-line curve in Figure 3, which represents a chart of power transfer efficiency versus β for the region $1<\beta<\infty$. A value of $\beta = 100$ would be required to reduce the power to 4 per cent of peak. In order to achieve the 85 per cent voltage modulation necessary in commercial transmission, the power would have to be reduced

to 2.25 per cent of peak. This would require an output cavity voltage of tremendous magnitude.

However, this disadvantage can be overcome by the use of a simple but highly successful artifice. This is accomplished by a collector at the exit to the output cavity which acts to decelerate and skew the electron beam in that cavity. Consider the output cavity geometry of the tube shown in Figure 1 for the case where the collector remains at the potential of the input cavity while the potential of the output cavity is varied. Figure 4(a) shows a field map of the direct-current space potential when a difference of potential exists between the output cavity and the collector. It is evident that the equipotential lines of voltage extend far into the coupling-beam space so that the electrons in the coupling beam experience two components of direct-current electric field—a radial component attempting to draw the electrons

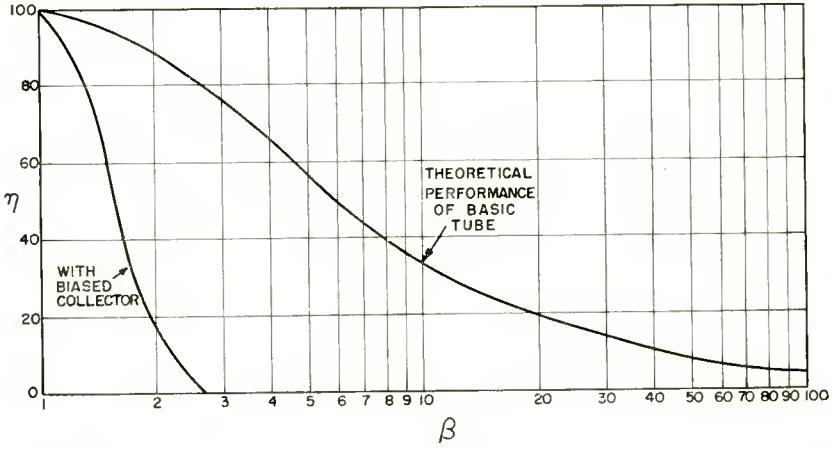

Fig. 3—Chart of β versus the power transfer efficiency of showing the theoretical performance based on Equation (12) and the experimentally achieved performance using a collector maintained at input cavity potential.

to the pole faces, and a reduction in magnitude of axial electric field component which reduces the electron velocity as it passes through the final portion of the output cavity thereby increasing the total transit time of each electron through the cavity.

As the electrons in the directrix beam approach the exit of the output cavity, a Lorentz force due to the radial field will be present which will cause translation of the electrons, resulting in a twisted or skewed beam as shown in Figure 4(b), or possibly grazing. This skewing of the coupling beam in the output cavity may be employed to drastically reduce the power to the output load. Note that for values of β in

the vicinity of 3 it is evident from Figure 4(a) that the radial component of the direct-current field will be comparable to the axial beam voltage.

In an experimental tube[2] of the type pictured in Figure 1, which utilized a value of $V_{b_{30}} = 600$ volts, the modulation characteristic curve shows that close to 100 per cent depth of modulation was obtained for $\beta = 2.75$, corresponding to a maximum cavity voltage of 1650 volts. This illustrates the vast improvement afforded by the use of the fixed-potential collector. (Note that phase modulation due to the skewing of the beam, is inherent in this method of amplitude modulation.)

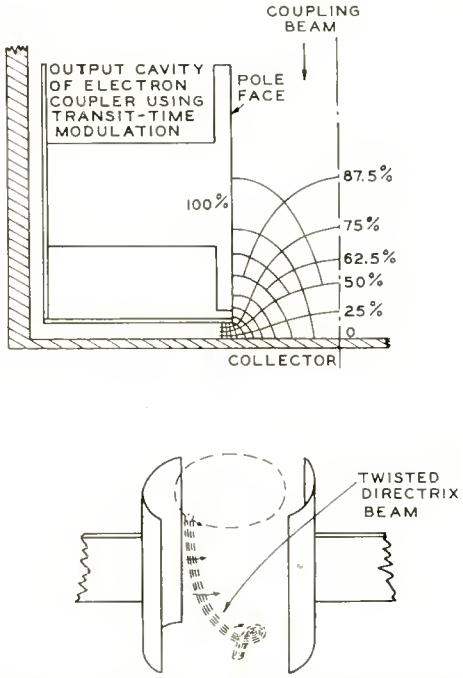

Fig. 4—(a) Field map of direct-current electric field in the output cavity of a vane-type Electron Coupler. (b) Illustration showing the skewing of the coupling beam in the output cavity as a result of the presence of the radial electric field components shown in (a).

Auxiliary Beam Modulation of the Electron Coupler

Transit-time modulation in the basic Electron Coupler is an effective and simple method of modulation; however, it possesses the disadvantage of requiring a high modulating voltage. From a purely engineering standpoint, it is much more desirable to use a method of modulation which uses as low a voltage swing as possible, provided that it does not unduly complicate the tube.

In general, when an electron beam of finite cross section is passed through a transverse electric field under conditions that grazing does not exist and that a magnetic field, parallel to the flow of the electrons be present and adjusted for cyclotron frequency, this electron beam will present the resistance,*

$$R = 8 \frac{V_b}{I} \left[\frac{d}{l} \right]^2, \tag{13}$$

where R is measured in ohms, V_b is the beam voltage in volts, I is the beam current in amperes, and d and l are the width of the transverse field boundaries and the distance traversed by the beam in centimeters, respectively. By controlling the magnitude of the beam current, I, it is evident that such a beam may be employed as a controllable shunt resistance or load.

Consider now the case when a shunt load, R_M, produced by an auxiliary beam is installed in the output cavity of an Electron Coupler; the fundamental mechanism of interaction is described as follows:

As the auxiliary beam current is turned on and increased, the output cavity experiences a mismatch between the coupling beam and the combined load presented by the combination of the output load and the shunting resistance presented by the auxiliary beam; this results in a decrease in transfer efficiency into the combined loads. In a basic Electron Coupler, the power-transfer efficiency is†

$$\eta = \frac{4\gamma}{[1+\gamma]^2} \times 100, \tag{14}$$

where $\gamma = R_o/R_{oo}$. For auxiliary beam modulation, let the output cavity be matched to the output load at the time when the auxiliary beams are turned off, i.e., $R_o = R_{oo}$. When the auxiliary beams are turned on, a new output load will exist which is a combination of the output load, R_o, and the auxiliary beam load, R_M. γ may then be written:

$$\gamma = \frac{R_M}{R_M + R_{oo}}. \tag{15}$$

* See Part I, Equation (18).
† See Part I, Equation (A-17).

The reduction in transfer efficiency when auxiliary beam modulation is employed is due to the fact that as a result of the mismatch, the power goes to three sinks, namely,

1. Output load,
2. Auxiliary beam,
3. Collector,

rather than to the output load alone. As an illustration of the concepts

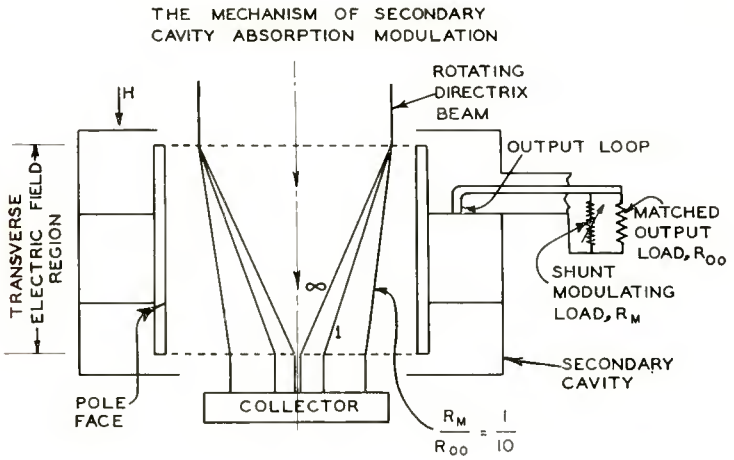

$\frac{R_M}{R_{00}}$	TRANSFER EFFICIENCY	% POWER TO COLLECTOR	% POWER TO OUTPUT LOAD, R_{00}	% POWER TO SHUNT LOAD, R_M
∞	100 %	0	100	0
1	88 %	12	44	44
$\frac{1}{10}$	30 %	70	2.72	27.28

Fig. 5—Diagram and chart showing the mechanism of secondary cavity modulation. The degree of convergence of the coupling beam in the output cavity is illustrated for three ratios of output load to auxiliary beam load. The distribution of output power corresponding to these three values is shown in the chart.

relating to load mismatch and output cavity auxiliary beam modulation, consider the beam configurations and chart pictured in Figure 5.

When the auxiliary beam is off, $R_M = \infty$; the beam configuration is that of a cone and the transfer efficiency is 100 per cent.

When the auxiliary beam is adjusted so that $R_M = R_{oo}$, the transfer efficiency is reduced to 88 per cent with 44 per cent of the power going to the output load, 12 per cent going to the collector, and 44 per cent to the auxiliary beam.

When the auxiliary beam is adjusted so that $R_M = (1/10)R_{oo}$, the transfer efficiency is 30 per cent. 70 per cent of the power will go to the collector, 27.28 per cent to the auxiliary beam, and only 2.72 per cent will reach the output load. This corresponds to 97.28 per cent power modulation or 83.5 per cent voltage modulation and demonstrates the capabilities of output cavity-auxiliary beam modulation method. It is possible to extend the discussion to the case when the coupling beam current is not the optimum value which corresponds to R_{oo}. Figure 6 shows a set of curves derived from Figure 8 of Part I,

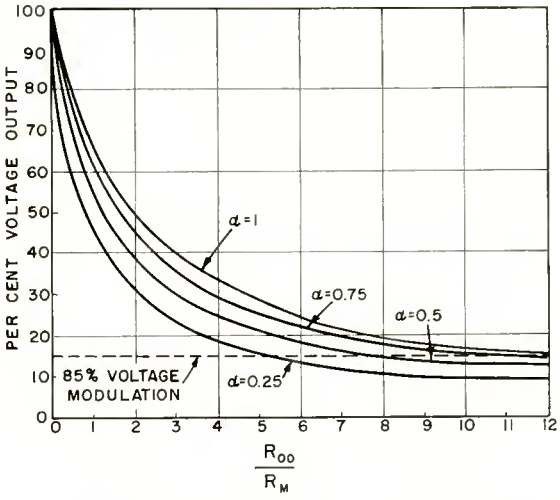

Fig. 6—Voltage transfer ratio versus R_{oo}/R_M as a function of $\alpha = I_o/I_{oo}$, R_M is the auxiliary-beam resistance, I_{oo} is the optimum value of coupling beam current, and I_o is an arbitrary value of coupling beam current.

illustrating the general behavior of the output voltage, expressed as a percentage of the input cavity voltage, $\frac{R_{oo}}{R_M}$, for various values of $\frac{I_o}{I_{oo}}$.

Directrix Beams in Coaxial Cavities

In order to make provisions for auxiliary-beam currents of large magnitude, consider now the use of a cavity of the closed half-wave coaxial-line variety. Such a cavity can be designed to accommodate many electron guns for either coupling or modulation, provided that

the center conductor is correctly shaped to provide transverse field regions of adequate rectilinearity.

Beam Deflection

The deflection x experienced by a directrix beam traveling through a transverse alternating electric field, $E\,e^{j\omega_c t}$, which is uniform along the z-axis (which is the axis of beam travel) is described by Equation (3). Consider the case in a coaxial cavity where the transverse alternating field is a function of z, i.e.,

$$e(z) = E \sin \frac{2\pi z}{L}\, e^{j\omega_c t}, \tag{16}$$

where $\frac{L}{2}$ is the length of the cavity. Letting

$$x = k\,\theta, \tag{17}$$

it follows from Equation (3) that

$$\theta = \frac{2\pi z}{L},\quad k = \frac{2.36}{\pi}\,\frac{E_1}{V_{b_1}^{\frac{1}{2}} f_c}\,\frac{L}{2}. \tag{18}$$

According to the superposition integral theorem, as described in Appendix A, using here the distance parameter θ rather than z,

$$x = k \int_{\theta}^{\phi} Z\,(\phi - \theta)\, e'(\theta)\, d\theta, \tag{19}$$

where, for the field configuration described by Equation (16),

$$e' = \cos\theta, \tag{20}$$

and ϕ is an arbitrary angle such that, $0 < \phi < \pi$. When $\phi = \pi$, $z = \frac{L}{2}$.

Upon integration,

$$x = \frac{2.36}{\pi}\,\frac{E_1}{V_{b_1}^{\frac{1}{2}} f_c}\,\frac{L}{2}\left[1 - \cos\frac{2\pi z}{L}\right]. \tag{21}$$

A beam having a deflection as described by Equation (21) is "milk-bottle" in shape. (See Figure 7.)

Beam Power

Consider now the power into the beam when the beam passes through a coaxial cavity such that the transverse electric field varies sinusoidally along the z-axis as described by Equation (16). Let the power be expressed

$$P = k' \theta^2. \tag{22}$$

From Equation (26) it follows that

$$\theta = \frac{2\pi z}{L} \text{ and } k' = \frac{1}{16} \frac{E_1^2 I_o}{V_{b_1}} \left[\frac{L}{2\pi} \right]^2. \tag{23}$$

Then, according to the superposition integral theorem,

$$P = k' \int_0^{\pi} [\pi - \theta]^2 \cos \theta \, d\theta, \tag{24}$$

where the length of the cavity is $L/2$, corresponding to the limit, π, used in the integral, and $\cos \theta$ is the time derivative of the variation of transverse electric field along the z axis. Solving the integral,

$$P = \frac{1}{8\pi} \frac{E_1^2 I_o}{V_{b_1}} \left[\frac{L}{2} \right]^2. \tag{25}$$

For equal peak field strengths, the power absorbed in a coaxial cavity is $2/\pi$ times that absorbed in a cavity with uniform field and length $L/2$.

If power as a function of final deflection is desired, Equation (25) can be written in the following way (compare with Equation (2)):

$$P = 1.768 \times 10^{-2} \times f_c^2 \times I_o \times x^2 \tag{26}$$

where f_c, I_o, and x are defined in Equation (2).

Beam Resistance

The resistance presented by a directrix beam which absorbs power P in a coaxial cavity is

$$R = \frac{d_1^2 E^2}{2P}, \tag{27}$$

where d_1 is the distance between field boundaries in centimeters and E

is the peak value of the alternating-current transverse electric field. Substituting Equation (25) into Equation (27) yields

$$R = 4\pi \frac{d_1^2 E_1^2 V_{b1}}{I_o E_1^2 l^2} \tag{28}$$

$$= 8 \left[\frac{d_1}{l\sqrt{\frac{2}{\pi}}} \right]^2 \frac{V_{b1}}{I_o} \tag{29}$$

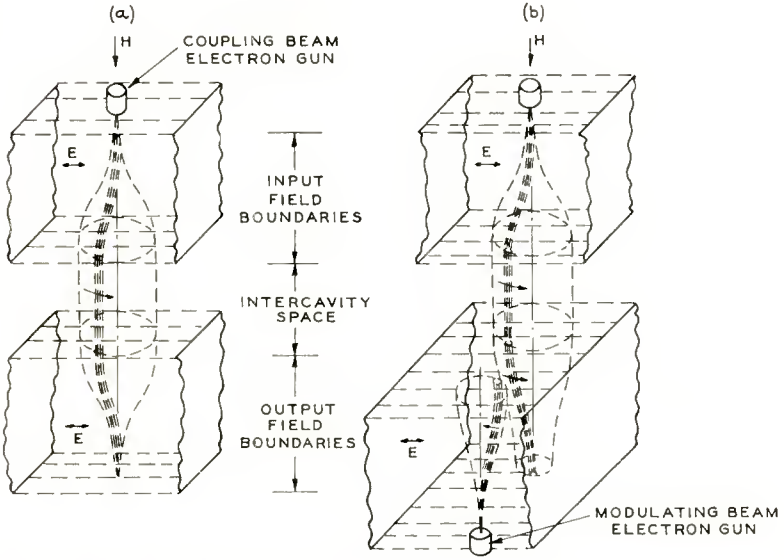

Fig. 7—Shape of the directrix coupling beam in a coaxial-cavity Electron Coupler (a) when the coupling beam is matched to the output load, (b) when an auxiliary electron-beam is introduced into the output cavity.

where $l = L/2$, I_o is the beam current, and V_{b1} the beam voltage. Equation (29) shows that the resistance presented by a directrix beam in coaxial cavity is the same as that presented by a cone directrix beam in a uniform-field cavity whose length is $\sqrt{2/\pi}$ times the length of the coaxial cavity.

Effect of Modulating Beam

The behavior of the coupling beam in the coaxial output cavity as a result of a change in output load by the introduction of an auxiliary beam is pictured in Figure 7. Figure 7a shows the case when the

output cavity is matched to the output load. Here the directrix beam in the output cavity is an exact image of the directrix beam in the input cavity, the apex of the directrix beam being at the exit of the output cavity. Figure 7b shows the configuration of the directrix beam resulting when an auxiliary beam is turned on in the output cavity.

Multi-beam Electron Coupler Design

Consider the multi-beam Electron Coupler[3] whose fundamental structure is shown in Figure 8. The structure consists of two coaxial cavities laid end to end with two apertures, through which coupling beams may pass from the input into the output cavity. These apertures

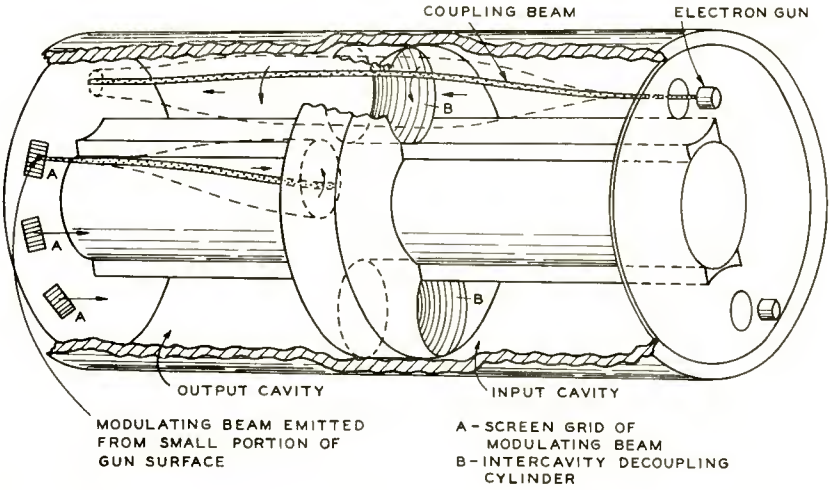

Fig. 8—Structural features of a two-cavity coaxial-type Electron Coupler showing provisions for two coupling beams and three of the five auxiliary modulating beams in the output cavity. The coupling loops are not shown.

are of sufficient length to discourage any electromagnetic coupling between the cavities. The beam-region structure is capable of utilizing two coupling beams that pass between specially shaped pole faces which maintain the rectilinearity of the transverse field. The output cavity is seen to be easily capable of utilizing a plurality of auxiliary beams which are confined to this cavity alone. The input and output coupling loops are not shown.

Consider first the power handling capabilities of a coupling beam in a tube utilizing the structure shown in Figure 8. Let it be specified

that two electron guns are present, each capable of yielding 200 milliamperes without space-charge discontinuities, and that these guns will produce a beam $\frac{3}{8}$ inch in diameter which will travel between pole faces $1\frac{1}{2}$ inches apart. The power handling capabilities of such a tube at 800 megacycles using 400 milliamperes of coupling beam current with a practical grazing limit set at 1.25 centimeters, may be calculated from Equation (26) as follows:

$$P = 1.768 \times 10^{-2} \times 800^2 \times 0.400 \times 1.25^2 = 7040 \text{ watts.} \tag{30}$$

This demonstrates the power handling capabilities of such an Electron Coupler; however, other considerations will place severe limitations on any value of peak power, these considerations being a function of both the input match of the input cavity and the modulation characteristics of the output cavity.

Consider the input cavity and the general problem of matching this cavity to the transmission line from the generator. It is easily shown that if the coupling beam presents a shunt resistance R_t across the pole faces, the transformed resistance R_a as seen at the input to the coupling loops by the transmission line is

$$R_a \approx K^2 \frac{L_1}{L_2} R_t, \tag{31}$$

where K is the coupling coefficient and L_1 and L_2 represent the lumped inductances of the coupling loop and the input cavity, respectively. It then follows from Equation (28) that

$$R_a = 4\pi K^2 \frac{L_1}{L_2} \frac{V_{b_1}}{I_o} \left[\frac{d_1}{l_1} \right]^2. \tag{32}$$

Table I yields a typical series of system parameters for which the input cavity with a coupling coefficient of 0.12 will terminate a 50-ohm transmission line with its optimum termination*. Note that for each value of I_o there corresponds a value of beam voltage and maximum power.

* Actually, an optimum termination of the transmission line by the input cavity may not necessarily be desirable. If the driving generator is a magnetron, for example, the magnetron will have region of high efficiency on its Rieke diagram which will exceed those values of efficiency which occur when the magnetron sees a matched line; it may be desirable to operate in such a region.

Table I — Calculated Electron Coupler Operating Parameters

I_o	K	L_1/L_2	d_1/l_1	V_{b1}	R_a	P_{max} (watts)
0.060	0.12	1	0.2	420	50	1060
0.100	0.12	1	0.2	700	50	1786
0.130	0.12	1	0.2	910	50	2290
0.165	0.12	1	0.2	1150	50	3910
0.200	0.12	1	0.2	1400	50	3520

Consider now a reconciliation of these figures with the practical depth-of-modulation requirements which are specified for modulation systems, i.e., that such modulation systems be capable of 85 per cent voltage modulation. Two cases which reveal the pertinent aspects of auxiliary-beam design are presented.

Case I—Figure 6 shows that if the coupling beam is matched to the output load ($\alpha = 1$), a value of $I_m = 12\ I_o$ will be required to yield 85 per cent voltage modulation. This will limit the value of coupling beam current to one twelfth of that which can be accommodated in the output cavity. If $I_o = 0.200$ is adopted, this beam being capable of a peak power of 3520 watts, $I_m = 2.4$ amperes may be a formidable amount of auxiliary-beam current to produce. If $I_o = 0.060$, thus reducing the power to 1060 watts, 720 milliamperes will be needed in the output cavity.

Case II—The output circuit is sufficiently versatile to make relatively unnecessary the possible stringent auxiliary-beam requirements described in Case I. Let the coupling beam be deliberately mismatched to, say, $\alpha = 0.5$. Note that this drops the voltage at full output to 96 per cent of its value at $\alpha = 1$. However, this has reduced by almost one third the amount of auxiliary-beam current necessary for commensurate modulation (taking into consideration the reduction in peak voltage). Some improvement may also be realized by the appropriate change of beam voltage to increase the mismatch as described in Appendix C.

Band Width Considerations in the Multi-Beam Electron Coupler

Band width considerations in a multi-beam Electron Coupler are derived from two output-cavity parameters, i.e., the transit-time of the directrix beams through the cavities, and the Q of the output cavity system.

One consideration based on the transit-time through the cavity involves possible distortion should the modulation rate become too

rapid. Smith and Shulman[5] have discussed the general aspects of this problem for general values of frequency, different from the cyclotron frequency. However, in the Electron Coupler operating at cyclotron frequency, the electrons are all properly phased and only the effect due to electron bunches being formed along the directrix beam or beams need be considered. It is evident that if, for an extreme case, the modulating rate approaches to the frequency of the resonant cavity, certain electrons as they issue from the cathode will not have time to reach the collector before a new quantity of electrons, as prescribed by the modulation rate, issue from the cathode. This resultant variation in electron density along the directrix beam will manifest itself in the form of different absorption characteristics as compared to a directrix beam with uniform axial constancy of electron density and considerable distortion may result. However, this type of distortion is easily discouraged by making the electron transit time through the tube very small compared to the period of the highest frequency modulating wave component, i.e.,

$$\tau << T, \tag{33}$$

where τ is the transit time through the tube and T is the period of the highest frequency modulating-wave component. In general, the inequality specified by Expression (33) is easily satisfied.

The other band width consideration is based on the Q of the output system. If the cavity is considered to be a system comprised by a lumped L, lumped C, and a resistance R_s, all in parallel, then the Q of the cavity is

$$Q = \frac{R_s}{\omega_c L}. \tag{34}$$

As long as the maximum value of R_s during a modulation cycle yields a value of Q compatible with band width requirements, it is evident that the performance of the modulation system during modulation will be commensurate with these requirements.

Experimental Tube Performance[3]

An experimental multi-beam Electron Coupler was built with an internal structure similar to that shown in Figure 10. It contained

[5] L. P. Smith and C. I. Shulman, "Frequency Modulation and Control by Electron Beams," *Proc. I.R.E.*, Vol. 35, pp. 644-657, July, 1947.

two coupling beams, each capable of 200 milliamperes, and 5 auxiliary-beams capable of a total modulating current of 650 milliamperes at a beam voltage of 750 volts or more, this current being subject to complete control of a grid in the range of $0 < E_g < -50$ when the beam voltage is 750 volts.

The tube was operated at the one-kilowatt level and exhibited a power transfer efficiency of 50 per cent at match, with no auxiliary beams turned on. This is lower than the value of 70 per cent achieved in tubes utilizing the geometry shown in Figure 3. The decrease is attributable to the fact that the great length of the tube (18 inches) made it difficult to achieve over-all rectilinearity of magnetic field as produced by solenoidal magnets.

Consider now the obtainable depth of modulation as predicted by the preceding theory. This information is contained in the curves in Figure 6.

The ordinate R_{oo}/R_M in Figure 6 is too cumbersome for direct use. By employing Equations (7) and (13), however, it follows that

$$\frac{R_{oo}}{R_M} = \frac{I_M}{I_{oo}} \frac{V_{b_{3o}}}{V_{b_{3M}}}, \tag{35}$$

where I_{oo} and $V_{b_{3o}}$ are the optimum values of coupling beam current and beam voltage in the output cavity as prescribed by the output load. I_M is the auxiliary beam present in the output cavity and $V_{b_{3M}}$ is the beam voltage experienced by this beam as referred to the auxiliary beam cathode.

Consider now three cases which illustrate both the theoretical and the practical considerations which are germane to the problem.

Case 1—Let $I_{oo} = 0.060$ and $V_{b_{3o}} = V_{b_{3M}} = 420$ volts (See Table 1). It then follows from Figure 6 that the magnitude of auxiliary beam current necessary to produce 85 per cent voltage modulation is $I_M = 12$ $I_{oo} = 720$ milliamperes. (Since the optimum values of I_{oo} and $V_{b_{3o}}$ are employed, $\alpha = 1$.) It is evident that this is more current than that which is available from the auxiliary beam guns (650 milliamperes max); however, practically speaking, it is not possible to produce even 450 milliamperes in the experimental tube at this low voltage.

Case 2—Let $I_{oo} = 0.165$ and $V_{b_{3o}} = V_{b_{3M}} = 1150$ volts. Following the same procedure as in Case 1, a total of $I_M = 1.920$ amperes is required. This is three times the current available from the auxiliary beam guns. The beam voltage, at least, will be more than sufficient to maintain the available auxiliary-beam current.

Case 3—The situation in Case 2 may be redeemed by mismatching the coupling beam current and the output load as follows: First, let the optimum values, $I_b = 0.165$ and $V_{b_{30}} = 1150$ volts, be set up. Note that according to Table 1, this corresponds to a peak power of 3910 watts. Then reduce the coupling beam current to 0.060, and, adjusting $V_{b_{3M}}$ to 750 volts, bias the auxiliary-beam guns to deliver the full 650 milliamperes. Thus,

$$\alpha = \frac{0.060}{0.165} = 0.37,$$

$$\frac{V_{b_{30}}}{V_{b_{3M}}} = \frac{1150}{750} = 1.532,$$

$$\frac{I_M}{I_{oo}} = \frac{0.650}{0.165} = 3.94,$$

$$\frac{R_M}{R_{oo}} = 3.94 \times 1.532 = 6.04. \tag{36}$$

Using these values for α and R_M/R_{oo}, it is found from Figure 6 that the output voltage is reduced to 15 per cent of the value corresponding to $I_M = 0$. Note that the maximum power which can be carried by a coupling beam of 0.060 milliampere in a tube of these dimensions is, according to Table I, 1060 watts.

The figure for voltage-modulation depth which was deduced in Case 3 was very closely corroborated in the experimental tube. The linearity as a function of auxiliary-beam-grid *voltage* was found to be excellent and the band width was measured to be in excess of 5 megacycles.

Acknowledgment

The author wishes to acknowledge the generous aid and counsel given by J. S. Donal, Jr.

Appendix A—The Superposition Integral Theorem

Consider the case in which an electron enters a transverse electric field whose instantaneous field strength is uniform along the path traversed by the electron. Let a magnetic field exist parallel to the path of the electron and let the magnetic field and the transverse

alternating-current field be adjusted to the cyclotron frequency. The path of the electron is illustrated in Figure 9a; the step-function nature of the transverse field is pictured in Figure 9b, where it is seen that the step function starts at $z = z_1$. The electron will yield what will be termed an electron-response function as a result of its encountering this step-function field. If the response is one of deflection,

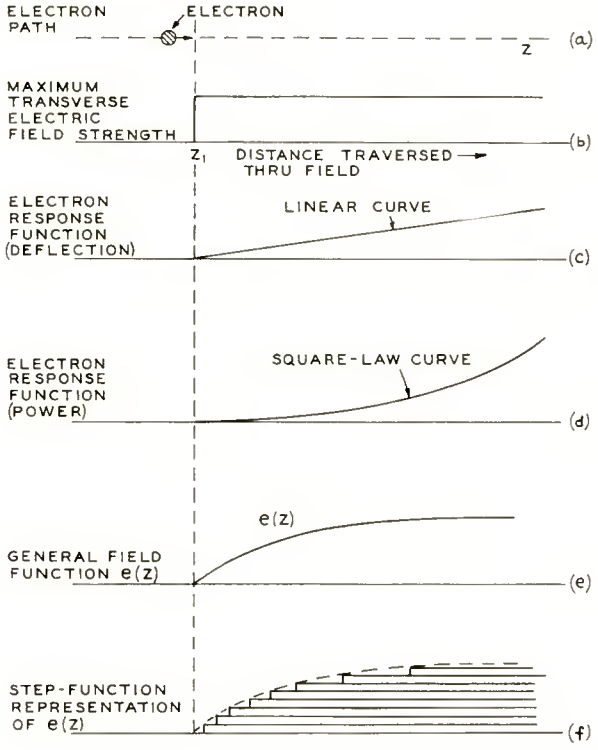

Fig. 9—(a) Path of electron traveling in the Z direction; (b) Diagram showing the step-function nature of axially-uniform transverse electric field as seen by an electron traveling in the Z direction; (c) Electron response function-deflection (linear); (d) Electron response function-power (square law); (e) General function denoting axial variation of transverse electric field; (f) Step function summation which simulates the curve in (e).

then the electron-response function is a linear-response function (see Equation (3)) as pictured in Figure 9c. If the response is one of power, then the electron-response function obeys a square law (see Equation (2)) as pictured in Figure 9d. This electron-response function is written symbolically as $Z(z)$ which is a function of the transit angle of the electron.

Now consider the axial variation of transverse electric field strength to be a general curve described by $e(z)e^{j\omega_e t}$, as pictured in Figure 9e. This curve can be decomposed into a set of step-function components as pictured in Figure 9f.

Let the first of the step-function components in Figure 9f have the amplitude, Δe. The electron response to this particular step-function component will be

$$\text{response} = Z(z)\left(\frac{\Delta e}{\Delta z}\right)\Delta z. \tag{37}$$

It follows that the sum of the responses in distance z is

$$\text{response} = \sum_{o}^{z} Z\,[z-\lambda]\,\frac{\Delta e}{\Delta \lambda}\,\Delta\lambda, \tag{38}$$

where λ is a convenient change of variable. Letting $\Delta\lambda$ approach $d\lambda$ and letting $\frac{\Delta e}{\Delta\lambda}$ approach the derivative of e with respect to λ, we get, as a summation of the responses from 0 to z, the integral

$$\text{response} = \int_{o}^{z} Z\,[z-\lambda]\,e'(\lambda)\,d\lambda, \tag{39}$$

which is recognized as the integral comprising the superposition integral theorem.

Appendix B—Directrix Beam Frequency Multipliers

If a cavity of the magnetron type is used for the output system of an Electron Coupler, and if its frequency is tuned to some integral multiple of the input cavity, frequency multiplication will take place. A directrix beam is formed in the input cavity which, when passed into the cavity-magnetron resonator close to the vane type as shown in Figure 10(a), will interact with the traveling fields of the resonator resulting in the extraction of rotating-beam power by the output cavity system.

Power transfer can only take place if the rotating electron beam sets up a traveling azimuthal electric field $E_\theta\ (r,\theta,t)$ whose angular velocity is that of the rotating beam and whose phase is such that the rotating field sees a retarding field.

An important difference between the interaction process in a frequency multiplier and the Electron Coupler is that, in the Electron Coupler, the transverse electric field extends throughout the interpole face region. In the frequency multiplier, the traveling electric field decreases rapidly along a radius from the vane tips to the center of the interaction space. It can be shown that*

$$E_\theta(r,\theta,t) \approx \sum_{m=-\infty}^{\infty} C_m \left[\frac{r}{r_a}\right]^{n|m|-1} \cos\,(nm\theta - \omega_n t), \qquad (40)$$

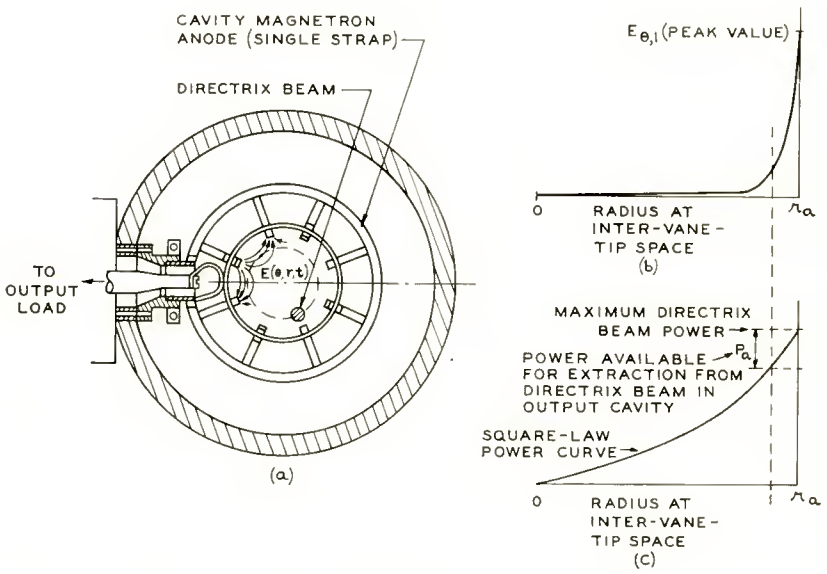

Fig. 10—(a) Vane tips and electric field configuration in a cavity-magnetron anode; (b) Variation of E_θ as a function of radius for the first Fourier component when the number of cavities is large, and the mode of operation is the π-mode; (c) Directrix-beam power as a function of radius.

where C_m is the mth Fourier component of the traveling field, r_a is the radius of the interaction space, θ is the azimuthal angle of the traveling field, and n is the mode number such that $o \leqq n \leqq N/2$, where N is the number of cavities. The π-mode rotating electric field will interact with the $m = 1$ component of correct direction described

* C. L. Cuccia, *Harmonics Sidebands and Transients in Communication Engineering*, McGraw-Hill Book Company, Inc., New York, 1952, p. 417.

by an electric field expression of the following form:

$$E_{\theta, m=1} = C_{\pm 1} \left[\frac{r}{r_a} \right]^{\frac{N}{2}-1} \cos \left[\frac{N}{2} \theta - \omega_n t \right]. \tag{41}$$

The precise value of $C_{\pm 1}$ is not important since it is evident that $(r/r_a)^{\frac{N}{2}-1}$ is the controlling factor as far as the variation of the electric field component along a radius is concerned.

Any power extracted from the rotating field will be described by the general expression

$$P = \int\int_r E_\theta \cdot J_\theta \, r dr d\theta, \tag{42}$$

where J is the current density. However, it is not necessary to pursue further the general formulation describing power extraction since the behavior of the output system follows from considerations of the magnitude of the fundamental azimuthal traveling-wave component as a function of radius.

As is predicted by Equation (41), the magnitude of $E_{\theta, m=1}$ will fall rapidly as a function of radius as measured from the vane tip toward the central axis. This is illustrated in Figure 10(b). It is evident therefore that interaction between the traveling wave and the directrix beam will take place chiefly near the vane tips. If this interaction causes a reduction in directrix-beam radius to, say, r_b, r_b will not be very much smaller than r_a and the power transfer efficiency will at best be

$$\eta = \left[1 - \frac{r_b}{r_a}^2 \right] \times 100. \tag{43}$$

If $r_b \lessapprox r_a$, it is evident that the power-transfer efficiency will be very low. This case is illustrated in Figure 10(c) where the vertical dash line denotes r_b and the power available for extraction from the directrix beam is P_a.

The preceding discussion is, of course, based on the proposition that there is no interaction from the radial component of field E_r (θ, r, t), that the cross section of the directrix beam is very small compared to the thickness of the vane tips, and that the directrix beam enters the output cavity nearly grazing the vane tips. Failure of these aspects to prevail will result in an even lower power-transfer efficiency.

An experimental frequency multiplier was built; the input cavity, tuned to 800 megacycles, was identical to the type used in the basic Electron Coupler in Figure 1; the output cavity was an 8-vane resonant cavity tuned to 3200 megacycles giving a frequency multiplication factor of 4. The distance between vane tips is the same as that between pole faces in the input cavity, or 1.5 inches, and the length of the vane is 2.4 inches. A beam .05 inch in diameter was used (as compared to the ⅜-inch-diameter beam used in the Electron Coupler).

Using cavity voltages of 600 volts, a beam of 45 milliamperes carrying an input radio-frequency power of around 100 watts was sent through the tube. The maximum output power obtainable from this tube was found to be 1.5 watts showing the transfer efficiency to be in the neighborhood of 1.5 per cent, thereby demonstrating the inherent inefficiency of a directrix-beam frequency-multiplier system.

Appendix C—Auxiliary Beam Modulation Using Inverse Feedback

There is a potentially important method, not yet used experimentally, for increasing the depth of modulation to a full 100 per cent. This method employs directrix-beam inverse feedback; an auxiliary beam of magnitude not exceeding that of the coupling beam is used for the modulation.

A directrix-beam inverse-feedback Electron Coupler is pictured in general form in Figure 11. The tube is seen to have a third resonant cavity added after the output cavity. (Note that the output loop remains in the second cavity.) The tube, without the auxiliary modulating beam, is a straightforward two-cavity Electron Coupler.

The principles of operation of this tube are described as follows:

Let the output load be matched to the output cavity when the auxiliary modulating beam is not on. All of the rotating beam power will go to the output load from the second cavity and the coupling beam will pass through the third cavity with only the direct-current energy due to the beam accelerating voltage remaining.

Let the auxiliary modulating beam be turned on slightly. The beam will pass through the third cavity into the second (output) cavity where it will cause mismatch between the directrix coupling beam and its effective load. The power transfer efficiency will be reduced resulting in some rotating beam power remaining in the coupling beam as it enters and passes through the third cavity. This rotating beam power is absorbed by the modulating beam in this third cavity. (Note that the directrix of the modulating beam will be 180 degrees out of phase with respect to the directrix of the third-cavity coupling beam.)

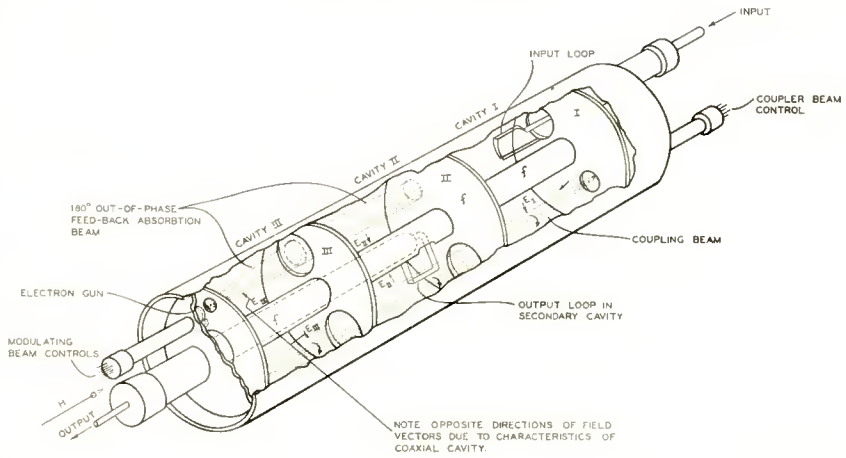

Fig. 11—Diagram of a three-cavity Electron Coupler using directrix-beam inverse feedback. Note that the output loop is in the middle cavity. (Although coaxial cavities are depicted, cone-directrix beams rather than "milk-bottle" beams are pictured in order to avoid undue complexity.)

The modulating beam will enter the output cavity and the rotating beam energy in the modulating beam will serve to further reduce the amount of power extracted from the coupling beam by the output load. As the auxiliary modulating beam is turned on further, more and more rotating beam energy enters the third cavity to be returned by the auxiliary modulating beam to the output cavity, 180 degrees out of phase, until, when the auxiliary modulation beam equals the coupling beam in magnitude, both electron beams will form cylinder-directrix beams of identical radius and no energy will reach the load.

ISRAEL INTERCITY VHF TELECOMMUNICATION SYSTEMS*

By

L. C. Simpson

Engineering Department, RCA International Division, New York, N. Y.

Summary—*Two 12-channel VHF relay systems which were recently installed to interconnect the cities of Jerusalem, Tel Aviv and Haifa are described. Frequency-modulated equipment operating in the 250-megacycle band is used with frequency-division multiplexing and toll dialing. Sources of noise and cross talk in relay systems of this type are discussed, and over-all performance figures are given. The system performance complies with CCIF recommendations.*

THE establishment of the State of Israel in 1948 coincident with the termination of the mandatory regime and followed by an almost three-fold increase in population, created many communication problems demanding rapid solution. As the result of immigration, increased industrial, agricultural and commercial operations, and the administrative activity incident to the formation of the new state, the requirements for national and international communications were multiplied many times.

Not the least important of the tasks confronting the Department of Posts, Telegraphs, Telephones and Radio was that of providing reliable telephone trunk circuits between the principal cities of the country. Traffic requirements were greatest between the cities of Tel Aviv, Haifa, and Jerusalem. In 1950, at the request of the Department, field tests were conducted by RCA to determine suitable station sites for two 12-channel 250-megacycle radio relay systems to interconnect these three cities. Installation work was commenced in mid 1951, and both systems were inaugurated April 14, 1952.

General Characteristics of the Systems

Each of the systems includes two radio hops as shown in Figure 1. In the Tel Aviv–Jerusalem system, a repeater station is located in the Judean Hills, and the radio path lengths are 26 miles and 8 miles. In the Tel Aviv–Haifa system, a repeater station is located on Mount Carmel, and the radio path lengths are 50 miles and 5 miles.

* Decimal classification: R423.15.

Terminal stations are located in the urban automatic telephone exchanges, with the antennas mounted on the roof. Each system is installed and wired as an integral part of the national telephone network. Toll dialing is provided, so that toll operators dial directly to subscribers in the distant city. Any or all channels of the two systems may be patched in tandem at Tel Aviv, as traffic demands, to provide direct circuits with toll dialing between Jerusalem and Haifa.

Performance

Each system provides 12 simultaneous two-way telephone circuits having a signal to noise and interchannel crosstalk ratio of 60 decibels or more. The frequency response of each voice channel between 220 cycles and 3550 cycles is within 2 decibels of the 1000-cycle value. Channel output levels remain within 2 decibels of the established test

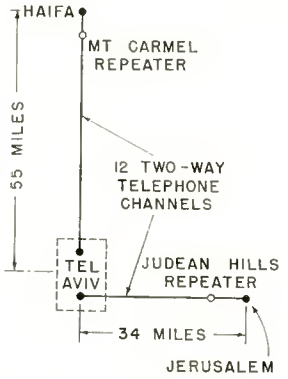

Fig. 1—Trunk facilities provided by intercity systems.

board level during a 24-hour day. The reliability factor of each system during a test week of 2016 channel hours exceeded 99.85 per cent, considering lost time due to all causes except loss of primary power.

Radio Equipment

Type CTR-2* transmitting and receiving equipment is used at all terminal and relay stations to provide a baseband extending from 50 to 112000 cycles. The transmitter operates in the 235-265 megacycle band, and delivers 50 watts output into a 50-ohm load. A master oscillator operating at about 5 megacycles is frequency modulated by means of push-pull reactance tubes. The oscillator frequency is multiplied 48 times in succeeding stages to excite a single 4X150 output tube. The maximum output frequency deviation is ±300 kilocycles.

* Later designation for this equipment is Type CTR-250L.

The center carrier frequency is automatically controlled by comparison with a quartz-crystal oscillator. By means of frequency divider chains, appropriate subharmonics of both master oscillator and crystal oscillator frequencies are applied to a comparison circuit. Any difference between the two subharmonic frequencies causes a correcting

Fig. 2—Tel Aviv terminal radio and carrier equipment.

voltage to be applied to one of the reactance modulator tubes.

The receiver is a single-conversion, crystal-controlled, superheterodyne, frequency-modulation receiver having an intermediate frequency of 32 megacycles. Two radio-frequency stages and five intermediate-frequency stages are used. The receiver noise factor is 9 to 11 decibels.*

* Noise factor of subsequent Model CTR-250 receiver is 6 decibels.

Antennas

Two types of antennas are used, one having 8 cophased elements with plane reflector and a gain of 15 decibels with respect to a half-wave dipole, and the other having a single element with plane reflector and a gain of 4 decibels. These antennas are fixed tuned to cover frequencies of 235-265 megacycles with standing wave ratios of 1.1

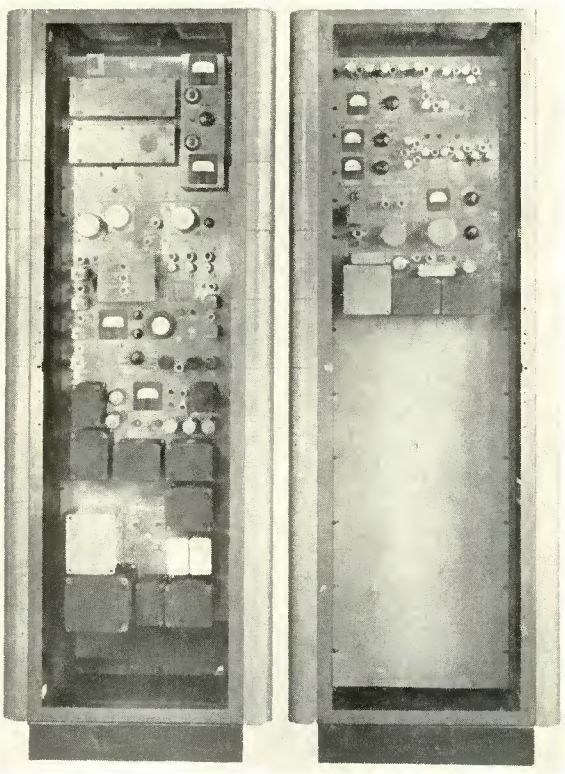

Fig. 3—RCA model CTR-2 VHF equipment transmitter (left) and receiver (right).

to 1.6. Antennas are supported 80 to 160 feet above ground level, with about 2 wave lengths horizontal separation between transmitting and receiving antennas. Approximately 150 feet of RG-17/U solid dielectric transmission line is used with each antenna. Receiving lines are equipped with coaxial filters to reject the adjacent transmitter fre-

quency having approximately 14 megacycles separation from the receiver frequency.

Multiplexing Equipment

Single-sideband carrier terminals are used to provide 12 high-quality telephone channels. Channel spacing is 4 kilocycles, and a multiplex transmission band of 60-108 kilocycles is required for each

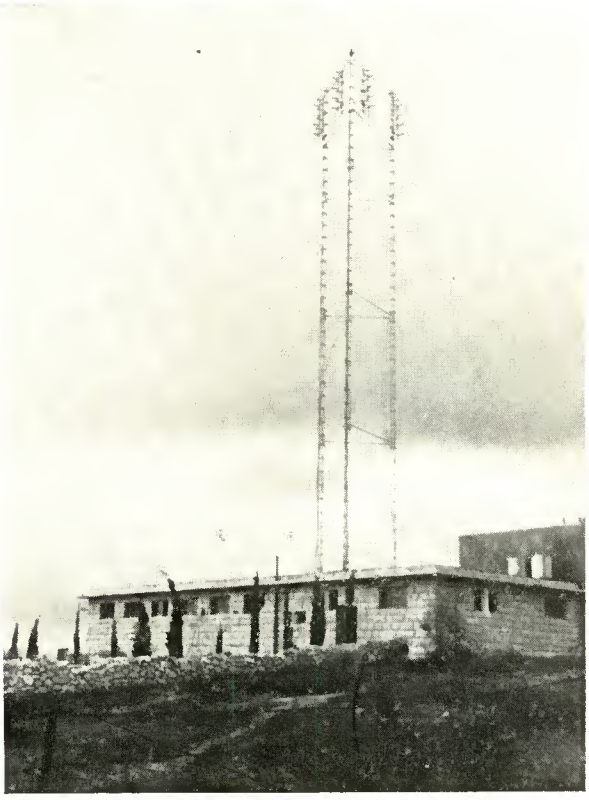

Fig. 4—Judean Hills relay station.

direction of transmission. Voice frequency tones for dialing and supervisory signaling, one for each channel and direction of transmission, are applied to a 13th channel and multiplexed to the 108-112 kilocycle band. The carrier equipment employs a double-modulation system wherein each voice band is first translated to the 8-12 kilocycle band and is then translated to its assigned position in the multiplex

transmission band. By virtue of this double modulation process, excellent channel separation is achieved with conventional band filters. The principal carrier circuits are shown schematically in Figure 12; a more complete description may be found in the literature.[1]

Trunk-Dialing Equipment

In each 12-channel system, 6 channels are used as trunks to handle calls originating at one terminal, and 6 channels for calls originating

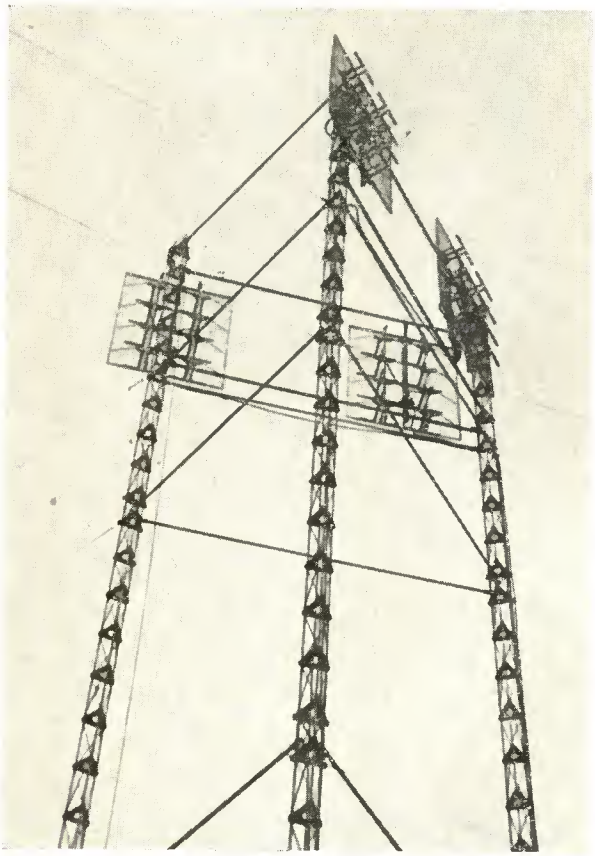

Fig. 5—Antennas at relay station.

at the other terminal. At each terminal, trunk-dialing relay sets are used to connect "outgoing" channels to the toll switchboard and "incoming" channels to the selectors of the automatic exchange. Carrier

[1] L. G. Erickson, "Simplified 48-Channel Carrier Telephone System," *Trans. A.I.E.E.*, Vol. 70, p. 56, January, 1951.

signaling tones are keyed on or off by action of the relay sets. The combined action of outgoing and incoming relay sets and carrier signaling equipment is such that a toll operator at the switchboard may seize, dial upon, or release a desired channel, and receive visual indication of subscriber station ringing, busy, answer, or disconnect conditions.

Propagation

While laying out the system prior to the fixing of the final station sites, a field survey was made. Field-strength measurements were made over all paths, using 20-watt, 150-megacycle mobile equipment at sites the same as, or similar to, those finally chosen for the permanent installation. The field strengths expected for the complete system were

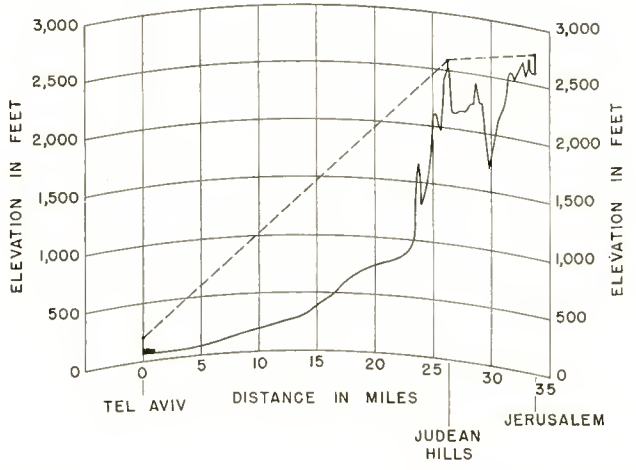

Fig. 6—Profile—Tel Aviv to Judean Hills to Jerusalem based on 1.33 × earth's radius.

derived from these measurements by taking into account the differences in frequency, power, antenna gain, and apparent effective height of antennas. It is of interest to note that for six of the eight paths the actual median receiver input power was within 2 decibels of the expected value. For the other two, Mount Carmel to Tel Aviv and Judean Hills to Tel Aviv, the actual field strengths were, respectively 5 and 9 decibels higher than expected.

The path profiles are shown in Figures 6 and 7. These are based on an earth's radius of 4/3 the actual value. Line-of-sight conditions exist for all paths.

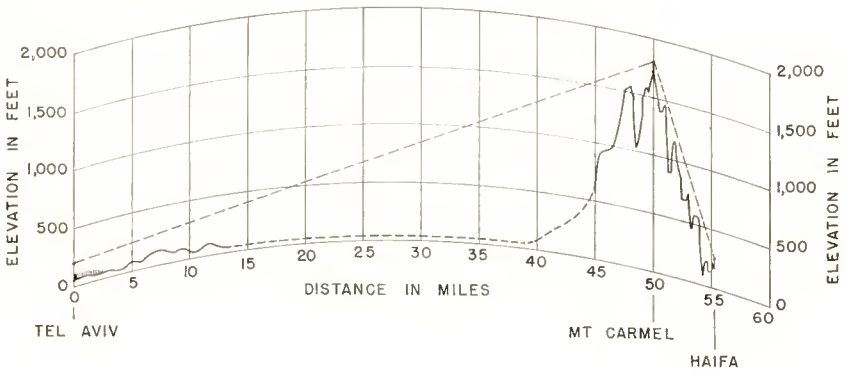

Fig. 7—Profile—Tel Aviv to Mt. Carmel to Haifa based on 1.33 × earth's radius.

The median receiver inputs observed for the various paths are given in the following tabulation. For comparison with published propagation data, such as the Bullington nomograms,[2] the received power which would have been obtained for a radiated power of 1 watt between half-wave dipole antennas is also shown. This is obtained by applying appropriate corrections for transmitter power, antenna gain, transmission line losses, and filter loss. Median receiver inputs are 2 to 17 decibels below free-space values.

Path	Distance, Miles	Receiver Input, Micro-Volts	Receiver Input, dbw*	Equivalent Receiver Input for 1 Watt Dipoles, dbw*	Equivalent Receiver Input, DB Below Free Space Value
Haifa–Mt. Carmel	5	1900	—71	—99	4
Mt. Carmel–Haifa	5	2400	—69	—97	2
Judean Hills–Jerusalem	8	1040	—77	—104	6
Jerusalem–Judean Hills	8	1470	—74	—101	3
Mt. Carmel–Tel Aviv	50	370	—86	—125	11
Tel Aviv–Mt. Carmel	50	260	—89	—128	14
Judean Hills–Tel Aviv	26	1130	—76	—115	7
Tel Aviv–Judean Hills	26	350	—86	—125	17

[2] Kenneth Bullington, "Radio Propagation at Frequencies above 30 Megacycles," *Proc. I.R.E.*, Vol. 35, p. 1122, October, 1947.

* Decibels referred to 1 watt.

Fading

No significant variations in signal strength were observed between Haifa and Mt. Carmel (5 miles) or between Jerusalem and the Judean Hills Station (8 miles).

Received signal strengths over the longer paths, Tel Aviv–Mt. Carmel (50 miles) and Tel Aviv–Judean Hills (26 miles) were observed more or less regularly for about 3 months, from mid-January until April 23, 1952. Figures 8A, 9A, 10A, and 11A are receiver input voltage distribution curves typical for this period.

During the 10 days from March 29 to April 7, much more fading was observed than that which was typical during the rest of the 3

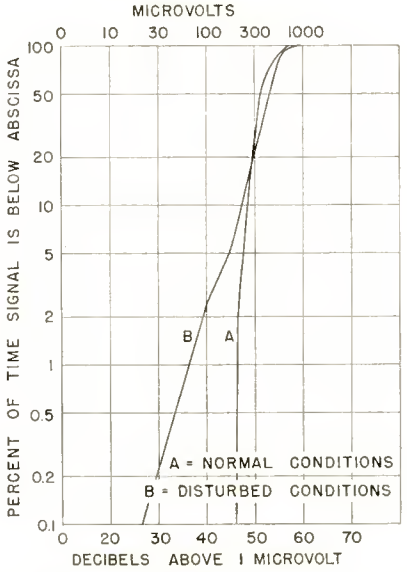

Fig. 8—Receiver input voltage distribution at Tel Aviv, from Mt. Carmel.

month period. This condition was most pronounced from April 2 to April 7 inclusive, and Figures 8B, 9B, 10B, and 11B are receiver input voltage distribution curves for these 6 days. This period of fading coincided with the occurrence of a "khamsin," which is the presence over Israel of a mass of hot dry air from the Arabian desert. The name signifies "fifty," it being said that about fifty such days may be expected each year, mostly during the spring and fall.

Under normal conditions the radio-frequency signals received over the four long hops faded 3 to 5 decibels below median values during only 1 per cent of the time. During the disturbed period, fades of 12

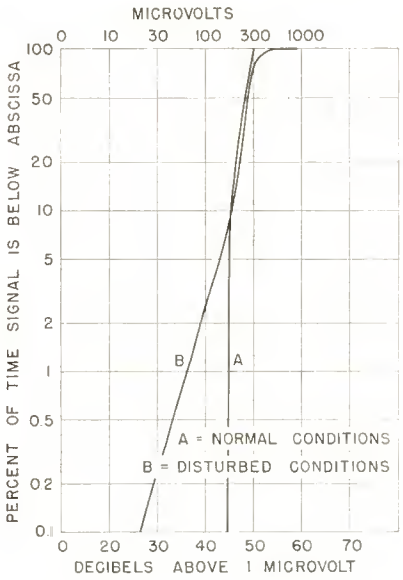

Fig. 9—Receiver input voltage distribution at Mt. Carmel, from Tel Aviv.

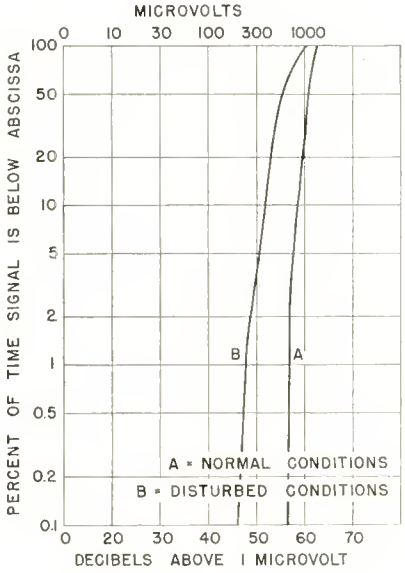

Fig. 10—Receiver input voltage distribution at Tel Aviv, from the Judean Hills.

to 20 decibels below median values were observed for 1 per cent of the time, and fades of 15 to 26 decibels for 0.1 per cent of the time.

Levels

Signal Levels

Multi-channel systems which provide intercity trunk connections between urban telephone exchanges are subjected to a wide range of speech input volumes. Such systems operate in accordance with usual carrier telephone practice whereby speech signals originating at subscribers' telephones are applied, via the local telephone exchange, directly to the channel inputs. No gain adjustments are made for

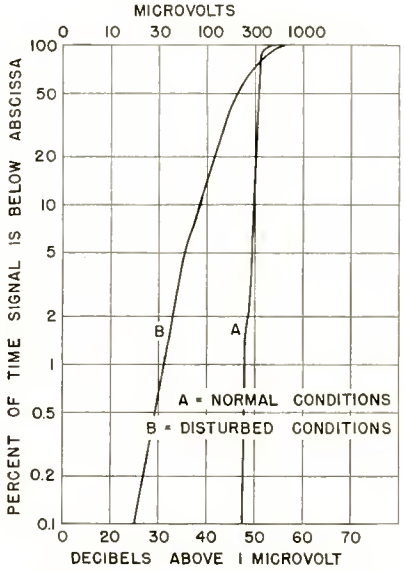

Fig. 11—Receiver input voltage distribution at the Judean Hills, from Tel Aviv.

individual calls, so that input volumes are uncontrolled except for peak limiting in each channel of the carrier equipment at high volume levels. This method of operating is in contrast with that employed in many high-frequency radiotelephone systems, where the input volume may be manually or automatically adjusted for each call to provide acceptable communication over a circuit having a low intrinsic signal-to-noise ratio.

The channel input volume for a given call depends upon such factors as the characteristics of individual telephone instruments, talker volume, length of subscriber line, and the loss of any intervening interoffice

trunk lines. The volume range covered by all calls depends upon the electrical characteristics of the particular telephone network and the talking habits of the subscribers. Typical volumes delivered to the channel inputs from toll switchboards in the United States cover a range of 33 decibels, varying from +8 VU to —25 VU, with a median value of about —8 VU.* Volumes observed in Israel were generally 2 or 3 decibels higher than these values.

The line-up and maintenance of the complete system requires adjustment of individual gains and losses so that the actual signal power at the various units will fall between the allowable limits imposed by noise and overload. This involves adjustments and measurements at a dozen or more points for each channel and direction of transmission. It is customarily done by applying a test tone of specified nominal power at the input of a single channel and measuring the resulting nominal power at each other point of interest. The optimum nominal power for each unit is determined from consideration of its overload characteristics together with the statistical relationship between the test tone and the actual speech signals.

A particular point in the circuit may be referred to in terms of the nominal power, in dbm†, at that point. It may also be referred to in terms of its relative transmission level, which is the gain or loss in decibels between the circuit input and the point considered. In a system having two-wire channel terminations, the sending hybrid input is usually designated a point of "zero transmission level," and a 1 milliwatt (0 dbm) 1000-cycle test tone is applied at this point as the nominal input power. In this case nominal power levels and transmission levels are numerically equal. Figure 12 is a schematic diagram of one of the 12-channel systems, with nominal levels shown.

The most important sources of noise and interchannel crosstalk are in those parts of the system which carry the combined signals of all the active channels. Achievement of the best signal-to-noise ratio with the lowest equipment cost requires that the combined signal level be as high as possible. On the other hand, peaks must not exceed some predetermined limit. This limit may be determined by equipment distortion which causes crosstalk, or, in a frequency-modulation system, by the allowable radio frequency spectrum.

---

* Volume in VU is determined by a device known as a volume indicator, and is numerically equal to the strength of the signal in decibels with respect to a reference volume. The indicator is calibrated so that a 1000-cycle signal whose power is 1 milliwatt in 600 ohms gives a reading of 0 VU. Reference volume is that strength of electrical speech or program waves which gives a reading of 0 VU.

† Decibels referred to 1 milliwatt.

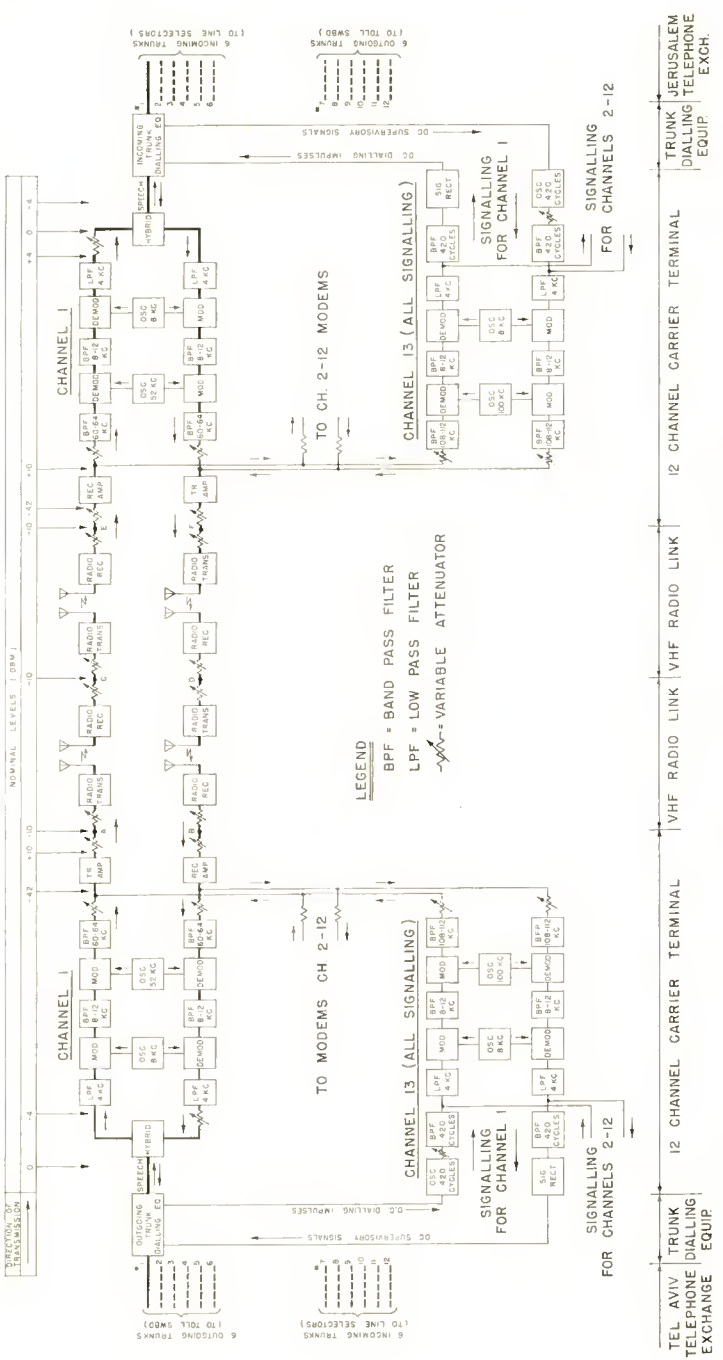

Fig. 12—Schematic diagram of 12-channel VHF telephone system with toll dialling.

The addition of multi-channel speech signals has been investigated in detail by Holbrook and Dixon.[3] Their results are expressed as the root-mean-square power of the single-frequency tone having a peak value which will not be exceeded by the peak value of the actual multi-channel signal more than 1 per cent of the time during the busy hour. Figure 13 is taken from Holbrook and Dixon's work and shows the required single-tone capacity, in dbm, at a point of zero transmission level, as a function of the total number of channels in the system. The curves are based on typical talker volume distribution in each active channel.

In practice, the system is so adjusted that, when a 0 dbm test tone is applied at the input of a single channel, the nominal level at the input of any unit which must carry the combined signal is below the

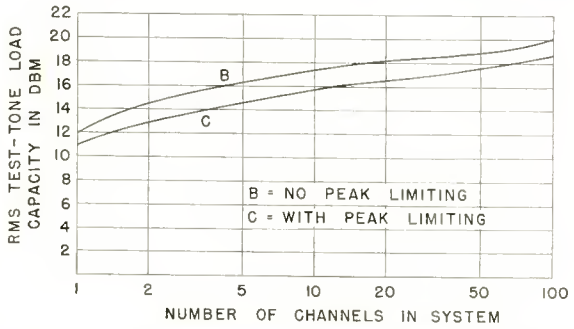

Fig. 13—Load capacity for system or N channels with uncontrolled volumes.

input level corresponding to the maximum single-tone capacity of the unit by the amount indicated in Figure 13.

In the case of the Israel systems, it was desired to limit the maximum frequency deviation of the frequency-modulation transmitters to the rated value or ±300 kilocycles. With 0 dbm test tone input to a single channel, the nominal level at the transmitter input was adjusted to be 16 decibels below the level which would produce 300 kilocycles frequency deviation. This is the value indicated in Figure 13C for a 12-channel system with typical peak limiting.

Oscillographic observation of the actual combined signal during heavy traffic showed maximum peaks, for speech, equivalent to those of a sinusoidal tone 14 decibels above nominal level. The maximum value for supervisory clicks was 19 decibels. A value of 13 decibels was obtained when 11 channels were simultaneously loaded with non-

[3] B. D. Holbrook and J. T. Dixon, "Load Rating Theory for Multi-Channel Amplifiers," *Bell Sys. Tech. Jour.*, Vol. 18, p. 624, 1939.

synchronous tones, each 4 decibels below nominal input level, for crosstalk measurements.

Noise Levels

Single-frequency noise components of different frequencies have different interfering effects on telephone circuits, and their relative interfering effects have been determined. In wire line practice, circuit noise at a point of specified transmission level is measured by means of a noise meter incorporating a frequency weighting network appropriate for the type of telephone instrument used in the system.

The Western Electric 2B noise measuring set is widely used for this purpose. Basically, the instrument indicates total weighted noise power in decibels above a 1000-cycle reference power of —90 dbm. However, for some weighting networks the meter reading is "adjusted" by an amount which is determined by the acoustical efficiency of the telephone instrument to which the weighting corresponds. In this way equal interfering effects on systems employing different telephone instruments are indicated by equal noise meter readings when appropriate weighting is used in each case. Such readings are expressed in dba (db adjusted). For F1A line weighting, which was used in the Israel tests, the readings in dba represent total weighted noise power in decibels above a 1000-cycle reference power of —85 dbm. The F1A line weighting curve is in conformity with that adopted by the CCIF (International Consultative Committee on Telephony) for use in measuring noise on international circuits.*

The average circuit noise for all channels of the systems installed in Israel, including residual noise and intermodulation crosstalk under heavy traffic conditions, was about 30 dba at a point of zero transmission level, or 26 dba at the hybrid output (—4 db transmission level).

It may be noted that had the channels been adjusted for 7 decibels net loss, the noise output would have been 23 dba, which more than fulfills the CCIF requirement of 27 dba (2 millivolts psophometric EMF) at a point of —7 db transmission level.

Signal-to-Noise Ratio

As an expression of circuit merit, signal-to-noise ratio is more widely used by radio engineers than is circuit noise level as expressed above. Maximum signal-to-noise ratio is usually taken as the ratio of

* CCIF recommendations for noise are not expressed in dba, but in noise electromotive force (psophometric emf). For example, 2 millivolts psophometric emf is equivalent to 27 dba. For definition see CCIF XV Plenary Assembly, Paris, July 1949, Volume IV, page 25.

maximum 1000-cycle sine wave output to weighted noise output. In the present case the maximum 1000-cycle output is limited to approximately +10 dbm at a point of 0 transmission level, or 95 dba when measured with F1A weighting. Thus, a noise level of 30 dba at a point of 0 transmission level corresponds to a maximum signal-to-noise ratio of 65 decibels.

The extent to which the available signal-to-noise ratio is made use of in a particular subscriber-to-subscriber connection depends upon the lengths of the subscriber loops and other characteristics of the wire telephone network. In general, a trunk signal-to-noise ratio of 60 decibels or more is desirable to assure satisfactory speech-to-noise ratios for difficult subscriber connections.

Channel Noise

The determination of residual noise on the speech channels is one of the most important performance tests. Also, a special effort was made to accumulate as much data as possible concerning noise, since such data would be useful in future design of very-high-frequency systems.

Channel noise caused by the equipment itself can be predicted fairly accurately from theoretical considerations and laboratory measurements, but man-made noise picked up by the receiving antenna and its effect on channel noise depends on local conditions and must be determined largely from empirical data. With this in mind steps were taken to evaluate separately the various components of the total noise output.

All noise measurements were made at the speech channel outputs, either at the carrier demodulator outputs (point of 0 transmission level) or at the receiving hybrid outputs (point of —4 decibels transmission level).

Considering a telephone connection from subscriber to subscriber, the sources of noise are as follows:

1. Lines to subscribers at each end.
2. Automatic exchanges at each end, and toll switchboard.
3. Toll dialing equipment at each end, and lines to exchange and to carrier equipment.
4. Carrier equipment at each end.
5. Radio transmitters at sending terminal and relay station.
6. Radio receivers at receiving terminal and relay station.
7. Man-made noise picked up by radio receivers.
8. Cosmic noise picked up by radio receivers.
9. Interfering radio signals picked up by receivers.

The subscriber lines, automatic exchanges, and toll switchboards were not part of the system supplied, and, therefore, noise from these sources will not be considered here. The outgoing and incoming toll dialing equipment and the relatively short lines connecting it into the system were not significant sources of noise.

Carrier Equipment Noise

Residual noise produced in the channels by the carrier equipment alone may be measured by looping the sending and receiving sides at a terminal. In equipment having alternating-current power supply, as in this case, noise consisting of harmonics of the power frequency may originate in the demodulators. Noise levels with F1A weighting varied from channel to channel between 12 and 20 dba with an average of 15 dba, at a point of 0 transmission level.

Radio Transmitter Noise

The only significant source of noise found in the CTR-2 Transmitter is in the frequency control circuits. The master oscillator and crystal oscillator frequencies are subdivided, for comparison, to a frequency around 22 kilocycles. The harmonics of this frequency modulate the transmitter at a level of 60 to 80 decibels below the full modulation level or about 45 to 65 decibels below single channel test tone level. The resulting channel noise level, if the tone in question falls at the peak of the F1A weighting curve, will be 20 to 40 dba at point of 0 transmission level.

In the Israel systems only the third, fourth, and fifth harmonics fall within the carrier range, some of the frequencies fall between channels, and others are attenuated by the weighting. Measurable noise of this type is between 20 and 30 dba at point of 0 transmission level on one or two channels.

Receiver Fluctuation Noise

Electron current fluctuation and thermal agitation in the early stages of the receiver cause noise in the receiver output which may be calculated from the input level and the receiver noise factor. The weighted noise level corresponding to each speech channel may likewise be calculated.

As determined by measurements at the factory, the noise factors of the CTR-2 Receivers used in the system ranged from 9 to 11 decibels with respect to theoretical thermal noise, and the measured base-band noise outputs were within ± 1.5 decibels of the values calculated from the noise factors. However, in order to be able to segregate accurately

all sources of noise during the installation, measurements of receiver fluctuation noise in the speech channels were made in Israel.

With the receiver fed from an unmodulated signal generator, the noise output of each carrier telephone channel was measured with a 2B Noise Measuring Set and compared with the calculated noise output. Carrier equipment noise was either deducted, or its effect eliminated by raising the level of the receiver noise by a known amount before entering the carrier equipment.

It was found that receiver fluctuation noise, as it appeared in the speech channels, was about 3 decibels higher than calculated.

Radio-frequency signal strengths and city noise conditions were such that fluctuation noise was of importance only at the relay stations. Measurements on receivers located at relay stations where there is no carrier equipment were made at the terminal stations. The input from the signal generator to the relay receiver was set low enough to make the relay receiver fluctuation noise completely override the terminal receiver fluctuation or city noise.

In the Israel systems, receiver fluctuation noise was largely determined by received signal strength at the relay stations, and was generally of the order of 20 to 23 dba at point of 0 transmission level for an average channel under median conditions of propagation.

City Noise

The noise output of a very-high-frequency receiver located in a city may be considerably higher than that which is caused by fluctuation noise in the receiver itself. This noise, which we will call city noise, is picked up by the antenna from motor vehicles, electrical machinery, electric signs, faulty high-voltage insulators and similar sources.[4] It usually varies in level with the activity of the city, from day to night and from working day to holiday. Because of its irregular and impulse-like nature, it causes a crackling sound which is easily distinguished from the characteristically "smooth" sound of fluctuation noise in a very-high-frequency telephone channel. Whether or not such noise contributes appreciably to the total system noise depends upon the signal field strength at the noisy location.

In the Israel system the terminal stations are located at city telephone exchanges in areas of high noise level. The signal strengths received from the relay stations are such that city noise contributes to the total noise output at Jerusalem and Haifa, while at Tel Aviv it is the largest single source of noise. However, the system was so

[4] L. C. Simpson, H. J. B. Nevitt, and E. J. Eriksen, "VHF Radio Multichannel Carrier Telephone Circuits in Colombia," *Ericsson Review*, Vol. 28, p. 62, 1951.

planned that signal field strengths were adequate to insure excellent performance.

Although city noise was the predominant noise source at only one terminal and did not constitute a problem at any terminal, measurements of it were made at all three terminals for use in designing future systems involving similar station sites. Noise level readings were taken at the channel outputs with the 2B noise measuring set, and any other noise power present, such as receiver fluctuation noise or carrier equipment noise, was then deducted to arrive at the output level of the city noise alone. This output level was then used to derive a city noise factor.

The 2B noise measuring set combines single-frequency components on a root-sum-square basis, but it is not known whether this occurs for sharply peaked impulse noise. Since city noise is usually a combination of noise from many sources, the pulse rate is high enough so that there is little difficulty in reading the instrument, though variations are generally greater than for receiver fluctuation noise. In any event, whether or not true power is indicated, this meter is widely used for measuring telephone circuit noise, and means for predicting its readings are necessary in system design.

The noise level in the telephone channels due to city noise picked up by the antenna will depend upon such factors as the received signal strength and the modulation level, which vary from system to system. In order that data obtained at the station sites of the present system may be made use of to estimate the circuit noise which may be introduced at similar sites in other systems, it is necessary to express it in relation to some fixed reference value.

Perhaps it would appear most logical that the noise be expressed as radio-frequency field strength. However, the conversion of circuit noise to radio frequency noise field strength requires that the gain of the antenna in the direction of the noise source be known. In the case of a fixed directive antenna mounted high above crisscrossed city streets, the direction from which the noise comes is difficult to determine. Though the direction may be estimated, the corresponding antenna gain can only be approximated unless an unusually complete antenna radiation pattern is available. Calculations of noise field strength based on such assumptions showed reasonable correlation with published radio-frequency noise data, but the complications seemed out of proportion with the degree of accuracy to be expected.

As a practical matter, city noise may be treated as though it originates in the antenna, and the power which it delivers to the transmission line evaluated in decibels above the thermal power which

would be delivered by an equivalent resistor replacing the antenna. Such a city noise factor for a given location, antenna height, and frequency, is comparable to the receiver noise factor which is used to evaluate receiver fluctuation noise, and may be used in a similar manner. In practical work, the two noise factors may be combined by subtracting the transmission line and filter loss from the city noise factor, adding the result to the receiver noise factor on a power basis, and using this over-all noise factor to establish the carrier-to-total-noise ratio at the receiver input.

During the installation in Israel, sufficient measurements were taken at the three terminals to establish the approximate range of the city noise factor as shown in the following tabulation:

Terminal	Time	City Noise Factor, decibels		
		Maximum	Usual	Minimum
Tel Aviv	0700-1900	30	28	25
	1900-0700	25		20
Haifa	0700-1900	30	28	12
	1900-0700	22		12
Jerusalem	0700-1900	28	25	12
	1900-0700	22		12

The total noise at a channel output is the power sum of city and fluctuation noise from the terminal and relay receivers, carrier equipment noise, and any spurious tones or heterodyne interference which may fall in the channel. The relative importance of these factors will vary from one system to another. It may also vary from hour to hour as city noise and propagations change, and with direction of transmission.

For example, at the Tel Aviv terminal the channel noise level was generally determined by city noise, and at the Haifa terminal it was determined by fluctuation noise from the relay receiver on Mt. Carmel. At Jerusalem the noise level was generally determined by fluctuation noise from the relay receiver in the Judean Hills, but quite often city noise, fluctuation noise, and carrier noise all contributed equally.

Measurements of total system noise, made on all 12 channels at the different terminals, fell within the limits given below. These measurements were made at various hours between 10:00 A.M. and 8:00 P.M., with F1A weighting, and are expressed in dba at a point of 0 transmission level.

	Average All Channels dba	Worst Channel dba
Tel Aviv (From Jerusalem)	20-23	23-27
Tel Aviv (From Haifa)	24-29	27-36
Jerusalem (From Tel Aviv)	25-29	27-30
Haifa (From Tel Aviv)	25-27	27-31

Interference from local transmitters, which may cause beat notes in the channels of very-high-frequency systems, was avoided by careful selection of operating frequencies. The reception of a small amount of cosmic noise may be expected, under certain conditions, at frequencies as high as 250 megacycles. No attempt was made to evaluate this during the present installation, since other noise sources were predominant.

Intermodulation Crosstalk

Interchannel crosstalk in a multichannel system of this type is caused by nonlinearity in those parts of the system which carry the combined signals of all the channels. Nonlinearity in the amplitude response of the radio equipment and the wide-band amplifiers of the carrier equipment results in the production of unwanted intermodulation products. These products, having frequencies other than the signals which caused them, appear as unwanted noise in other channels. This crosstalk is unintelligible.

Crosstalk caused by intermodulation may vary between rather wide limits, as it depends upon the number, position, and talker volume of the other channels which may be active at any particular moment. For system adjustments and performance tests, it is convenient to simulate traffic conditions in some way, so that steady crosstalk readings may be obtained which are reasonably indicative of the readings which will prevail when the system is carrying its heaviest traffic.

The method used for simulating traffic during adjustment of the present systems was the simultaneous modulation of all channels, except the one being measured, with sine wave tones of the same level. A generator having 11 separate oscillator outputs at frequencies between 300 and 3300 cycles was used for this purpose.

Crosstalk measurements were made with tone levels varying from —12 to 0 dbm at the transmitting hybrid. Final performance tests were made with a tone level of —4.5 dbm.

No practical means were available for obtaining complete statistical data on crosstalk while the system was carrying traffic. However, it was observed that for the greater part of the time during the busiest

period, the over-all channel noise, including crosstalk, dialing and switching peaks, and residual noise, did not exceed the values obtained when the system was loaded with tones of —4.5 dbm.

Occasional maximum circuit noise peaks during the busiest period were somewhat higher than with multitone loading. Each channel was observed for 3 to 5 minutes and the maximum values of circuit noise caused by crosstalk, dialing and switching peaks, the residual noise were recorded. This data is summarized in the following tabulation, which also includes, for comparison, a summary of measurements made when the channels were loaded with tones of —4.5 dbm at the transmitting hybrid.

Circuit Noise and Crosstalk,
dba F1A at Point of 0 Transmission Level

		11 Tone Test		Traffic Test (Max. Values)			
Direction of Transmission	Channel	Residual Noise	Crosstalk Plus Residual Noise	Crosstalk Plus Residual Noise	Dialing Peaks	Switching Peaks	Residual Noise
Tel Aviv to Jerusalem	Worst	30	31	39	34	38	30
	Average	27	30	31	32	32	26
	Best	23	26	28	28	N	25
Jerusalem to Tel Aviv	Worst	24	29	36	35	42	27
	Average	22	27	28	30	32	22
	Best	19	23	23	N	N	19
Tel Aviv to Haifa	Worst	30	29	34	30	36	31
	Average	27	27	30	29	32	25
	Best	25	24	28	N	N	22
Haifa to Tel Aviv	Worst	27	32	36	32	34	31
	Average	25	29	29	30	33	26
	Best	22	28	26	N	N	22

Referring to the tabulation, it may be seen that for the average channels the maxima observed during the traffic test were from 0 to 3 decibels above the values obtained with tone loading. Making the same comparison for the worst channel in each case, the highest peaks were from 4 to 8 decibels above the values obtained with tone loading.

Noise peaks caused by dialing impulses are shown separately, and are seen to be 4 or 5 decibels below the highest crosstalk peaks. Isolated peaks caused by switching and supervisory relays in the toll dialing equipment were comparable with the highest crosstalk peaks. Under normal operating conditions these switching peaks were not frequent enough to be noticeable.

It is considered that the performance obtained when 11 channels are loaded with tones of —4.5 dbm provides a realistic approximation of the actual system performance under traffic conditions. However, it may be noted that an increase in tone level of 2 or 3 decibels would be required to produce crosstalk levels equal to the highest peaks observed under traffic conditions.

Loop Measurements (Two-Hop)

During the initial adjustments, crosstalk measurements were made on a loop basis, from terminal to relay station and back again, rather than from terminal to terminal. Such a loop circuit involves the same amount of equipment as a two-hop terminal-to-terminal circuit, and

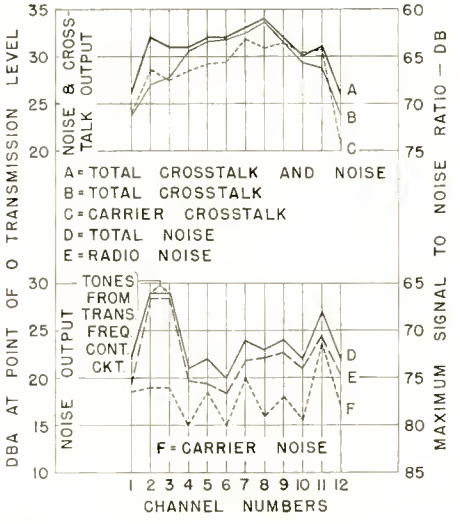

Fig. 14—Noise and crosstalk in each channel of 12-channel system when remaining 11 channels are modulated with nonsynchronous tones of —4 dbm at point of 0 transmission level (20 decibels below 300-kilocycle transmitter frequency deviation). Jerusalem–Judean Hills–Jerusalem loop.

has the advantage that the channel inputs and outputs are at one point. In addition, the amount of crosstalk and noise originating in the carrier equipment alone may be determined by making a loop connection from carrier output to carrier input. In order to facilitate such loop tests, the system was so lined up that the levels at the wide-band terminals of all radio and carrier equipment were the same.

Figure 14 shows measurements made on each channel for the

Jerusalem–Judean Hills–Jerusalem loop, and illustrates how crosstalk and noise vary from channel to channel. The actual measurements taken for each channel were (1) carrier residual noise, (2) total residual noise, (3) carrier crosstalk plus noise for —4 dbm tone loading, and (4) total crosstalk plus noise for —4 dbm tone loading. The total residual noise was then subtracted from the total crosstalk plus noise, on a power basis, to obtain the total crosstalk alone. The carrier residual noise was likewise subtracted from the total residual noise to obtain the radio noise alone. All levels are in dba, F1A weighting, at the demodulator output jacks of the carrier equipment (point of 0 transmission level).

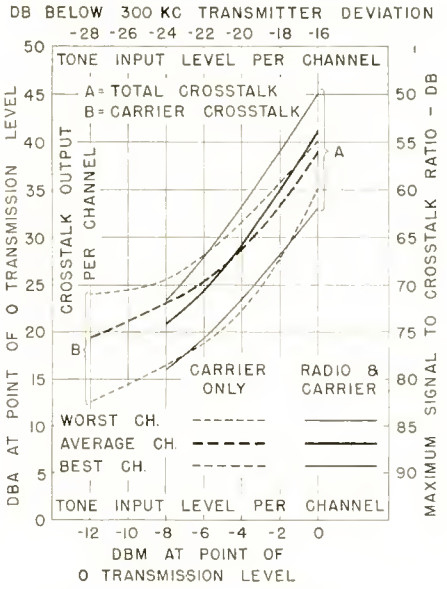

Fig. 15—Crosstalk in single channel of 12-channel system when 11 remaining channels are modulated with nonsynchronous tones. Jerusalem–Judean Hills–Jerusalem loop.

Figure 15 also applies to the Jerusalem–Judean Hills–Jerusalem loop. It illustrates how the total crosstalk and carrier crosstalk for each channel vary when the level of the tones loading the remaining 11 channels is varied.

Acknowledgments

The installation work was carried out by the Department of Posts, Telegraphs, Telephones and Radio of the Ministry of Transport and

Communications of Israel, with supervision by RCA International Division. Credit is due to Mr. M. E. Berman, Head of Engineering Services (Radio and Transmission), to Mr. M. S. Friedman, Head of Engineering Services (Equipment and Lines), to the engineering personnel of the district offices, and to Mr. T. Katz, Transmission Engineer, and Mr. M. Offner, Radio Engineer who collaborated in all phases of the installation.

The support and encouragement received from Dr. David Pinkas, late Minister of Transport and Communications, from Mr. Ch. Ben Menachem, Director General of Posts, Telegraphs, Telephones and Radio, and from Mr. Zvi Prihar, former Director General of Posts, Telegraphs, Telephones and Radio, are gratefully acknowledged.

The system design at RCA International Division was under the direction of G. G. Gerlach, who also conducted the field survey, and D. H. Pain. The radio equipment was designed under the supervision of J. C. Sutherland of RCA Victor Company Limited (Canada). Carrier telephone equipment was supplied by the Lenkurt Electric Company. In particular the author wishes to acknowledge the work of J. C. Barron of RCA Victor Company Limited who collaborated with the writer in the supervision of the installation in Israel.

RCA TECHNICAL PAPERS †

Fourth Quarter, 1952

Any request for copies of papers listed herein should be addressed to the publication to which credited.*

"An All-Band Antenna and Coupler," J. H. Owens, *Ham Tips* (November) 1952

"Application of Linear Active Four-Terminal Network Theory to Transistors," L. J. Giacoletto, *RCA Industry Service Laboratory Bulletin LB-889* (October 14) 1952

"Attenuation of Wire Helices in Dielectric Supports," R. W. Peter, J. A. Ruetz, and A. B. Olsen, *RCA Review* (December) 1952

"Broadcasting TV in the UHF Band," J. Epstein and D. W. Peterson, *Electronics* (November) 1952

"A Building-Block Approach to Magnetic Recording Equipment Design," K. Singer and J. L. Pettus, *Jour. S.M.P.T.E.* (October) ... 1952

"Ceramic-Metal Seals of the Tungsten-Iron Type," D. G. Burnside, *RCA Industry Service Laboratory Bulletin 894* (November 10) .. 1952

"The Control of Frequency Response and Stability of Point-Contact Transistors," B. N. Slade, *Proc. I.R.E.* (November) 1952

"Development of an Improved Graphechon Storage Tube," W. T. Dyall, G. R. Fadner, and M. D. Harsh, *RCA Review* (December) 1952

"A Developmental Germanium P-N-P Junction Transistor," R. R. Law, C. W. Mueller, J. I. Pankove, and L. D. Armstrong, *Proc. I.R.E.* (November) 1952

"Electrical Measurements on Germanium," E. C. Giaimo, A. R. Moore, and J. Kurshan, *RCA Industry Service Laboratory Bulletin LB-885* (October 8) 1952

"Electron Microscopy of Some Marine Egg Inclusions," J. Hillier, A. I. Lansing, and T. B. Rosenthal, *Biological Bulletin* (October) 1952

"Electron Microscopy of Some Marine Egg Surfaces," J. Hillier, A. I. Lansing, and T. B. Rosenthal, *Biological Bulletin* (October) 1952

"Electronic Structure of the Diamond Crystal," F. Herman, *Phys. Rev.* (December) (Letter to the Editor) 1952

"Equipments for Measurement of Junction Transistor Small-Signal Parameters for a Wide Range of Frequencies," I. J. Giacoletto, *RCA Industry Service Laboratory Bulletin LB-900* (December 30) 1952

"Experimental 850-Mc TV Transmitter," G. A. Olive, *Electronics* (November) 1952

"Experimentally Determined Radiation Characteristics of Conical and Triangular Antennas," O. M. Woodward, Jr. and G. H. Brown, *RCA Industry Service Laboratory Bulletin LB-893* (October 31) .. 1952

"Experimentally Determined Radiation Characteristics of Conical and Triangular Antennas," G. H. Brown and O. M. Woodward, Jr., *RCA Review* (December) 1952

† Report all corrections or additions to RCA Review, Radio Corporation of America, RCA Laboratories Division, Princeton, N. J.

* *RCA Industry Service Laboratory Bulletins* are not published and are issued only as a service to licensees of the Radio Corporation of America.

"Field Strengths Recorded on Adjacent FM Channels at 93 Megacycles over Distances from 40 to 150 Miles," G. S. Wickizer and A. M. Braaten, *Proc. I.R.E.* (December) 1952
"High-Efficiency Coolers for Power Tubes," M. B. Lemeshka and A. G. Nekut, *Tele-Tech* (November) 1952
"Junction Transistor Equivalent Circuits and Vacuum-Tube Analogy," L. J. Giacoletto, *Proc. I. R. E.* (November) 1952
"Laboratory Equipment for Germanium Purification," E. C. Giaimo, *RCA Industry Service Laboratory Bulletin LB-891* (October 17) 1952
"Low-Temperature Electrical Measurements on Semiconductors," R. L. Bjork, E. E. Hahn, and M. L. Schultz, *RCA Industry Service Laboratory Bulletin LB-886* (October 8) 1952
"Methods of Processing Silver-Magnesium Secondary Emitters for *Electron Tubes*," P. Rappaport, *RCA Industry Service Laboratory Bulletin LB-897* (November 28) 1952
"Miniature High-Performance Personal Radio Receivers," J. C. Bleazey, J. Preston, and H. F. Olson, *RCA Industry Service Laboratory Bulletin LB-888* (October 14) 1952
"A New Superhet S-Meter Circuit," J. H. Owens, *Ham Tips* (November) 1952
"One-Channel Converter for UHF Television," W. Y. Pan, *Electronics* (December) 1952
"Photoconductivity Study of Activation of Barium Oxide," H. B. DeVore, *RCA Review* (December) 1952
"P-N Junctions by Impurity Introduction Through an Intermediate Metal Layer, L. D. Armstrong, *Proc. I.R.E.* (November) 1952
"Potential Distribution for Space-Charge Limited Current between a Flame Accelerating Grid and Parallel Anode," E. G. Ramberg and L. Malter, *Jour. Appl. Phys.* (December) 1952
"Preparation of Single Crystals of Germanium and Silicon," B. Selikson, *RCA Industry Service Laboratory Bulletin LB-892* (October 23) 1952
"A Profile of the Man in Industrial Research," E. W. Engstrom and E. H. Alexander, *Proc. I.R.E.* (December) 1952
"Progress Report on Transistor Research and Circuit Applications," *RCA Industry Service Laboratory Bulletin LB-898* (December 17) 1952
"Purification of Germanium by Gradient Freezing," S. M. Christian, *RCA Industry Service Laboratory Bulletin LB-890* (October 17) 1952
"Q-Meter Correction Chart for Distributed Capacitance," R. Lafferty, *Tele-Tech* (November) 1952
"Q-Meter Correction Chart for Q-Voltmeter Loading," R. Lafferty, *Tele-Tech* (October) 1952
"Reflexed Intercarrier Sound," J. Avins, *RCA Industry Service Laboratory Bulletin LB-887* (October 10) 1952
"Resistivity Striations in Single-Crystal Germanium," P. R. Camp, *RCA Industry Service Laboratory Bulletin LB-896* (November 14) 1952
"R-F Coupling Nomograph," R. E. Lafferty, *Electronics* (October) .. 1952
"Some Applications of Permanently Magnetized Ferrite Magnetostrictive Resonators," W. Roberts, *RCA Industry Service Laboratory Bulletin LB-884* (October 6) 1952
"Stable Oscillator for UHF TV Receivers," K. E. Loofbourrow and C. M. Morris, *Electronics* (December) 1952
"Studies of the Oxide Cathode," L. S. Nergaard, *RCA Review* (December) 1952
"Survey of Transistor Development, Part 2," B. N. Slade, *Rad. and Tele. News* (October) 1952
"A Sweep Method for Measuring Envelope Delay," A. C. Schroeder, *RCA Industry Service Laboratory Bulletin LB-883* (October 3) .. 1952

"Theoretical Relativity and Hall Coefficient of Impure Germanium Near Room Temperature," P. G. Herkart and J. Kurshan, *RCA Industry Service Laboratory Bulletin LB-899* (December 18).... 1952
"Transistor Trigger Circuits," A. W. Lo, *Proc. I.R.E.* (November).. 1952
"Transistors Operate at 300 MC," G. M. Rose and B. N. Slade, *Electronics* (November) 1952
"Universal Design Curves for Tone-Control Circuits, Part 4," M. B. Knight, *Rad. and Tele. News* (October) 1952
"The Use of Radioactive Material for the Generation of High Voltage," E. G. Linder and S. M. Christian, *Jour. Appl. Phys.* (November) 1952
"The Vibrating-Plate Viscometer—An Aid in Slip-Casting Control," J. G. Woodward, *American Ceramic Bulletin* (October)..... 1952

Correction:

In the paper entitled "Analysis of Microwave Antenna Sidelobes," by N. I. Korman, E. B. Herman, and J. R. Ford, which appears in the September 1952 issue, the last sentence of the first full paragraph on page 326 should read:

"If d is the peak-to-peak linear error of the largest sinusoidal component, then $\pi d/\lambda$ is the peak-to-peak error of this component, and the largest sidelobe will have a peak value of $\pi d/2\lambda$."

AUTHORS

JOHN C. BLEAZEY received the B.S. degree in Electrical Engineering from the Drexel Institute of Technology in 1940. In 1941 he was commissioned in the U.S. Army Signal Corps. While in the Army, he was promoted to the rank of Captain and commanded a Radar Maintenance Unit in the European Theatre till the end of the war. In 1945 he joined the RCA Laboratories Division, Princeton, N. J. and has been engaged in research in acoustics. Mr. Bleazey is a member of the Acoustical Society of America.

C. LOUIS CUCCIA received the B.S. degree in E.E. in 1941 and the M.S. degree in 1942 from the University of Michigan. From 1941 to 1942 he was affiliated with the department of engineering research of the University of Michigan for Fisher Body Division of the General Motors Corporation. In June 1942, he joined the research department of the RCA Manufacturing Company in Harrison, N. J. In November 1942, he transferred to the research staff of RCA Laboratories Division in Princeton, N. J. Mr. Cuccia is a member of Sigma Xi.

L. J. GIACOLETTO received the B.S. degree in Electrical Engineering from Rose Polytechnic Institute, Terre Haute, Indiana, in 1938, and the M.S. degree in Physics from the State University of Iowa in 1939. From 1939 to 1941, while a Teaching Fellow in the department of Electrical Engineering at the University of Michigan, he engaged in frequency-modulation research. He received the Ph.D. degree in Electrical Engineering from the University of Michigan in 1952. He was associated with the Collins Radio Company during the summers of 1937 and 1938, and with the Bell Telephone Laboratories in 1940. From 1941 to 1945 he served with the Signal Corps and returned to inactive status as a major in the Signal Corps Reserve in May, 1946. Since June, 1946, he has been serving as a research engineer at RCA Laboratories Division, Princeton, N. J. Dr. Giacoletto is a member of the American Association for the Advancement of Science, Gamma Alpha, Iota Alpha, Phi Kappa Phi, Tau Beta Pi, and Sigma Xi.

RALPH W. KLOPFENSTEIN received the B.S. degree in Electrical Engineering from the University of Washington in 1944 and the degree of M.S. in Applied Mathematics from Iowa State College in 1951. During 1945 and 1946 he served as a Radio Materiel Officer in the U.S. Navy and during 1947 and 1948 he was a Mathematics instructor at the South Dakota School of Mines and Technology. In 1948 he joined the Broadcast Engineering Section of the RCA Victor Division in Camden, N. J. where he worked on advanced development of television and FM transmitting antennas and filters. He is now on leave of absence pursuing graduate study in Applied Mathematics at Iowa State College where he is also serving as a Mathematics instructor. Mr. Klopfenstein is an Associate Member of Sigma Xi and a Member of Phi Kappa Phi, the Mathematical Association of America and the Institute of Radio Engineers.

HARRY F. OLSON received the B.S. degree in 1924, the M.S. degree in 1925, the Ph.D. degree in 1928 and the E.E. degree in 1932 from the University of Iowa. From 1928 to 1930 he was in the Research Department of Radio Corporation of America; from 1930 to 1932, in the Engineering Department of RCA Photophone; from 1932 to 1941, in the Research Division of RCA Manufacturing Company; since 1941, with RCA Laboratories Division. Dr. Olson is a member of Tau Beta Pi, Sigma Xi and the American Physical Society and a Fellow of the Institute of Radio Engineers. He is a Fellow of the Acoustical Society of America and is serving as its President 1952-1953.

JOHN PRESTON received his education in England, attended Manchester Scientific Institute taking courses in Mechanical Engineering. He then joined the engineering staff of the Bolton Power and Electrical Company. He became a member of Radio Corporation of America in 1929 and was associated with the Research Department of RCA Victor from 1930 to 1935; the Research Department of RCA Manufacturing Company from 1935 to 1941, and RCA Laboratories Division from 1941 to date. His work has been in the field of acoustics since joining Radio Corporation of America. Mr. Preston is a member of the Acoustical Society of America and of Sigma Xi and a Fellow of the Audio Engineering Society.

WALTER VAN B. ROBERTS received the B.S. degree from Princeton University in 1915, the E.E. degree in 1917, the M.A. in 1923, and the Ph.D. in Physics in 1924. He served as the technical officer of a sound ranging station during World War I. From 1919-1924 he was an Instructor in physics and electrical engineering at Princeton University. In 1924, he joined the Radio Corporation of America in the Technical and Test Department, and from 1927 to 1943 served in the Patent Department. From 1943-1946 he was on leave of absence from RCA performing development work at Johns Hopkins and Princeton on proximity fuses, guided missiles and telemetering. He returned to RCA Laboratories Division, Princeton, N. J., as a research engineer in 1946. Dr. Roberts is a Member of Sigma Xi and Phi Beta Kappa and a Fellow of the Institute of Radio Engineers.

LEROY C. SIMPSON received the B.S. degree in Electrical Engineering from the University of New Hampshire in 1928. From 1928 to 1934 he was engaged in the design and installation of high power transmitters for the General Electric Company. In 1934 he joined RCA Victor Argentina, S.A. as Manager of the Engineering Products Division, and was concerned with the production, sale and installation of communications equipment. Since 1948 he has been with RCA International Division in New York, where he is now Assistant Chief Engineer. Mr. Simpson is a Senior Member of the Institute of Radio Engineers.

BERNARD N. SLADE received the B.S. degree in Electrical Engineering from the University of Wisconsin in 1948. He joined the RCA Victor Division immediately after graduation. Mr. Slade is associated with the Advanced Development Group at Harrison where he is working on the development of semiconductor devices. He is also doing graduate work in electrical engineering at Stevens Institute of Technology. Mr. Slade is a Member of the Institute of Radio Engineers.